Robust Adaptive Controls of Nonlinear Systems with Actuator Hysteresis Represented by Prandtl-Ishlinskii Models

Qingqing Wang

A Thesis

in

The Department

of

Mechanical and Industrial Engineering

Presented in Partial Fulfillment of the Requirements

for the Degree of Doctor of Philosophy at

Concordia University

Montréal, Québec, Canada

December 2006

Your file Votre référence
ISBN: 978-0-494-30144-9
Our file Notre référence
ISBN: 978-0-494-30144-9

ABSTRACT

Robust Adaptive Controls of Nonlinear Systems with Actuator Hysteresis Represented by Prandtl-Ishlinskii Models

Qingqing Wang, Ph.D.

Concordia University, 2006

The development of control techniques to mitigate the effects of unknown hysteresis preceding with plants, has recently re-attracted significant attention. This thesis deals with robust adaptive control of nonlinear systems preceded by unknown hysteresis nonlinearities. In the literature, the most common methods to reduce hysteresis effects to the controlled systems are based on the inverse hysteresis compensations. Due to the complexity of hysteresis behavior, this approach has its limit. By thoroughly investigating the Prandtl-Ishlinskii models of hysteresis, a robust adaptive control scheme was developed, which makes it possible to fuse the model of hysteresis with the available control techniques without necessarily constructing a hysteresis inverse. The global stability of the adaptive system and to track a desired trajectory to a certain precision are achieved.

Two classes of nonlinear systems preceded by unknown hysteresis nonlinearities are studied. One class of systems is with parametric uncertainties and known nonlinear functions. By integrating proposed hysteresis adaptation law with sliding mode control and back-stepping techniques, the global stability and tracking a desired trajectory to a certain precision are achieved. Simulation results attained

for an example of this class of nonlinear system are presented to illustrate and further validate the effectiveness of the proposed approaches. Then the approach is extended to a more general class of systems in the presence of parametric uncertainties and unknown nonlinear functions with bounded disturbances and preceded by unknown hysteresis nonlinearities. Combined with neural networks adaptation control method, it is proved that for any bounded initial conditions, all closed-loop signals are bounded and the state vector $x(t)$ converges to a neighborhood of the desired trajectory.

Concerning the practical applications, determination of the density function of the Prandtl-Ishlinskii model is crucial. In this study, a discretional approach is developed to approximate density function $p(r)$ based on the memory effects of the play operator $F_r[v](t)$.

ACKNOWLEDGEMENTS

I would like to express my sincere gratitude to **Dr. Chun-Yi Su** of Concordia University for his time, support and guidance through out the course of this research. He spent many hours of his time to teach and guide me. His supervision and encouragement was really of a paramount importance to me in completing this work. The journal papers and refereed conference proceedings published from my thesis and those submitted for review were made possible by his most responsive follow-ups and incisive critiques on the original drafts. I would like to thank Dr. W. Lin, the External Examiner, Dr. S. Zad, Examiner (External to Program), and the internal examiners, Dr. B. Gordon and Dr. H. Hong for their time and helpful suggestions. I also would like to thank Dr. F. Defersha for his help in formatting this thesis document using LaTeX software.

I sincerely appreciate the financial support for my study from Concordia ENCS SRT Grant and NSERC Research Grant through Dr. Chun-Yi Su.

I would like to thank my family for their support and understanding for the time I spent in the Ph.D. Program.

TABLE OF CONTENTS

LIST OF FIGURES

LIST OF SYMBOLS

$C^{(n)}(R)$	-	The n-dimensional space of continuous functions defined on R
$C\lceil 0, t_E \rceil$	-	The space of continuous functions defined on the time interval $[0, t_E]$
$C_m\lceil 0, t_E \rceil$	-	The space of piece-wise monotone continuous functions defined on the time interval $[0, t_E]$
Ω	-	A compact set, a set which is closed and bounded
$\mathbf{x}$	-	The system state vector $\mathbf{x} = [\mathbf{x}, \dot{\mathbf{x}}, ..., \mathbf{x^{(n-1)}}]^{\mathbf{T}}$
$\mathbf{x_d}$	-	The desired trajectory vector $\mathbf{x_d} = [\mathbf{x_d}, \dot{\mathbf{x}}_\mathbf{d}, ..., \mathbf{x}_\mathbf{d}^{(\mathbf{n-1})}]^{\mathbf{T}}$
$\tilde{\mathbf{x}}$	-	The tracking error vector $\tilde{\mathbf{x}} = \mathbf{x} - \mathbf{x_d}$
$s(t)$	-	The filtered tracking error $s(t) = [\Lambda^T 1]\tilde{\mathbf{x}}(t)$ with $\Lambda^T = [\lambda^{(n-1)}, (n-1)\lambda^{(n-2)}, ..., (n-1)\lambda]$
s_ϵ	-	A tuning error $s_\epsilon = s - \epsilon sat(\frac{s}{\epsilon})$
$v(t)$	-	The system input
$v_h(t)$	-	The term of the controller input designed to compensate the effect of hysteresis
$w(t)$	-	The output of the hysteresis operator
$d_e(t)$	-	The term of the system uncertainties
$Fr\lceil v \rceil$	-	The play hysteresis operator
$F_r\lceil v; \psi \rceil$	-	The play hysteresis operator with general initial condition
$f_r(v, w)$	-	$f_r(v, w) = \max(v - r, \min(v + r, w))$
$E_r\lceil v \rceil$	-	The stop hysteresis operator
$e_r(v)$	-	$e_r(v) = \min(r, \max(-r, v))$
$R_{s-r,s+r}\lceil v \rceil(t)$	-	A relay hysteresis operator
$p(r)$	-	The density function of the Prandtl-Ishlinskii hysteresis model
p_0	-	$p_0 = \int_0^R p(r)dr$

p_{0min} - The lower bound of p_{0min}, i.e., $p_0 > p_{0min}$

$p_{max}(r)$ - The upper bound of $p(r)$, $p(r) \leq p_{max}(r)$ for all $r \in [0, R]$

$\tilde{p}(t,r)$ - $\tilde{p}(t,r) = \hat{p}(t,r) - p(r), \quad for\ all\ r \in [0,R]$

$d[v](t)$ - $d[v](t) = \int_0^R p(r) F_r[v](t) dr$

$\Re_{supp}(\psi)$ - $\Re_{supp}(\psi) = sup\{r | r \geq 0, \psi(r) \neq 0\} < +\infty$

Ψ - The set of functions $\psi : \Re_+ \mapsto \Re$, satisfying

$$|\psi(r_1) - \psi(r_2)| \leq |r_1 - r_2| \quad for\ all\ r_1, r_2 \geq 0, \tag{1}$$

and

$$\Re_{supp}(\psi) = sup\{r | r \geq 0, \psi(r) \neq 0\} < +\infty. \tag{2}$$

In [9] it is called the set of Preisach memory curves.

ψ - The general initial condition of the hysteresis operator

$B(v(t))$ - $B(v(t)) \triangleq \int_0^R p(r) \frac{|F_r[v](t)|}{p_{0min}} dr$

$\tilde{B}(t)$ - $\tilde{B}(t) = \int_0^R (\hat{p}(t,r) - p(r)) \frac{|F_r[v](t)|}{p_{0min}} dr$

$g(x)$ - $g(x) = b(x) p_0 / \bar{b}(x) p_{0max}$

$V(t)$ - The Lyapunov function

$Proj(z,y)$ - The projection operator

Chapter 1

Introduction

1.1. Hysteresis and Systems Control

The hysteresis phenomenon occurs in a wide range of physical systems. For example, smart material-based actuators, such as piezoceramics and shape memory alloys, exhibit hysteresis phenomena [5]. The principal characteristic of hysteresis is that the output of the system depends not only on the instantaneous input, but also on the history of its operation. The relationship between the output and the input takes form of branches, as shown in Fig. 1.1. This usually causes undesirable inaccuracies or oscillations and even instability [15, 59] when controlling a system exhibiting hysteresis behavior.

The development of control techniques to mitigate the effects of unknown hysteresis has been studied for decades and has recently re-attracted significant attention of many researchers. Much of this renewed interest is a direct consequence of the importance of hysteresis in current applications. Interest in studying dynamic systems with actuator hysteresis is also motivated by the fact that they are nonlinear systems with non-smooth multi-valued nonlinearities for which traditional control

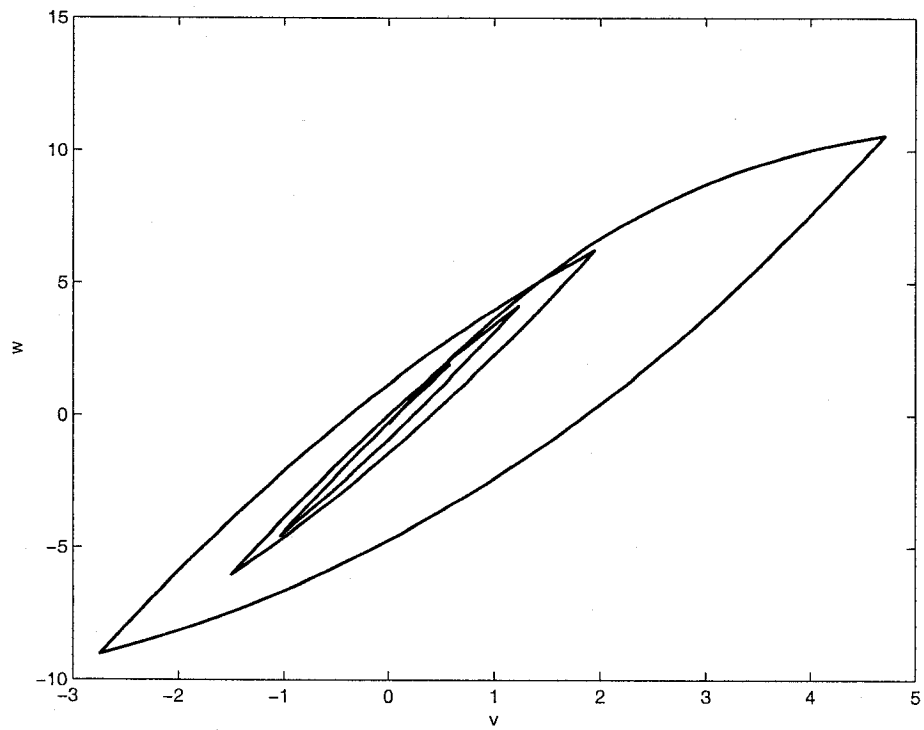

Figure 1.1: Hysteresis nonlinearity

methods are insufficient and so requiring development of new approaches [60]. It is typically challenging in developing a general frame for control of a system in the presence of unknown hysteresis nonlinearities.

To address such a challenge, the development of purely phenomenological models is necessary. Such models will characterize these nonlinearities with sufficient accuracy. They should be amenable to control design for nonlinearity compensation and efficient enough for use in real-time applications. Several models of hysteresis have been developed since the end of the 19th century (see, for instance, [10, 37, 45, 63]). The reader may refer to [43] for a recent review of research in this area. One of such models is the Preisach model, which can be considered as a superposition of one of the elementary hysteresis operators, called "relay". This model has been widely utilized in modelling piezoelectric, magnetostrictive and shape memory alloy hysteresis. An extensive review on this subject can be found in [45]. Models set up by the composition of "play" or "stop" operators are referred to as Prandtl-Ishlinskii models in the literature (see, e.g., [37, 63]). Although the model itself was introduced much earlier [31], the reader may refer to [10, 37, 63] for a systematic mathematical investigation of Prandtl-Ishlinskii models.

In the literature, the most common approach to mitigate the effects of hysteresis is to construct an inverse operator, which was pioneered by Tao and Kokotovic [59]. The reader may refer to, for instance, [17, 23, 38] for recent progress in such development. Essentially, the inversion problem depends on the phenomenological modelling methods (for example, using Preisach models) and strongly influences practical applications of controller design. Due to multi-valued and non-smoothness features of hysteresis, those inverse based methods are sometimes complicated, computationally costly and highly sensitive to the model parameters with unknown measurement errors. These issues are directly linked to the difficulty of stability analysis

of the systems except for certain special cases [59].

In the past decades, robust adaptive control of uncertain nonlinear dynamics has undergone rapid developments. Systematic design procedures for globally stable and asymptotically tracking controllers have been developed for reasonably large classes of nonlinear systems, including systems with nonlinear parameters, in the presence of parametric uncertainties and unknown nonlinear functions [30, 41, 36]. Although the phenomenological models, such as Prandtl-Ishlinskii model, have been successfully applied in modelling piezoceramic and shape memory alloy hysteresis [27, 23, 58], methods to integrate them with available control techniques to have the basic requirement of system stability are not apparent. In this thesis research, by thoroughly investigating the Prandtl-Ishlinskii models of hysteresis, it is noticed that the Prandtl-Ishlinskii model can be transformed into the Preisach model. Under certain definition of the measurement, they are all defined as Preisach type models. These two models have the same type of memory, which is completely determined by a curve of the play operator in the $(F_r[v](t), r)$ plane. Based on this consideration, the experimental results applied to the Preisach models can be adjusted to suit to the Prandtl-Ishlinskii models. Secondly, it is noticed that the Prandtl-Ishlinskii model decomposes the hysteresis behavior into two terms. The first term is a linear function of the control signal $v(t)$, and the second term describes the nonlinear hysteretic part. This decomposition is crucial since it facilitates the utilization of the currently available robust adaptive control techniques for the controller design. It will become more clear later that this structure makes design the adaptive control algorithm possible. This is also the primary motivation to use the Prandtl-Ishlinskii model in this thesis research.

1.2. Contributions of the Thesis

1.2.1 Summary of Research Contributions

This thesis deals with robust adaptive control of nonlinear systems preceded by unknown hysteresis nonlinearities. In recent development in this area, the most common methods to reduce hysteresis effects to the controlled systems are based on the inverse hysteresis compensations. Due to the complexity of hysteresis behavior, this approach has its limit. By thoroughly investigating the Prandtl-Ishlinskii models of hysteresis, a novel robust adaptive control scheme is developed , which makes it possible to fuse the model of hysteresis with the available control techniques without necessarily constructing a hysteresis inverse.

Two classes of nonlinear systems preceded by unknown hysteresis nonlinearities are studied. One class of systems with known nonlinear functions and unknown parameters. By combining the proposed hysteresis adaptation method with two control techniques, sliding mode control and back-stepping, it is proved that the closed-loop systems are globally stable, and the system states track the desired trajectory to a designed precision. Simulation results attained for a nonlinear system are presented for both methods to illustrate and further validate the effectiveness of the proposed approaches.

Then the approach is extended to a more general class of systems. The systems are in the presence of parametric uncertainties and unknown nonlinear functions, bounded disturbances caused by the system uncertainties such as the external disturbances and modelling errors, and unknown hysteresis nonlinearities preceded by the plant. Combined the technique designed to reduce the hysteresis effects with neural network adaptation control method given in [19], it is proved that if the system states defined in a bounded domain, for any bounded initial conditions, all

closed-loop signals are bounded and the state vector $x(t)$ converges to a neighborhood of the desired trajectory. To illustrate this robust adaptive control algorithm, simulations are conducted to a variable length pendulum plant. The pendulum is considered to be driven by an input v though an actuator with hysteresis. The output of the actuator applied to the pendulum is the torque w, see Fig.6.1. The results show the effectiveness and robustness of the approach under different set of parameters.

As for practical applications, it is noticed that the Prandtl-Ishlinskii model is determined by its density function. In this study, a discretional approach is developed to approximate the density function $p(r)$ based on the memory effects of the play operator $F_r[v]$. By measuring the outputs corresponding to a designed decreasing input function, the density function can be estimated.

1.3. Organization of the Thesis

The remaining part of this thesis is organized as follows. Extensive literature review in mathematical models of the hysteresis nonlinearity and control methods of the systems with hysteresis is presented in Chapter 2. From the numerous recent publications in this area, it is noticed that such controller design is an open question and requires further study. In Chapter 3, the Prandtl-Ishlinskii model and its major properties to be used in our controller design are presented. And also a model identification methodology for the density function of the Prandtl-Ishlinskii model for practical applications is developed. Controller design based on sliding mode control and back-stepping control are discussed in Chapters 4 and 5, respectively, with analysis and simulation results. Controller design with neural network for even more complicated systems is presented in Chapter 6. Summary and concluding remarks

from the results of this thesis research are presented in Chapter 7.

Chapter 2

Literature Review

2.1. Hysteresis

The phenomenon of hysteresis is encountered in many different areas of engineering and science. However, the vary meaning of hysteresis varies from one area to another. Usually people refer hysteresis phenomenon to a relation between two quantities with the formation of hysteresis loops. As pointed out by Mayergoyz [45], this may be misleading and can create the impression that the looping is the essence of hysteresis. In 1905, by experimentally observing ferromagnetic hysteresis and noticing its complexity, Madelung [10] summarized the following rules to describe ferromagnetic hysteresis effect, with reference to Fig.2.1.

Madelung's Rules:

1) Any curve C_1 emanating from a turning point A of the input-output graph is uniquely determined by the coordinates of A.

2) If any point B on the curve C_1 becomes a new turning point, then the curve C_2 originating at B leads back to the point A.

3) If the curve C_2 is continued beyond the point A, then it coincides with the

continuation of the curve C which led to the point A before the C_1-C_2 cycle was traversed.

In order to avoid confusion and ambiguity, the definition given in [45] is adopt:

Definition of Hysteresis

Consider a transducer which can be characterized by an input $v(t)$ and an output $w(t)$. This transducer is called a hysteresis transducer if its input-output relationship is a multi-branch nonlinearity for which branch-to-branch transition occur after extrema.

This is a phenomenological definition. It is not related to any specific physical meanings of the input and output functions. Thus it gives more mathematical generality. This definition emphasizes that branching is the most important characteristic of hysteresis. The Preisach models and the Prandtl-Ishlinskii models are examples of hysteresis transducers under this definition. It can be seen in Fig.2.1 that looping is a particular case of branching, and hysteresis loops are formed only when the input function is back and forth between two consecutive extremum values.

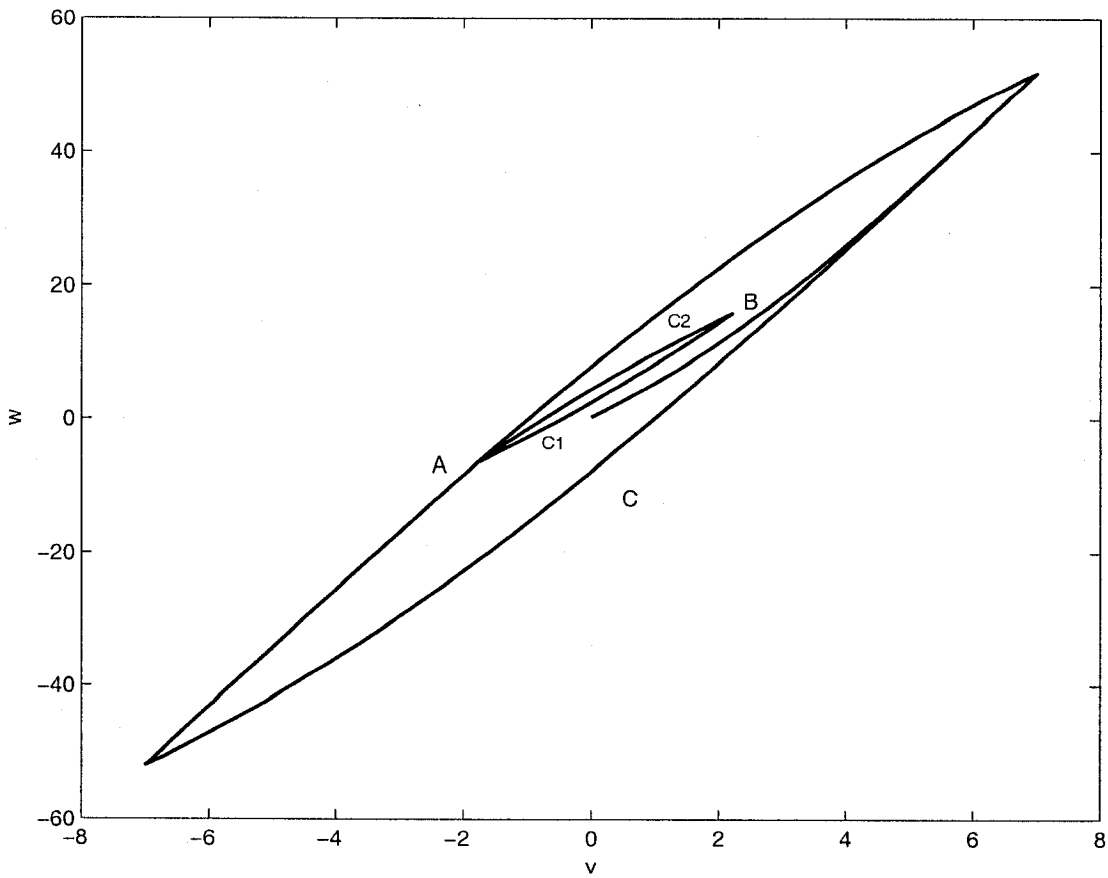

Figure 2.1: Madelung's rules

2.2. Mathematical Models of Hysteresis

To develop general models that can accurately represent diverse hysteresis behaviors has been a subject of interest since the end of the 19th century. Several models of hysteresis have been proposed and each has found applications in certain areas. For instance, the Duhem models and the Preisach models are mainly used in applied electromagnetics while the Prandtl-Ishlinskii models are used to describe elastic-plastic behavior of certain systems. Since early 1970s, systematic mathematical investigations on hysteresis phenomenon have been carried out by many research. The most widely accepted hysteresis models are the Duhem type models usually in the form of differential equations, the Preisach and Prandtl-Ishlinskii models based on basic hysteresis operators, and the Krasnosel'skii-Pokrovskii hysteron. There are monographs for hysteresis modelling and for dynamical systems with hysteresis, [10, 37, 45, 63]. The reader may refer to [43, 52] for recent review.

2.2.1 The Duhem Type Hysteresis Models

The Duhem model focusses on the fact that the output can only change its character when the input changes direction. In general, for suitable functions f_1 and f_2, the hysteresis is given by the two families of curves in the (v, w) plane defined as the solution to the differential equation

$$\dot{w}(t) = f_1(w, v)\dot{v}_+(t) + f_2(w, v)\dot{v}_-(t)$$

with $\dot{v}_+(t) = max[0, \dot{v}(t)]$, $\dot{v}_-(t) = min[0, \dot{v}(t)]$. A special case given in Bouc [43] is

$$\frac{dw}{dt} + a|\frac{dv}{dt}|g(v, w) = b\frac{dv}{dt}, \tag{2.1}$$

where a typical choice for g is $g(v, w) = w - b\phi(v)$. Coleman and Hodgdon [12, 13] extensively studied this model, using the equation

$$\frac{dB}{dt} = \alpha|\frac{dH}{dt}|[f(H) - B] + \frac{dH}{dt}g(H), \tag{2.2}$$

where $\alpha > 0$ is a constant, H is the applied magnetic field and B is the level of magnetization of the medium. They proved that the following conditions for f and g are necessary and sufficient for equation (2.2) to give a hysteresis diagram,

(1) $f(.)$ is piecewise smooth, monotone increasing, odd, with $lim_{H\to\infty}f'(H)$ finite;

(2) $g(.)$ is piecewise continuous, even, with $lim_{H\to\infty}g(H) = lim_{H\to\infty}f'(H)$;

(3) $f'(H) > g(H) > \alpha e^{\alpha H}\int_H^\infty |f'(\eta) - g(\eta)|e^{-\alpha\eta}d\eta$ for all $H > 0$.

And the solution can be explicitly expressed as

$$B = f(H)+[B_0-f(H_0)]e^{-\alpha(H-H_0)sgn\dot{H}}+e^{-\alpha H sgn\dot{H}}\int_{H_0}^{H}[g(\eta)-f'(\eta)]e^{-\alpha\eta sgn\dot{H}}d\eta \tag{2.3}$$

for H piecewise monotone and $\dot{H}$ constant. The functions and parameters in (2.2) can be fine-tuned to match experimental results for rate-independent hysteresis in ferromagnetic soft materials.

A modification based on exchanging the positions of B and H in the differential equation (2.2) was studied by Hodgdon [24, 25].

The Bouc-Wen model: Bouc-Wen model is another modification of the Bouc's model. The model was applied to describe hysteresis in a single degree of freedom oscillator [56], and a magnetorheological damper attached to a scaled three-degree of freedom building [52]. Suppose x is the position of a oscillator system given by

$$\ddot{x} = f(x, \dot{x}, z, u), \tag{2.4}$$

where z is the hysteretic variable proportional to the restoring force acting on the oscillator described by the first order differential equation

$$\dot{z} = A\dot{x} - \beta\dot{x}|z|^n - \gamma|\dot{x}||z|^{n-1}z, \tag{2.5}$$

the parameters n, A, β, and γ are shape parameters of the hysteresis curves which can also be functions of time. Note that in this model $\dot{x}$ acts as an input, and the equation is not involved in x although the hysteresis phenomenon is observed between x and z. When $n = 1$, (2.5) becomes a linear ordinary differential equation which can be solved according to the signs of $\dot{x}$ and z. As n increases to ∞, the hysteresis loop will converge to a bilinear curve defined by $\dot{z} = \dot{x}[sgn(z + A) - sgn(z - A)]/2$.

The Jiles-Atherton model: This model is widely used in modelling ferromagnetic hysteresis [34, 35, 33]. In its original form [35], magnetization $M = M_{rev} + M_{irr}$ was decomposed into its reversible component M_{rev} and irreversible component M_{irr}. The differential equations with respect to the frequency of the imposed magnetic field $H(t)$ are represented in the form

$$\frac{dM_{irr}}{dH} = \frac{M_{an} - M_{irr}}{\delta k - \alpha(M_{an} - M_{irr})} \tag{2.6}$$

$$\frac{dM_{rev}}{dH} = c(\frac{dM_{an}}{dH} - \frac{dM_{irr}}{dH}), \tag{2.7}$$

where M_{an} is the anhysteretic magnetization

$$M_{an} = M_s\{coth(\frac{H + \alpha M}{a}) - (\frac{a}{H + \alpha M})\} \tag{2.8}$$

and δ is a directional parameter. It takes the value $+1$ for $dH/dt > 0$ and -1 for $dH/dt < 0$. a, α, c, k, and the saturation magnetization M_s are the parameters to be determined from experimental measurements of the hysteresis loops, see [35, 40, 53]. The Jiles-Atherton model and the Preisach model are often used in

magnetodynamic field. The former is based on the real physical systems, and the latter is a phenomenological model. Philips [49] compared the computation results of these models with experimental measurements. It was found that the identification of the parameters in the Jiles-Atherton model requires less measurements, while the Preisach model fits the hysteresis loops better.

2.2.2 Hysteresis Models Based on Hysteron

The Krasnosel'skii-Pokrovskii hysteron: In 1970s, Krasnosel'skii and Pokrovskii systematically investigated the hysteresis phenomenon from mathematical point of view, see the monograph [37]. They defined their basic model of hysteresis, referred as hysteron, in a geometric way.

Considering a transducer W with input $u(t)$ and output $x(t)$ as

$$x(t) = W[t_0, x_0]u(t), \qquad t \geq t_0. \tag{2.9}$$

For a piecewise monotone and continuous input function $u(t)$, the domain $\Omega(W)$ of the transducer W must satisfy the following hypotheses:

(1) The intersection $K(u_0)$ of the domain $\Omega(W)$ with any vertical straight line $u = u_0$ is a nonempty interval. It can be a singleton.

(2) The endpoints of the interval $K(u_0)$ for all $u = u_0$ define two continuous functions $\Phi_l(u)$ in $u \in (-\infty, a_l)$ and $\Phi_r(u)$ in $u \in (b_r, \infty)$; When $K(u_0)$ is a singleton, $\Phi_l(u)$ and $\Phi_r(u)$ coincide.

(3) The region $\Omega(W)_0 \in \Omega(W)$ defined by the points not belonging to either $\Phi_l(u)$ or $\Phi_r(u)$ is stratified into families of nonintersecting graphs of continuous functions. The left endpoint of all graphs belong to $\Phi_l(u)$; and the right endpoint of all graphs belong to $\Phi_r(u)$. The remaining points of the graphs belong neither to $\Phi_l(u)$ nor to $\Phi_r(u)$.

(4) If two points M and N belong to different graph families , then

$$[u_l(M) - u_l(N)][u_r(M) - u_r(N)] > 0.$$

This definition is very general and can cover various forms of hysteresis loops whereas some modifications are needed to give minor loops. A simple example is a play operator.

Banks, Kurdila and Webb [3, 4] developed a model using generalized play operators, called Krasnosel'skii-Pokrovskii (KP) operators. The model represents hysteresis as the cumulative effect of weighted KP operators distributed over a domain in $\Re^2$. Galinaitis investigated the KP model focusing on the properties of inverse and approximation [17].

The Preisach model: The most popular hysteresis model is certainly the Preisach's model. This model can be considered as a superposition of elementary hysteretic "relay" operators

$$W(t) = \int_0^{+\infty} \int_{-\infty}^{+\infty} \mu(\alpha, \beta) \gamma_{\alpha,\beta}[v](t) d\alpha d\beta, \tag{2.10}$$

where $\gamma_{\alpha,\beta}[v](t)$ is a relay hysteresis defined as

$$\gamma_{\alpha,\beta}[v](t) = \begin{cases} +1 & \text{if } v(t) > \alpha, \\ -1 & \text{if } v(t) < \beta, \\ \text{remains unchanged} & \text{if } \beta < v(t) < \alpha. \end{cases} \tag{2.11}$$

An extensive review on the Preisach model, its modified forms, and model identification methods can be found in monographs [10, 45] and papers [51, 67]. There are many experimental setups to show that this model can describe the hysteresis behavior in smart material-based actuators and sensors, such as magnetostrictive [58], piezoceramic in a stacked form [26], and shape memory alloy [23] actuators.

The Prandtl-Ishlinskii model There are other types of basic hysteresis operators such as "play" and "stop" operators. The models set up by composition of play or stop type operators are referred to as Prandtl-Ishlinskii models. Suppose $E_r[v]$ are basic elastic-plastic elements or stop operators for all $r \in [0, R]$, then the model can be expressed as

$$w(t) = \int_0^R p(r) E_r[v](t) dr, \tag{2.12}$$

where $p(r)$ is a given density function. Although the model itself was introduced much earlier [50, 31], the reader may refer to [10, 37, 38] for recent development. Kuhnen and Janocha [39] give a modified Prandtl-Ishlinskii model. Instead of using all stop or play operators, they combined the one-sided dead-zone operators and the play operators to formulate hysteresis loops. They demonstrated that the modified Prandtl-Ishlinskii model is applicable to a broad class of hysteretic actuator nonlinearities.

Hysteresis models based on hysteron are phenomenological. They have been intensively and extensively studied and proved to be effective in capturing important properties of hysteresis phenomena. In this research, the Prandtl-Ishlinskii model is used to define the hysteretic behavior appeared in the system. The detailed discussion about this model will be given in Chapter 3.

2.3. Control Methods for Systems with Hysteresis Nonlinearity

In the literature, control schemes for systems with unknown hysteresis have been developed. The most common approach to mitigate the effects of hysteresis is to construct an inverse operator, which was pioneered by Tao and Kokotovic [59]. For

hysteresis with major and minor loops, they used a simplified linear parameterized model to develop an adaptive hysteresis inverse model with parameters updated on line by adaptive laws. Model-based compensation of hysteresis has been addressed in many research papers. The main issue is how to find the inverse of the hysteresis.

Compensation of hysteresis effects in smart material actuation systems using Preisach model-based control architectures has been studied by many researchers. Ge and Jouaneh [18] proposed a static approach to reduce the hysteresis effects in tracking control of a piezoceramic actuator for desired sinusoidal trajectory. The relationship between input and output of the actuator was first initialized by a linear approximation model of a specific hysteresis. The Preisach model of the hysteresis was then used to redefine the corresponding input signals for the desired output of the actuator displacements. PID feedback controller was used to adjust the tracking errors. The developed method worked for both specific trajectories and required resetting for different inputs. Galinaitis [17] analytically investigated the inverse properties of the Preisach model and proved that a Preisach operator can only be locally invertible. He presented a closed form inverse formula when the weight function of the Preisach model was taking a specific form. Mittal and Meng [46] developed a method of hysteresis compensation in electromagnetic actuator through inversion of numerically expressed Preisach model in terms of first-order reversal curves and the input history. Croft, Shed and Devasia [14] used a different approach. Instead of modelling the forward hysteresis in piezoceramic actuators and then finding the inverse, they directly formulated the inverse hysteresis effect using Preisach model. Also in [8], an inverse Preisach model was proposed with magnetic flux density and its rate as inputs, and the magnetic fields as the output.

Methods based on the inverse of KP model can be found in [17, 64]. Galinaitis mathematically investigated the properties and the discrete approximation method

of the KP operators [17]. Webb defined a parameterized discrete inverse KP model, combined with adaptive laws to adjust the parameters on-line to compensate hysteresis effects [64]. Recently, a feed-forward control design based on the inverse of Prandtl-Ishlinskii model was also applied to reduce hysteresis effects in piezoelectric actuators [38].

In addition to the above mentioned model-based inverse methods, neural networks and fuzzy system models were also developed. It is well known that the universal approximation property is one of the most important properties of neural networks and fuzzy systems. However, this property is generally proven for continuous and one-to-one functions. Wei and Sun [65] studied the rate-independent memory property. After conducting analysis on multi-layer feed-forward, recurrent and reinforcement learning networks, they found that networks with only computational nodes and links cannot function as hysteresis simulators. They proposed a propulsive neural unit to construct hysteretic memory. Several propulsive neural units with distinct sensible ranges were used to form a model. The neural network can be trained to follow the loops given by the Preisach model. Selmic [54] gave a neural network structure to approximate piecewise continuous functions appearing in friction, or functions with jumps. Hwang [29, 28] developed a neuro-adaptive control method for unknown piezoelectric actuator systems. The proposed neural network included two different nonlinear gains according to the change rate of a input signal and a linear dynamic system, to learn the dynamics of the piezoelectric actuators. A forward control based on the inverse of learned model was used to achieve an acceptable tracking result. Because the tracking performance by a control could not be guaranteed as the system was subject to uncertainties, a discrete-time variable-structure control was synthesized to improve the performance. Readers can refer to [47, 42] for further details.

Essentially, the inversion methods treat hysteresis and structure response functions separately. That is, the inverse models are used in the forward loop to cancel hysteresis behavior. Then a feedback controller is designed to compensate the structural dynamic effects. However, the hysteresis operator is usually a part of a system. It is difficult to decouple the effects from the hysteresis and the structural dynamics from experimental measurements. As a result, the input is determined by the interaction of the operator with the rest of the system. Since the input is not predictable beforehand, it is impossible to specify ahead of time the branches of hysteresis nonlinearity which will be followed in a particular regime of the system. Due to the complexity of the hysteresis characteristics, especially the multi-value and non-smoothness properties, it is quite a challenge to find the inverse hysteresis models. Thus, inversion methods usually using approximated inverse models are complicated, computationally costly and strongly sensitive to the model parameters to unknown measurement errors. These issues are also directly linked to the difficulty of stability analysis of the systems except for certain special cases [59]. It would be better to develop an approach that can consider both effects simultaneously [61].

Passivity-based stability and control of hysteresis in smart actuators were attempted by Pare and Gorbet [48, 23]. In [23], energy properties of the Preisach hysteresis model were investigated, and passivity was demonstrated for the relationship between the input and the derivative of the output. The result only leads to stability of rate control of hysteresis systems.

The differential models of hysteresis were used for control purposes [6, 16, 20, 52, 57]. The Bouc-Wen model was applied to develop a semi-active structural control model for a magnetorheological damper attached to a three-story scaled building, see

[52]. Su used Duhem form model investigated by Coleman and Hodgdon. He combined the solution properties of the model with adaptive control techniques and developed a robust adaptive control algorithm. This method integrates the hysteresis compensation and control techniques without constructing an inverse of hysteresis. Research presented in this thesis follows this direction. The dynamic characteristic of this type of models can be implemented in state-space. The main challenge is resulted from high nonlinearity and the lack of knowledge about mathematical properties of the differential models when they are applied to system control.

Chapter 3

The Prandtl-Ishlinskii Hysteresis Models

3.1. Hysteresis Operators

Some basic well-known hysteresis operators are first listed below. A detailed discussion on this subject can be found in monographs [10, 37, 63].

3.1.1 The Stop Operator

One of the basic elements of the theory of hysteresis operators came from the continuum mechanics for elastic-perfectly plastic constitutive laws as illustrated in Fig.3.1. As shown in Fig.3.1, as long as the applied stress w is smaller than the yield stress r of the material, strain v is related to w through the linear Hooke's law. As soon as w reaches the yield stress, the stress w will remain constant with further increase of the strain. However, the elastic behavior is instantly recovered when the strain is lowered again. This input-output relationship can be expressed by an elastic-plastic, or **stop**, operator, $w(t) = E_r[v](t)$, with threshold r.

Analytically, suppose $C_m[0, t_E]$ is the space of piece-wise monotone continuous functions, for any input $v(t) \in C_m[0, t_E]$, the stop operator $w = E_r[v](t)$, for any $r \geq 0$, can be given by the inductive definition

$$\begin{aligned} &E_r[v](0) = e_r(v(0)), \\ &E_r[v](t) = e_r(v(t) - v(t_i) + E_r[v](t_i)), \quad \text{for } t_i < t \leq t_{i+1} \text{ and } 0 \leq i \leq N-1, \end{aligned} \tag{3.1}$$

with

$$e_r(z) = \min(r, \max(-r, z)). \tag{3.2}$$

where $0 = t_0 < t_1 < \cdots < t_N = t_E$ is a partition of $[0, t_E]$ such that the function v is monotone on each of the sub-intervals $[t_i, t_{i+1}]$. The argument of the operator is written in square brackets to indicate the functional dependence, since it maps a function to a function. The stop operator however is mainly characterized by its threshold parameter r which determines the height of the hysteresis region in the (w, v) plane.

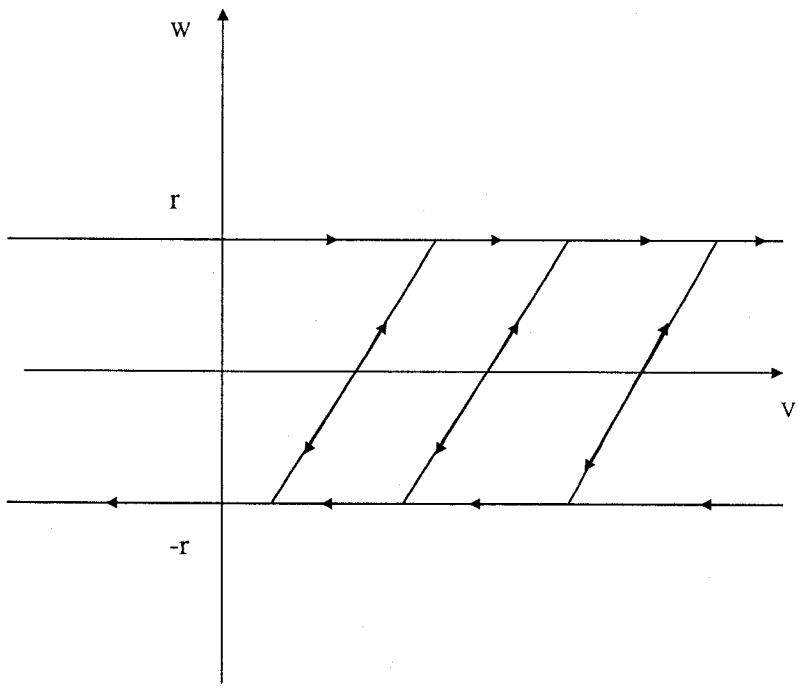

Figure 3.1: Stress-strain behavior in a one-dimensional elastic-plastic element

3.1.2 The Play Operator

Another basic hysteresis nonlinearity operator is the **play** operator. The one-dimensional play operator can be considered as a free-to-move cylinder of length $2r$ and a moving piston. The output $w(t)$ is the position of the center of the cylinder, and the input is the piston position $v(t)$. The input-output behavior can be given by the hysteresis diagram shown in Fig.3.2.

For a given input $v(t) \in C_m[0, t_E]$, the play operator $w = F_r[v](t)$ with threshold r is then inductively defined by

$$\begin{aligned} &F_r[v](0) = f_r(v(0), 0), \\ &F_r[v](t) = f_r(v(t), F_r[v](t_i)), \quad \text{for } t_i < t \leq t_{i+1} \text{ and } 0 \leq i \leq N-1, \end{aligned} \tag{3.3}$$

with

$$f_r(v, w) = \max(v - r, \min(v + r, w)). \tag{3.4}$$

where $0 = t_0 < t_1 < \cdots < t_N = t_E$ is a partition of $[0, t_E]$, such that the function v is monotone on each of the sub-intervals $[t_i, t_{i+1}]$.

From the definitions given in (3.1) and (3.3), it can be proved [10] that the operator F_r is the complement of E_r, i.e., they are closely related through the equation

$$E_r[v](t) + F_r[v](t) = v(t), \tag{3.5}$$

for any piece-wise monotone input function $v \in C_m[0, t_E]$ and $r \geq 0$.

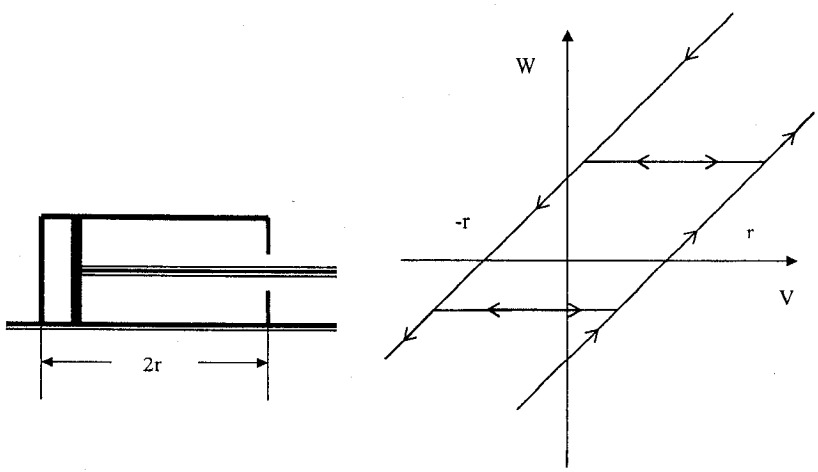

Figure 3.2: A piston with plunger of length 2r (left), and the rules of motion

3.1.3 Properties of the Play Operator

Listed below are some basic properties of the play operator. In the study of the Prandtl-Ishlinskii model in the following sections, the play operator will serve as an building element. Since the stop operator E_r is complement to F_r, the discussion will mainly focus on the play operator. Further details on the relationship of these two operators can be found in [10].

General Initial condition: In the definition of the play operator in (3.3), it is assumed that, before $v(0)$ was applied to the system at time $t = 0$, the internal state was 0 . In more general cases, the definition can be extended to the following: Let Ψ denote the set of functions $\psi : \Re_+ \mapsto \Re$, satisfying

$$|\psi(r_1) - \psi(r_2)| \leq |r_1 - r_2| \quad for\ all\ r_1, r_2 \geq 0, \tag{3.6}$$

and

$$\Re_{supp}(\psi) = sup\{r | r \geq 0, \psi(r) \neq 0\} < +\infty. \tag{3.7}$$

The play operator $F_r : C_m[0, t_E] \times \Psi \mapsto C_m[0, t_E]$, for $r \geq 0$, can then be inductively defined by

$$\begin{aligned} &F_r[v; \psi](0) = f_r(v(0); \psi), \\ &F_r[v; \psi](t) = f_r(v(t), F_r[v; \psi](t_i)), \quad \text{for } t_i < t \leq t_{i+1} \text{ and } 0 \leq i \leq N-1, \end{aligned} \tag{3.8}$$

where f_r is the same function as the one defined in (3.4).

From the recursive equation (3.4), it is easy to determine that $F_r[v; \psi](t) \in \Psi$ for all $v \in C_m[0, t_E]$. Thus, Ψ was called the set of memory curves in [10]. This definition is consistent with the previous definition for $\psi = 0$. In the sequel, $F_r[v]$ will be simply written as $F_r[v; \psi]$ so long as doing so does not affect the proof.

Due to the natural characteristics of the play and stop operators, above discussions are for continuous and piecewise monotone functions defined on the space

$C_m[0, t_E]$. However, they can also be extended to continuous functions in $C[0, t_E]$ space and satisfy the following theorem.

Theorem: Lipschitz Continuity on $C[0, t_E]$ For any $r \geq 0$, the operator F_r can be extended uniquely to a Lipschitz continuous operator $F_r : C[0, t_E] \times \Re \rightarrow C[0, t_E]$. In addition, it holds, for all $v_1, v_2 \in C[0, t_E]$, for all initial values $\psi_1, \psi_2 \in \Re$, and for all $0 \leq t' < t < t_E$,

$$|F_r[v_1; \psi_1](t) - F_r[v_2; \psi_2](t)| \leq max \sup_{0 \leq \tau \leq t} |v_1(\tau) - v_2(\tau)|, |\psi_1 - \psi_2| \quad (3.9)$$

$$|F_r[v_1; \psi_1](t) - F_r[v_1; \psi_1](t')| \leq \sup_{t' \leq \tau \leq t} |v_1(\tau) - v_1(t')| \quad (3.10)$$

$$F_r[v_1; \psi_1](t) \leq F_r[v_2; \psi_2](t), \quad if \;\; v_1 \leq v_2 \;\; and \;\; \psi_1 \leq \psi_2 \quad (3.11)$$

Proof: see [10] Section 2.3.

Bound of the Play Operator: From the above theorem, it is notice that the bound of the play operator is related to its initial condition and the maximum difference of the input function on the time interval. Especially, in (3.9), if let $v_2(t) \equiv 0$, and $\psi_2 = 0$, then $F_r[v_2; \psi_2](t) \equiv 0$, we have

$$|F_r[v_1; \psi_1](t)| \leq max \sup_{0 \leq \tau \leq t} |v_1(\tau)|, |\psi_1| \quad (3.12)$$

3.2. The Prandtl-Ishlinskii Model

3.2.1 Definition

With the introductory discussion in the previous section, it is ready to introduce the Prandtl-Ishlinskii model defined by the stop or play hysteresis operators. The Prandtl-Ishlinskii model was originally developed to describe elastic-plastic behavior through a weighted superposition of basic elastic-plastic elements $E_r[v]$, or **stop**, as following:

$$w(t) = \int_0^R p(r) E_r[v](t) dr, \tag{3.13}$$

where $p(r)$ is a given density function, satisfying $p(r) \geq 0$ with $\int^{\infty} rp(r)dr < \infty$. $p(r)$ can be identified from experimental data. With the defined density function, this operator maps $C[t_0, \infty)$ into $C[t_0, \infty)$, i.e., the Lipschitz continuous input will lead to the Lipschitz continuous output [37]. Since the density function $p(r)$ vanishes for large values of r, the choice of $R = \infty$ as the upper limit of the integration is specified mainly for the sake of convenience as discussed in [10].

Since the operator F_r is the complement of E_r, the Prandtl-Ishlinskii model can also be expressed through the play operator. Using Equation (3.5) and substituting E_r in (3.13) by F_r, the Prandtl-Ishlinskii model defined by the play hysteresis operator is expressed as follows:

$$w(t) = p_0 v(t) - \int_0^R p(r) F_r[v](t) dr, \tag{3.14}$$

where $p_0 = \int_0^R p(r)dr$ is a constant which depends on the density function. It should be noted that Equation (3.14) decomposes the hysteresis behavior into two terms. The first term describes the linear reversible part and the second term describes the nonlinear hysteretic part. This decomposition is crucial for the research as it

facilitates the utilization of the currently available robust adaptive control techniques for the controller design.

As an illustration, Fig.1.1 shows the function $w(t)$ generated by the model given in (3.14), with $p(r) = e^{-0.067(r-1)^2}$, $r \in [0, 10]$, and input $v(t) = 7sin(3t)/(1+t)$, $t \in [0, 2\pi]$ with $\psi = 0$. This numerical result shows that the Prandtl-Ishlinskii model (3.14) indeed generates the hysteresis curves.

3.2.2 Properties of the Prandtl-Ishlinskii Model

The Prandtl-Ishlinskii hysteresis operator has some important properties. List below are some fundamental characteristics which will be helpful to understand the results of this research.

Memory Effects: The hysteresis operators are nonlinearities with memory. In general, they fall into two categories: hysteresis nonlinearities with local memories and hysteresis nonlinearities with nonlocal memories. For hysteresis nonlinearities with local memories the past exerts its influence upon the future through the current value of output. While for hysteresis nonlinearities with nonlocal memories, future values of output depend not only on the current value of output but on past extremum values of input as well [45]. The play and the stop operators are examples of hysteresis nonlinearities with local memories. The Preisach and the Prandtl-Ishlinskii hysteresis operators are hysteresis nonlinearities with nonlocal memories. In this study, we solely concern with hysteresis nonlinearities with nonlocal memories.

At any time instant $t \geq 0$, for a given input function $v(t) \in C_m[0, t_E]$, $F_r[v](t)$ is a function of r. For $r \geq 0$, it forms a curve in the (r, F_r) plane. Fig.3.3 to Fig.3.5 illustrates that this curve depends not only on the current input, but also on the past history of some local extreme values of the input function. The form of the curves is independent of the speed at which they are traversed, and satisfies the wiping out property. A geometrical interpretation of this discussion is given below.

For example, we consider an input function $v(t)$, with $v(t_0) = 0$, which has the following local extreme values: $v(t_1) = 4$, $v(t_2) = -2$, $v(t_3) = 5$. $v(t)$ is monotonicity for $t \in (t_i, t_{i+1})$, $i = 0, 1, 2$. At $t = t_0 = 0$, we have $F_r[v](0) \equiv 0$, $\forall r \geq 0$. As the

input function v increases, by definition,

$$F_r[v](t) = f_r(v(t), 0) = max(v(t) - r, 0),$$

for $t \in (0, t_1)$, until $v(t)$ reaches its local maximum $v(t_1) = 4$. At $t = t_1$, $F_r[v](t_1)$ is the line segments ABC shown in Fig.3.3. Then, v decreases with respect to $t \in (t_1, t_2)$, and

$$F_r[v](t) = f_r(v(t), F_r[v](t_1)) = min(v(t) + r, F_r[v](t_1)).$$

When $v(t)$ reaches its local minimum $v(t_2) = -2$, $F_r[v](t_2)$ is the line segments $DEBC$, see Fig.3.4. If $v(t)$ then reverses to reach maximum value $v(t_3) = 5$, $F_r[v](t_3)$ is formed by the line segments $A'B'C$, shown in Fig.3.5. Thus, it can be seen that the memory behavior at time t is completely described by the curve $F_r[v](t)$.

Rate Independency: The form of the hysteresis diagrams is independent of the speed with which they were traversed. Notice that, in Fig.3.3 to Fig.3.5, the speed at which the input function $v(t)$ moves is only reflected in the speed of the output; how fast $v(t)$ reaches monotonically from one extreme value $v(t_i)$, for $i = 0, 1, 2$, to other alternating extreme value $v(t_{i+1})$ will not affect the form of the curve $F_r[v](t_{i+1})$ in the (F_r, r) plane. Since the Prandtl-Ishlinskii model is completely defined by the integration of $F_r[v](t)$ curve on $[0, R]$ for any input $v(t)$, the Prandtl-Ishlinskii model is rate independent. For input functions v_1 and v_2 in different time frames, they reach the same successive extreme values accordingly, see Fig.3.6. These inputs result in the same (F_r, r) diagram of hysteresis as shown in Fig.3.7.

Wiping-out Property: In Fig.3.3 to Fig.3.5, we see that the memories impressed by the previous smaller local extreme values have been deleted by a larger local extreme value. That is, the previous records of $F_r[v](t_1)$ and $F_r[v](t_2)$ have

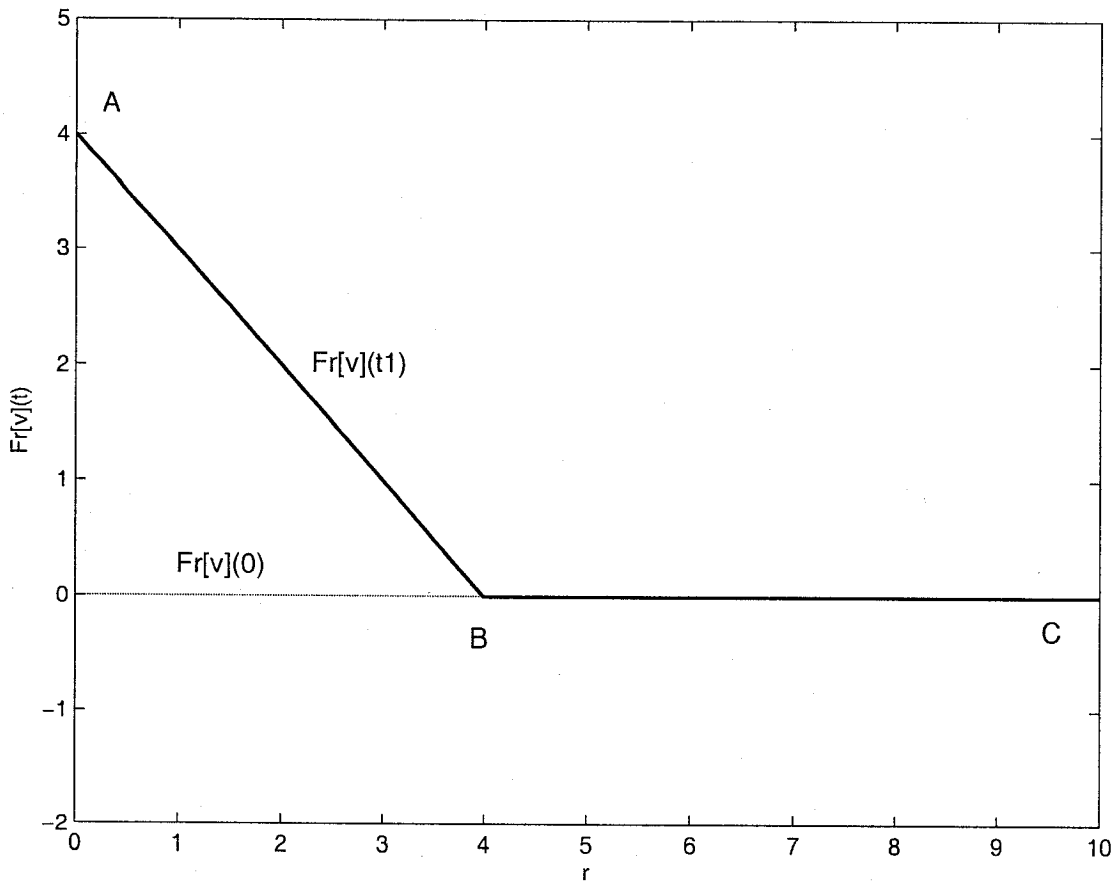

Figure 3.3: Geometrical interpretation of $F_r[v](t)$ in $(r, F_r[v](t))$ plane: $F_r[v](t_1)$

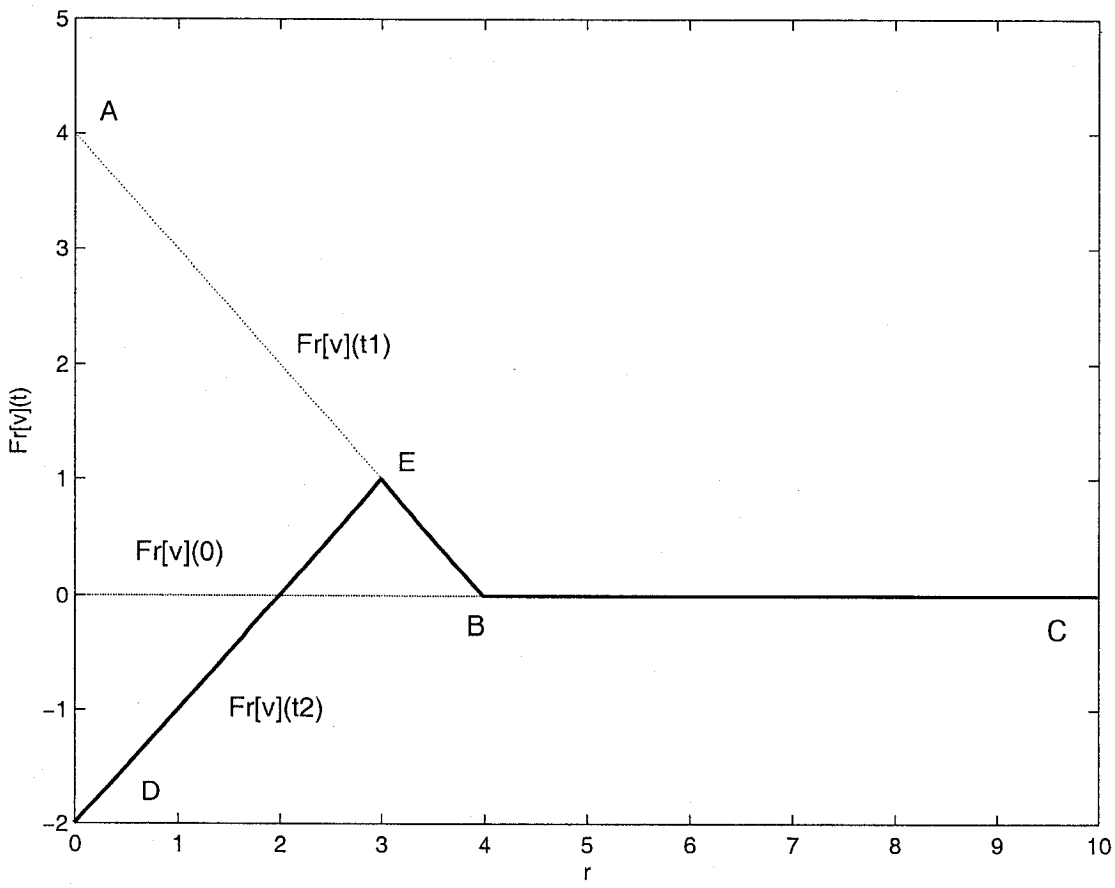

Figure 3.4: Geometrical interpretation of $F_r[v](t)$ in $(r, F_r[v](t))$ plane: $F_r[v](t_2)$

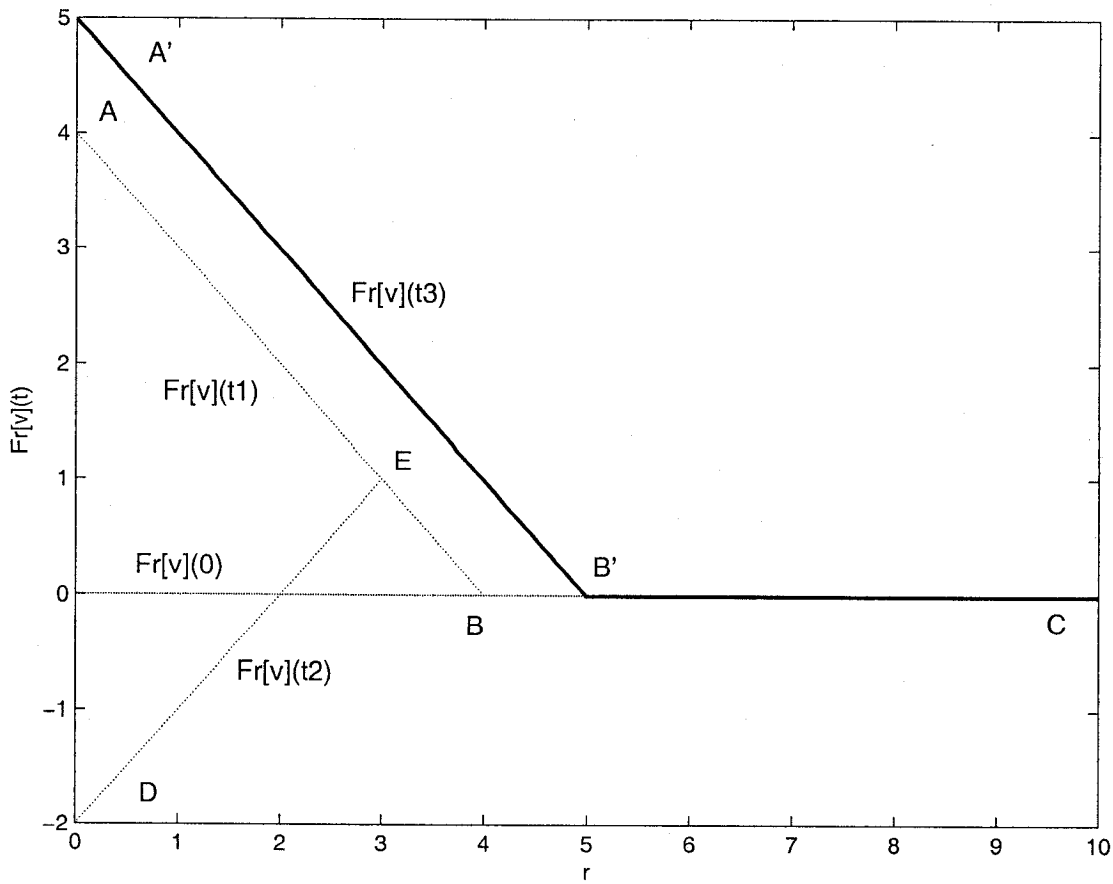

Figure 3.5: Geometrical interpretation of $F_r[v](t)$ in $(r, F_r[v](t))$ plane: $F_r[v](t_3)$

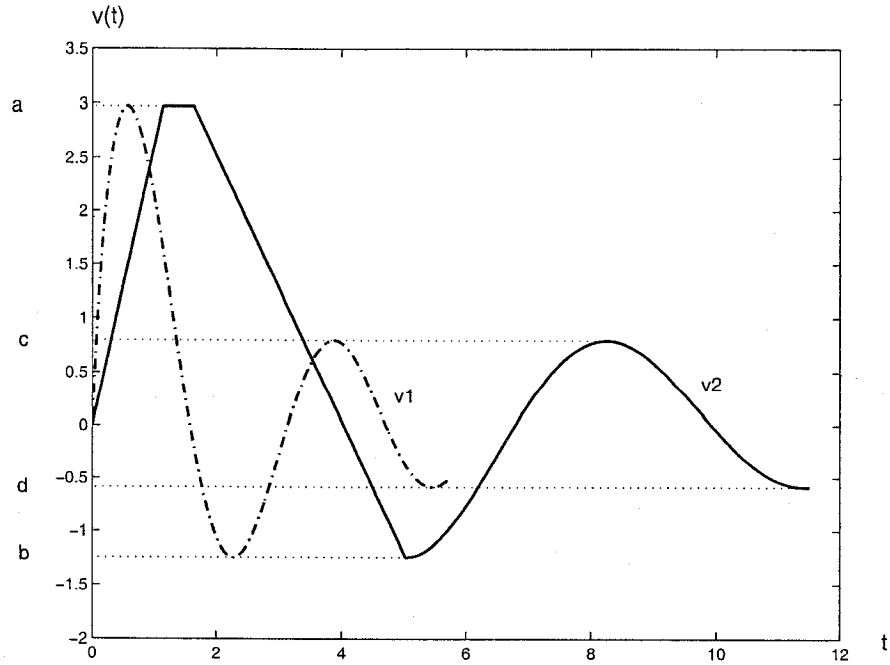

Figure 3.6: Rate independent: The input functions $v_1(t)$ and $v_2(t)$ reach the same successive extreme values in different velocities.

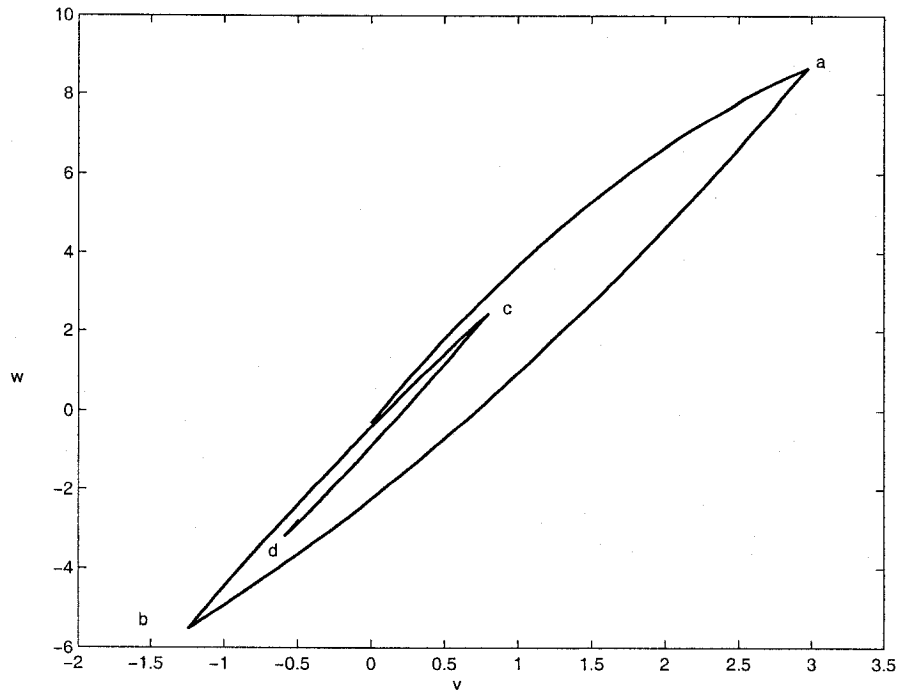

Figure 3.7: Rate independent: The same hysteresis diagram generated by the input functions $v_1(t)$ and $v_2(t)$.

been wiped out. This property is defined by Mayergoyz [45] as wiping-out property: Only the alternating series of the dominant input extrema are stored by the hysteresis model. All other input extrema are wiped out. In [10] section 2.7, it is defined as deletion rule and proves that the Prandtl-Ishlinskii model satisfies this property.

The Prandtl-Ishlinskii model also possesses some very unique properties such that it is invertible and the inverse has the same structure. A detailed discussion on this subject can be found in the monograph [10]. We will now prove an important property of the Prandtl-Ishlinskii model which will be useful in the sequel.

Lemma: Let $w(t)$ be a hysteresis defined by the Prandtl-Ishlinskii model (3.13)

$$w(t) = \int_0^R p(r)E_r[v](t)dr, \tag{3.15}$$

where $p(r)$ is a density function, satisfying $p(r) \geq 0$ with $\int^\infty rp(r)dr < \infty$. Then, for any $v(t) \in C[t_0, \infty)$, there exists a constant $K \geq 0$, s.t.

$$|w(t)| \leq K < \infty. \tag{3.16}$$

Proof: Let $r > 0$ be given. From the definition of E_r operator, we have

$$|E_r[v](t)| \leq r, \quad \textit{for all } v(t) \in C[t_0, \infty), \tag{3.17}$$

$$\begin{aligned} |w(t)| &= |\int_0^R p(r)E_r[v](t)dr| \\ &\leq \int_0^R |p(r)E_r[v](t)|dr \\ &\leq \int_0^R p(r)rdr, \end{aligned} \tag{3.18}$$

and from the definition of $p(r)$, one can conclude that $K = \int_0^R p(r)rdr < \infty$.

$\triangle\triangle\triangle$

3.3. Experimental Determination of the Density Function

It is clear that the Prandtl-Ishlinskii model is defined by its density function $p(r)$. Determination of the density function is crucial for practical applications of the Prandtl-Ishlinskii model. In this study, a discretional approach to approximate $p(r)$ is developed. Based on the memory effects of the play operator $F_r[v](t)$, especially the wiping-out property, and by devising the input in a certain sequence, $p(r)$ can be derived directly from the output measurements.

We consider that the system input v is a continuous bounded function contained in the interval $[-R, R]$. The memory set Ψ_0 is defined by

$$\begin{aligned} \Psi_0 &= \{\psi |\ \psi : [0, R] \mapsto \Re,\ |\psi(r)| \leq R, \\ &\quad |\psi(r) - \psi(r')| \leq |r - r'|,\ \ \forall\, r, r' \in [0, R]\} \end{aligned} \tag{3.19}$$

where r is on the interval $[0, R]$. The identification scheme is based on the measurements of the hysteresis outputs.

Step 0: Initial condition normalization

For arbitrary initial conditions $v_0 \in [-R, R]$ and internal state $\psi_1 \in \Psi_0$, if the input $v(t)$ monotonically increases to the positive saturate value $v(t_{01}) = +R$, by definition,

$$\begin{aligned} F_r[v; \psi_1](t_{01}) &= max\{R - r, min\{R + r, \psi_1\}\} \\ &= max\{R - r, \psi_1\} \\ &= \begin{cases} R - r & \text{if } R - r \geq \psi_1 \\ \psi_1, & \text{if } R - r < \psi_1 \end{cases} \qquad \forall r \in [0, R] \end{aligned} \tag{3.20}$$

If $v_0 \leq \psi_1$, for $t \leq t_0$ and $v_t \leq \psi_1$, $F_r[v; \psi_1](t)$ is formed by line $R + r$ from a to b and ψ_1 from b to c, shown in Fig.3.8. When $v_t \geq \psi_1$ and reaches $v(t_{01}) = R$,

$F_r[v;\psi_1](t_{01})$ erased the portion of the initial condition which is under the line of $R-r$. In addition, $F_r[v;\psi_1](t_{01})$ is formed by the line $R-r$ from $a1$ to $b1$ and the segment of the initial condition ψ_1 from $b1$ to c which has not been erased, Fig.3.9.

Then let the input decrease to the negative saturate value $v(t_{02}) = -R$, by definition,

$$\begin{aligned} F_r[v;\psi_1](t_{02}) &= max\{-R-r, min\{-R+r, F_r[v;\psi_1](t_{01})\}\} \\ &= \begin{cases} max\{-R-r, min\{-R+r, R-r\}\} & \text{if } R-r \geq \psi_1 \\ max\{-R-r, min\{-R+r, \psi_1\}\}, & \text{if } R-r < \psi_1 \end{cases} \\ &= max\{-R-r, -R+r\} \\ &= -R+r \quad \forall r \in [0,R] \end{aligned} \tag{3.21}$$

As we see in Fig.3.10, when $v(t)$ decreases, $F_r[v;\psi_1](t)$ erases every lines above the line $v(t)+r$ at that instant of time t. Using the above procedures, the initial state set by any initial input v_0 and internal state ψ_1 is erased. Therefore, it can be assumed that the identification procedures always start from a well defined initial state :

$$\begin{aligned} v_0 &= -R \ ; \\ F_r[v_0;\psi_1](t_0) &= -R+r \qquad \forall r \in [0,R] \end{aligned} \tag{3.22}$$

line from $(0,-R)$ to $(R,0)$ shown in boldface in Fig.3.11.

For the hysteresis definition interval $[0,R]$, let N be a positive integer, define

$$\triangle = R/N \tag{3.23}$$

Step 1: Define

$$r_{11} = R - \frac{1}{2}\triangle \tag{3.24}$$

$$r_{12} = R - i\triangle \tag{3.25}$$

and let the input function v monotonically increases from $v(t_0) = -R$ to the point $v(t_{11}) = R - \triangle$ at $t = t_{11}$:

$$\begin{aligned} F_r[v;\psi_1](t_{11}) &= max\{R-\triangle-r, min\{R-\triangle+r, F_r[v_0;\psi_1](t_{11})\}\} \\ &= max\{R-\triangle-r, -R+r\} \\ &= \begin{cases} R-\triangle-r & \text{if } 0 \le r \le r_{11} \\ -R+r, & \text{if } r_{11} < r \le R \end{cases} \end{aligned} \tag{3.26}$$

In Fig. 3.12, we can see that for all $r \le r_{11}$, $F_r[v_0;\psi_1](t_0)$ is erased by $F_r[v_{11};\psi_1](t_{11})$. The new memory curve $F_r[v_{11};\psi_1](t_{11})$ is shown in boldface in the figure. The hysteresis output w_{11} at time t_{11} is determined by

$$\begin{aligned} w_{11} &= p_0 v(t_{11}) - \int_0^R p(r)F_r[v](t_{11})dr \\ &= p_0(R-\triangle) - \int_0^R p(r)F_r[v](t_{11})dr \\ &= p_0(R-\triangle) - \int_0^{r_{11}} p(r)(R-\triangle-r)dr \\ &\quad - \int_{r_{11}}^R p(r)(-R+r)dr \end{aligned} \tag{3.27}$$

We now reverse the input and let $v(t)$ monotonically decrease from $v(t_{11}) = R - \triangle$ to $v(t_{12}) = -R + \triangle$ at $t = t_{12}$. By definition

$$\begin{aligned} F_r[v;\psi_1](t_{12}) &= max\{-R+\triangle-r, min\{-R+\triangle+r, F_r[v_{11};\psi_1]\}\} \\ &= \begin{cases} -R+\triangle+r & \text{if } 0 \le r \le r_{12} \\ F_r[v](t_{11}), & \text{if } r_{12} < r \le R \end{cases} \end{aligned} \tag{3.28}$$

where $r_{12} = R - \triangle$. Fig.3.13 shows that $F_r[v;\psi_1](t_{11})$ is erased by $F_r[v_{12};\psi_1](t_{12})$ for all $r \le r_{12}$. The hysteresis output w_{12} at time t_{12} is

$$\begin{aligned} w_{12} &= p_0 v(t_{12}) - \int_0^R p(r)F_r[v](t_{12})dr \\ &= p_0(-R+\triangle) - \int_0^{r_{12}} p(r)(-R+\triangle+r)dr \\ &\quad - \int_{r_{12}}^R p(r)F_r[v](t_{11})dr \end{aligned} \tag{3.29}$$

Noticing that in (3.27) the first term and the integrands in the second term on the interval $r \in [0, r_{12}]$ have opposite signs and compare the first and second terms in (3.29), if we add w_{11} and w_{12} together, we have

$$\begin{aligned} w_{11} + w_{22} &= p_0(R - \triangle) - \int_0^R p(r) F_r[v_{11}](t_{11}) dr \\ &\quad + p_0(-R + \triangle) - \int_0^{r_{12}} p(r)(-R + \triangle + r) dr \\ &\quad - \int_{r_{12}}^R p(r) F_r[v_{11}](t_{11}) dr \\ &= p_0(R - \triangle) - \int_0^{r_{12}} p(r)(R - \triangle - r) dr \\ &\quad - \int_{r_{12}}^R p(r) F_r[v_{11}](t_{11}) dr + p_0(-R + \triangle) \\ &\quad - \int_0^{r_{12}} p(r)(-R + \triangle + r) dr - \int_{r_{12}}^R p(r) F_r[v_{11}](t_{11}) dr \\ &= -2 \int_{r_{12}}^R p(r) F_r[v_{11}](t_{11}) dr \end{aligned} \tag{3.30}$$

Step i: For $i = 2, \ldots, n$, we define

$$r_{i1} = R - \frac{(2i-1)}{2} \triangle \tag{3.31}$$

$$r_{i2} = R - i\triangle, \quad i = 2, \ldots, N \tag{3.32}$$

Let the input function $v(t)$ monotonically increase from $v(t_{(i-1)2}) = -R + (i-1)\triangle$ to the point $v(t_{i1}) = R - i\triangle$ at $t = t_{i1}$, then decrease to the point $v(t_{i2}) = -R + i\triangle$ at $t = t_{i2}$:

$$\begin{aligned} F_r[v; \psi_1](t_{i1}) &= max\{R - i\triangle - r, min\{R - i\triangle + r, F_r[v](t_{(i-1)2})\}\} \\ &= max\{R - i\triangle - r, F_r[v](t_{(i-1)2})\} \\ &= \begin{cases} R - i\triangle - r & \text{if } 0 \le r \le r_{i1} \\ F_r[v](t_{(i-1)2}), & \text{if } r_{i1} < r \le R \end{cases} \end{aligned} \tag{3.33}$$

The hysteresis output w_{i1} at time t_{i1} is

$$w_{i1} = p_0 v(t_{i1}) - \int_0^R p(r) F_r[v](t_{i1}) dr$$

$$
\begin{aligned}
&= p_0(R - i\triangle) - \int_0^R p(r)F_r[v](t_{i1})dr \\
&= p_0(R - i\triangle) - \int_0^{r_{i1}} p(r)(R - i\triangle - r)dr \\
&\quad - \int_{r_{i1}}^R p(r)F_r[v](t_{(i-1)2})dr
\end{aligned} \tag{3.34}
$$

To reverse the input and let $v(t)$ monotonically decrease from $v(t_{i1}) = R - i\triangle$ to $v(t_{i2}) = -R + i\triangle$ at $t = t_{i2}$, by definition

$$
\begin{aligned}
F_r[v;\psi_1](t_{i2}) &= max\{-R + i\triangle - r, min\{-R + i\triangle + r, F_r[v](t_{i1})\}\} \\
&= \begin{cases} -R + i\triangle + r & \text{if } 0 \le r \le r_{i2} \\ F_r[v](t_{i1}), & \text{if } r_{i2} < r \le R \end{cases}
\end{aligned} \tag{3.35}
$$

where $r_{i2} = R - i\triangle$. The hysteresis output w_{i2} at time t_{i2} is

$$
\begin{aligned}
w_{i2} &= p_0 v(t_{i2}) - \int_0^R p(r)F_r[v](t_{i2})dr \\
&= p_0(-R + i\triangle) - \int_0^{r_{i2}} p(r)(-R + i\triangle + r)dr \\
&\quad - \int_{r_{i2}}^R p(r)F_r[v](t_{i1})dr \\
&= p_0(-R + i\triangle) - \int_0^{r_{i2}} p(r)(-R + i\triangle + r)dr \\
&\quad - \int_{r_{i2}}^{r_{i1}} p(r)F_r[v](t_{i1})dr - \int_{r_{r_{i1}}}^R p(r)F_r[v](t_{(i-1)2})dr
\end{aligned} \tag{3.36}
$$

Notice that the first two terms in (3.34) and (3.36) are in the opposite signs, add w_{i1} and w_{i2} together, we have

$$
\begin{aligned}
w_{i1} + w_{i2} &= -2\int_{r_{i2}}^R p(r)F_r[v](t_{i1})dr \\
&= -2\{\int_{r_{i2}}^{r_{(i-1)2}} p(r)F_r[v](t_{i1})dr + \sum_{k=1}^{i-1}\int_{r_{k2}}^{r_{(k-1)2}} p(r)F_r[v](t_{k1})dr\}
\end{aligned} \tag{3.37}
$$

for $i = 1, \ldots, n$.

If the number N is large enough, the intervals $[r_{i2}, r_{(i-1)2})$ will be small for $i = 1, \ldots, n$. It can be assumed that $p(r)$ are constants on each interval $[r_{i2}, r_{(i-1)2})$

and take $p(r_{i1}) \approx p(r)$ as an approximate value of the density function. Substituting $p(r)$ by $p(r_{i1})$ in the summation of (3.37) and based on the definition of (3.32), the integration of $F_r[v](t_{i1})$ on each interval $[r_{i2}, r_{(i-1)2}]$ equals

$$\begin{aligned}\int_{r_{i2}}^{r_{(i-1)2}} F_r[v](t_{i1})dr &= -\int_{r_{i2}}^{r_{i1}}(R - i\triangle - r)dr - \int_{r_{i1}}^{r_{(i-1)2}}(-R + (i-1)\triangle + r)dr \\ &= -\frac{\triangle^2}{4} \end{aligned} \tag{3.38}$$

we have

$$w_{i1} + w_{i2} = \frac{\triangle^2}{2}\{\sum_{k=1}^{i} p(r_{k1})\} \qquad i = 1, \ldots, n \tag{3.39}$$

We now can solve $p(r_{i1})$ from the above equations: for $i = 1$

$$p(r_{11}) = \frac{2}{\triangle^2}(w_{11} + w_{12}) \tag{3.40}$$

and for $i = 2, \ldots, n$

$$p(r_{i1}) = \frac{2}{\triangle^2}[(w_{i1} + w_{i2}) - (w_{(i-1)1} + w_{(i-1)2})] \tag{3.41}$$

Figs.3.8 - 3.14 present such identification process for $[0, R] = [0, 10]$ and $N = 10$.

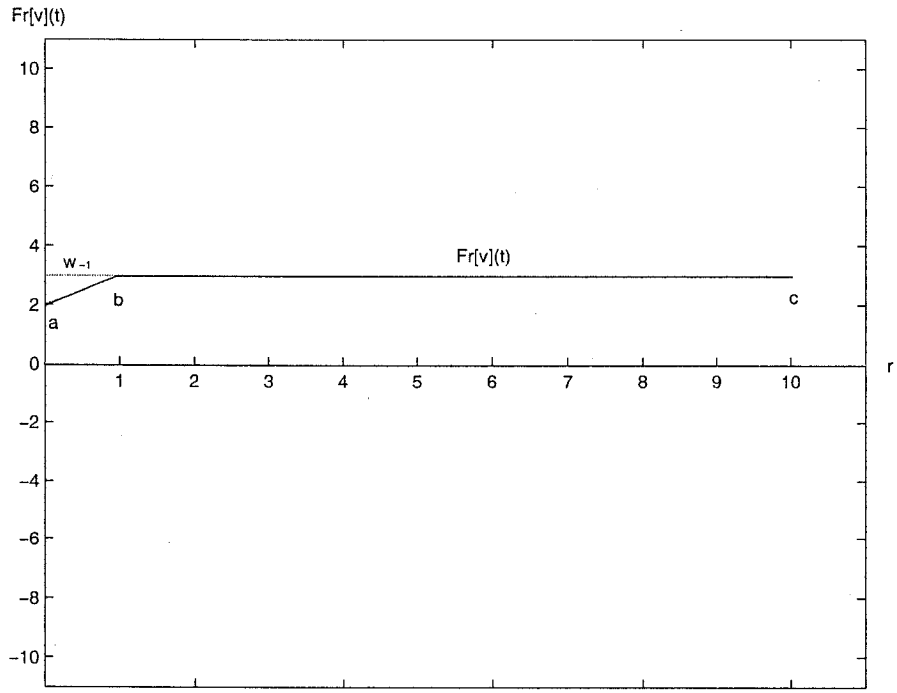

Figure 3.8: $p(r)$ identification-1

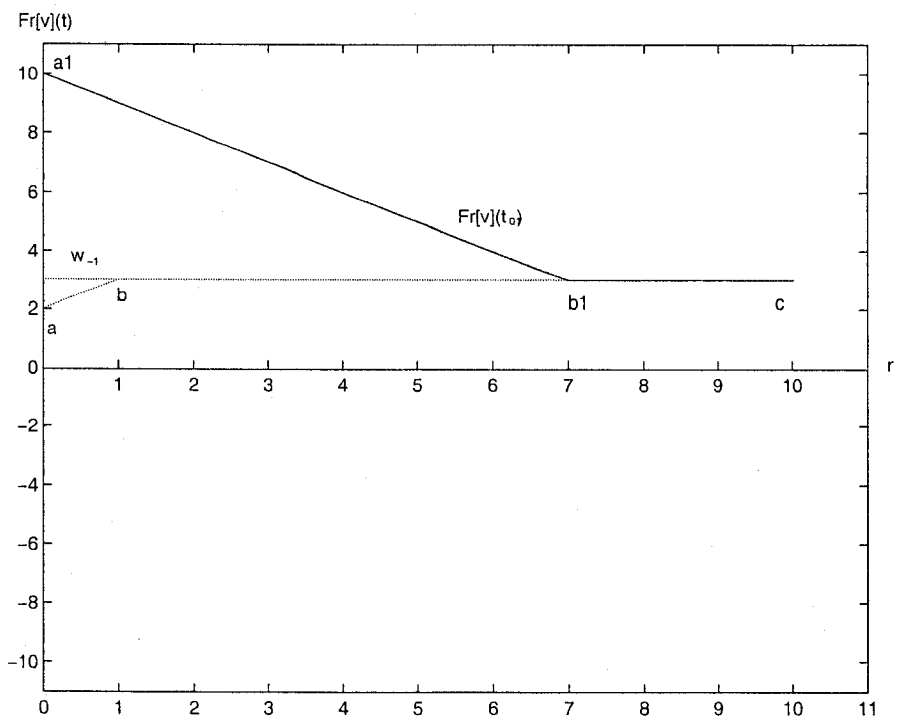

Figure 3.9: $p(r)$ identification-2

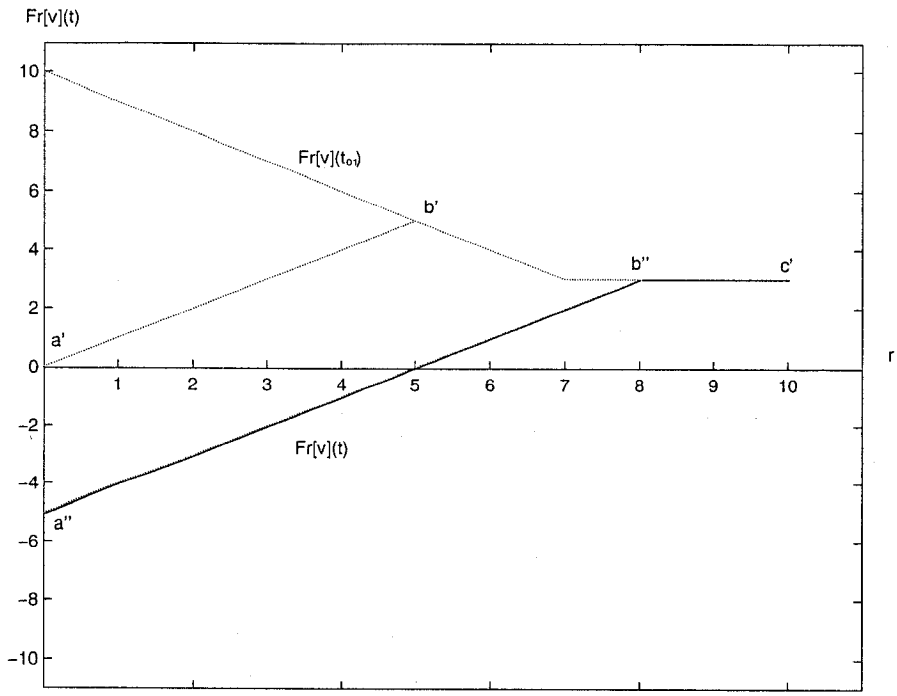

Figure 3.10: $p(r)$ identification-3

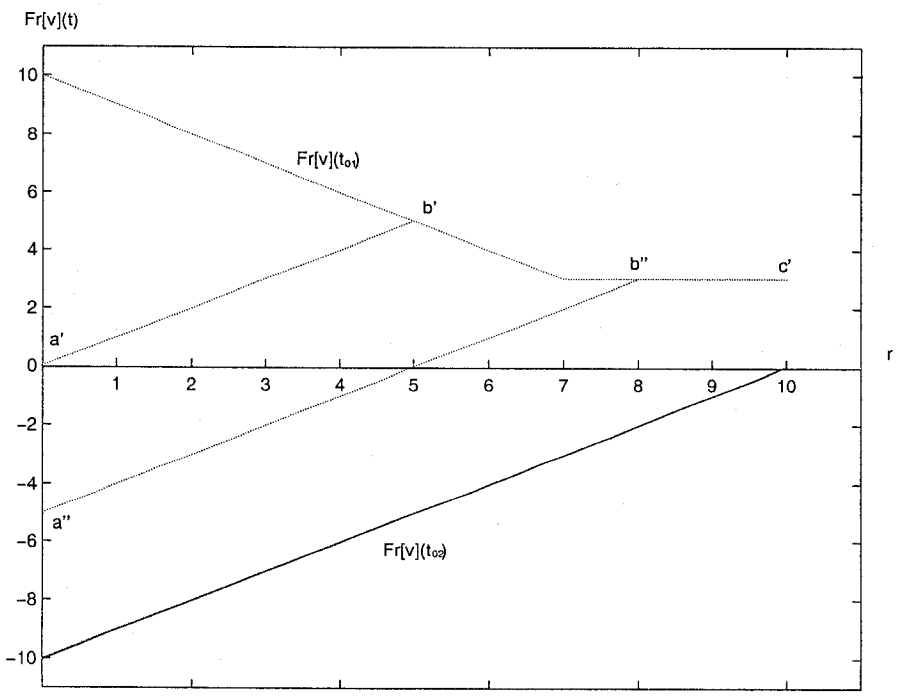

Figure 3.11: $p(r)$ identification-4

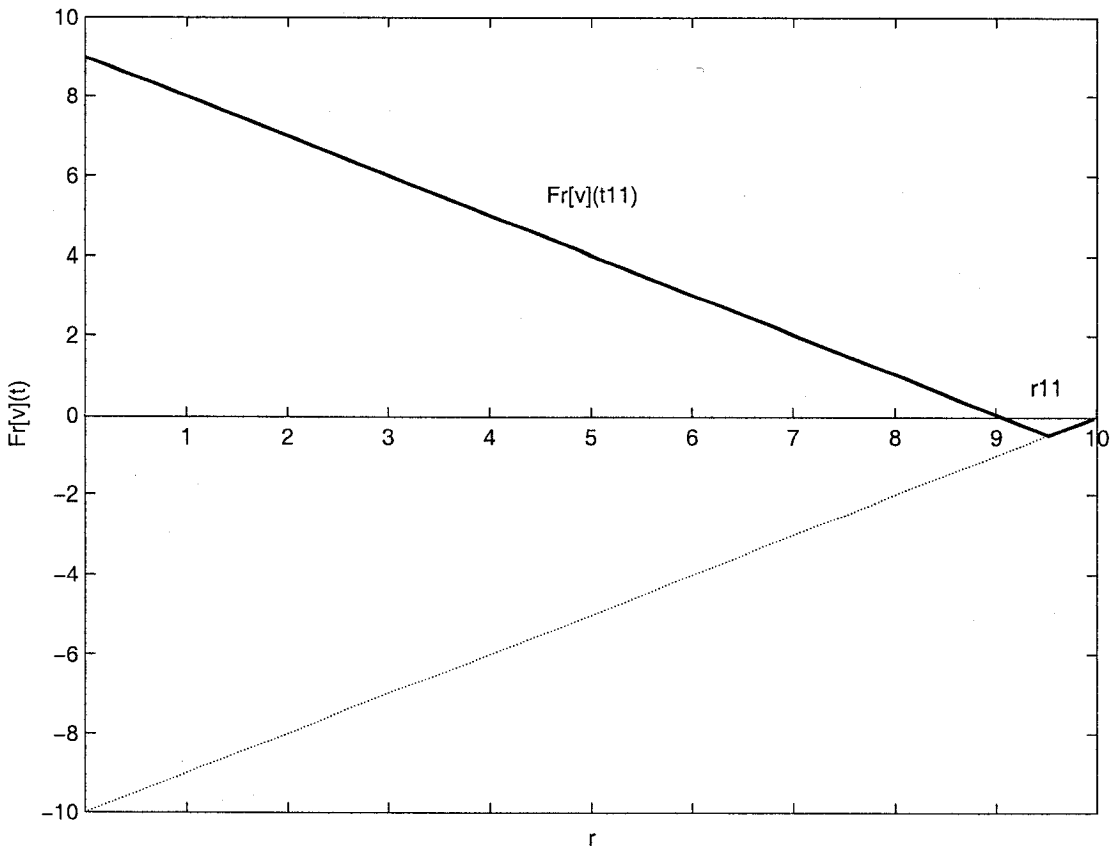

Figure 3.12: $p(r)$ identification-5

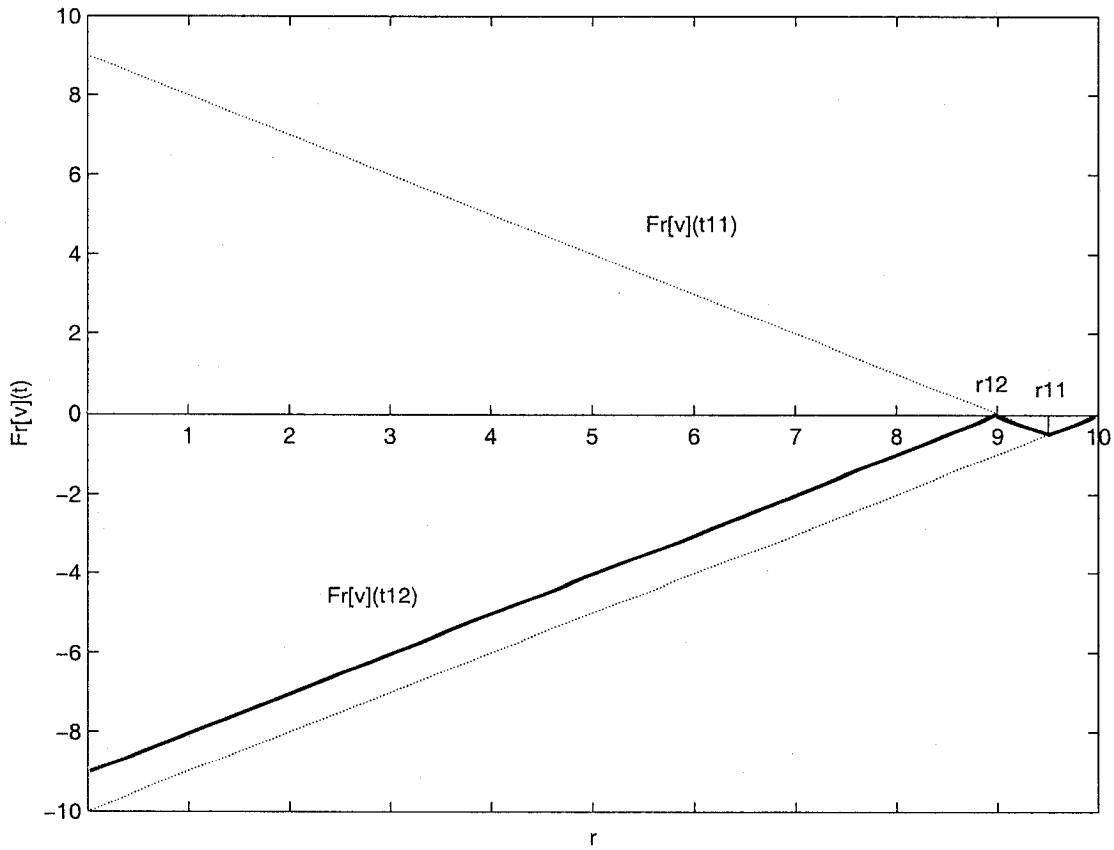

Figure 3.13: $p(r)$ identification-6

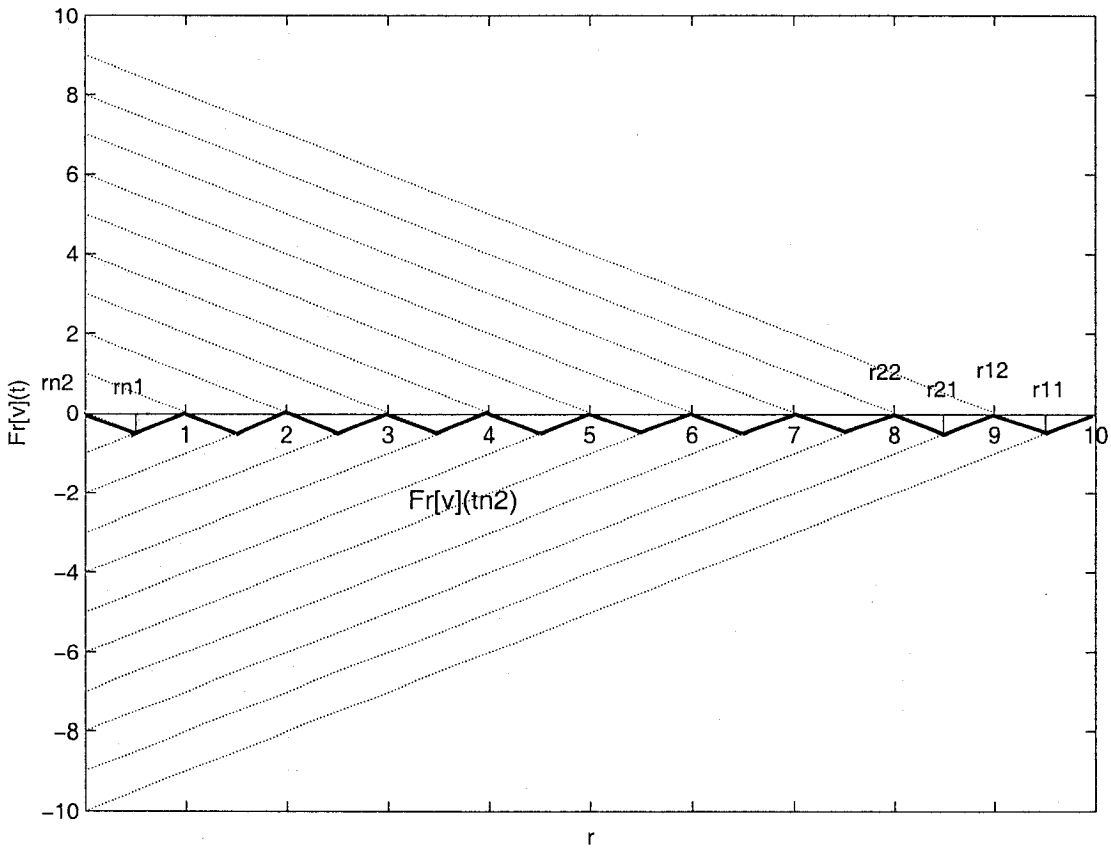

Figure 3.14: $p(r)$ identification-7

3.4. Relationship with Preisach Hysteresis Models

As discussed previously, the most popular hysteresis model is the Preisach model. In fact, the play operator is closely related to the Preisach operator [10]. In 1935, Preisach, based on his studies about the magnetization in ferromagnetic materials, developed a relation between the magnetization w and the magnetic field v through a linear superposition of relays with hysteresis, and also provided a simple geometrical interpretation for the Preisach model.

The Preisach model can be given as

$$W(t) = \int_0^{+\infty} \int_{-\infty}^{+\infty} \omega(r,s) R_{s-r,s+r}[v](t) ds dr, \tag{3.42}$$

where $R_{s-r,s+r}[v](t)$ is a relay hysteresis defined by

$$R_{s-r,s+r}[v](t) = \begin{cases} +1, & \text{if } v(t) \leq s-r \text{ or if } v(t) \in (s-r, s+r) \text{ and } v(\tau(t)) = s-r; \\ -1, & \text{if } v(t) \geq s+r \text{ or if } v(t) \in (s-r, s+r) \text{ and } v(\tau(t)) = s+r; \end{cases} \tag{3.43}$$

with $r \geq 0$, $\tau(t) = sup\{\alpha/\alpha \leq t, v(\alpha) = s-r \text{ or } v(\alpha) = s+r\}$, i.e., $\tau(t)$ is the value of time at the last threshold attained. The initial value of the relay $R_{s-r,s+r}[v]$ is taken as -1 if $s \geq 0$, and +1 otherwise.

It is known that the memory of the Preisach model is completely determined by the dividing line, $\phi(t)(r)$. It separates the areas in which the relays attain the value 1 from those having the value -1 at time t

$$A_{\pm}(t) = \{(r,s) \in \Re_+ \times \Re \mid R_{s-r,s+r}[v](t) = \pm 1\}.$$

Brokate in [9] described the connection between the dividing line $\phi(t)(r)$ and the play operator $F_r[v](t)$. If $\phi(t)(r)$ is given by the functional relation $s = \phi(t)(r)$,

where t is to be considered as a parameter fixed for each curve, then it can be proven that

$$\phi(t)(r) = F_r[v](t)$$

. The play operator is called the Preisach memory operator. In general, the Prandtl-Ishlinskii model is defined as a subclass of the Hysteresis Operators of Preisach Type. The reader may refer to [10], Sections 2.1 and 2.4, for detailed analysis.

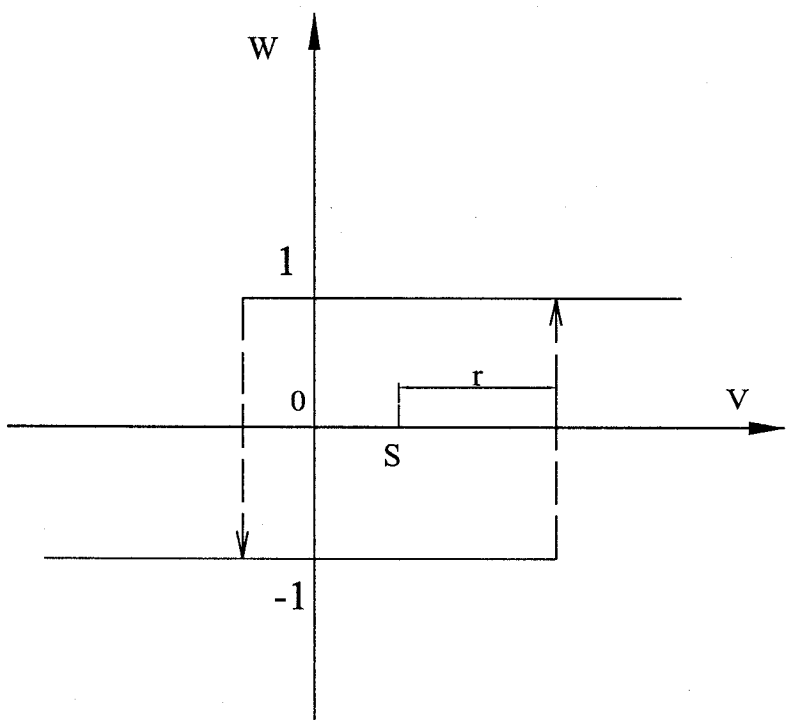

Figure 3.15: Relay with hysteresis

Chapter 4

Sliding Mode Control Based Design

4.1. System Description

Consider a controlled system consisting of a nonlinear plant preceded by an actuator with hysteresis nonlinearity, that is, the hysteresis is presented as an input of the nonlinear plant, and denoted as an operator

$$w(t) = P[v](t) \tag{4.1}$$

with $v(t)$ as the input and $w(t)$ as the output. The operator $P[v]$ will be discussed in detail in the following section of this chapter. The nonlinear dynamic system being preceded by the above hysteresis is described in the canonical form as

$$x^{(n)}(t) + \sum_{i=1}^{k} a_i Y_i(x(t), \dot{x}(t), ..., x^{(n-1)}(t)) = bw(t) \tag{4.2}$$

where Y_i are known continuous and linear or nonlinear functions. Parameters a_i and controller gain b are constants. It is a common assumption that the sign of b is known. Without loss of generality, we assume that $b > 0$.

The control objective is to design a control law $v(t)$, to force the state vector $\mathbf{x} = [\mathbf{x}, \dot{\mathbf{x}}, ..., \mathbf{x}^{(\mathbf{n-1})}]^{\mathbf{T}}$ to follow a desired trajectory $\mathbf{x_d} = [\mathbf{x_d}, \dot{\mathbf{x}}_\mathbf{d}, ..., \mathbf{x}_\mathbf{d}^{(\mathbf{n-1})}]^{\mathbf{T}}$, i.e., $\mathbf{x} \rightarrow \mathbf{x_d}$ as $t \rightarrow \infty$.

Consider the Prandtl-Ishlinskii model expressed by the play operator given in (3.14), the hysteresis output $w(t)$ can be written as

$$w(t) = p_0 v(t) - d[v](t), \tag{4.3}$$

where

$$d[v](t) = \int_0^R p(r) F_r[v](t) dr, \tag{4.4}$$

with $p_0 = \int_0^R p(r)dr$. For convenience, $F_r[v, \psi]$ is denoted by $F_r[v]$ for a given initial state $\psi \in \Psi$.

If the hysteresis in the system is known, that is, $p(r)$ and ψ are given or can be accurately estimated, for any continuous input function $v(t)$ at a time instant t, $F_r[v](t)$ will be a set of line segments determined by some extreme values of $v(t)$ (refer to Fig.3.3 to Fig.3.5)). The integration of $d[v]$ can be calculated online, and $d[v]$ can be used as a feed forward compensator to cancel the second non-linear term of the dynamic system.

However, in most cases, it is difficult or even impossible to accurately estimate the hysteresis of the system. Using the hysteresis model of (4.3), the system (4.2) becomes,

$$x^{(n)}(t) + \sum_{i=1}^{k} a_i Y_i(x(t), \dot{x}(t), ..., x^{(n-1)}(t)) = b\{p_0 v(t) - d[v](t)\}, \tag{4.5}$$

which leads to a linear relation to the input signal $v(t)$ plus a shifting term $bd[v]$.

Remark: It is clear that the first term on the right-hand side of (4.5) is a linear function of the control signal $v(t)$. In this case, it is possible to fuse the currently available controller design techniques with the hysteresis model for the

controller design. It will become more clear later that such a structure in fact makes it possible to design the adaptive control algorithm. This was also the primary motivation of using the Prandtl-Ishlinskii model.

If in the system (4.5), there is no hysteresis effect, that is, $d[v](t) = 0$, shown as

$$x^{(n)}(t) + \sum_{i=1}^{k} a_i Y_i(x(t), \dot{x}(t), ..., x^{(n-1)}(t)) = bp_0 v(t), \tag{4.6}$$

adaptive sliding mode control method can be effectively used to construct a robust controller for tracking and stabilization even when system uncertainties are present. In the context of robust control, the term $bd[v](t)$ is normally treated as a disturbance function, which is assumed to be bounded by a constant or bounded by a known function. However, being different from the traditional expressions of the disturbance, $d[v](t)$ is presented as an integral function. Therefore the assumption cannot be made on its boundedness. In addition, it is in fact a function of the input signal $v(t)$ and requires a special treatment for the adaptive controller design.

Define the tracking error vector $\tilde{\mathbf{x}}$ as

$$\tilde{\mathbf{x}} = \mathbf{x} - \mathbf{x_d},$$

and a filtered tracking error as

$$s(t) = (\frac{d}{dt} + \lambda)^{(n-1)} \tilde{x}(t), \qquad \lambda > 0 \tag{4.7}$$

$s(t)$ can be rewritten as $s(t) = \Lambda^T \tilde{\mathbf{x}}(t)$ with $\Lambda^T = [\lambda^{(n-1)}, (n-1)\lambda^{(n-2)}, ..., 1]$.

It has been shown in [55] that the definition given in (4.7) has the following properties:

(i) the equation $s(t) = 0$ defines a time-varying hyperplane in $\Re^n$ on which the tracking error vector $\tilde{\mathbf{x}}(t)$ decreases exponentially to zero;

(ii) if $\tilde{\mathbf{x}}(0) = 0$ and $|s(t)| \leq \epsilon$, where ϵ is a constant, then $\tilde{\mathbf{x}}(t) \in \Omega_\epsilon \triangleq \{\tilde{\mathbf{x}}(t) \mid |\tilde{\mathbf{x}}_i| \leq 2^{i-1}\lambda^{i-n}\epsilon, i = 1, ..., n\}$ for $\forall t \geq 0$;

(iii) if $\tilde{\mathbf{x}}(0) \neq 0$ and $|s(t)| \leq \epsilon$, then $\tilde{\mathbf{x}}(t)$ will converge to Ω_ϵ within a time-constant $(n-1)/\lambda$.

In sliding mode control design, the controller contains the discontinuous nonlinearity $sgn(\cdot)$. It will cause chattering due to practical imperfections in switching devices and delays. In order to eliminate chattering, rather than deriving the adaptive laws with the filtered error $s(t)$, we introduce a tuning error, s_ϵ, as follows:

$$s_\epsilon = s - \epsilon sat(\frac{s}{\epsilon}) \tag{4.8}$$

where ϵ is an arbitrary positive constant and $sat(\cdot)$ is the saturation function. The tuning error, s_ϵ, disappears when the filtered error, s, is less than ϵ.

In developing robust adaptive control laws, the following assumptions regarding the plant and the hysteresis are made:

Assumption 1: The desired trajectory $\mathbf{x}_d = [x_d, \dot{x}_d, ..., x_d^{(n-1)}]^T$ is continuous and available. Furthermore, $[\mathbf{x}_d^T, x_d^{(n)}]^T \in \Omega_d \subset \Re^{n+1}$ with Ω_d a compact set.

Assumption 2: There exist known constants $0 < b_{min} \leq b_{max}$ such that the control gain b in (4.2) satisfies $b \in [b_{min}, b_{max}]$.

Assumption 3: Define $\theta \triangleq [\frac{a_1}{bp_0}, ..., \frac{a_k}{bp_0}]^T \in \Re^k$, then

$$\theta \in \Omega_\theta \triangleq \{\theta : \theta_{imin} \leq \theta_i \leq \theta_{imax}, \forall i \in \{1, ..., k\}\}$$

where θ_{imin} and θ_{imax} are some known real numbers.

Assumption 4: There exist known constants p_{0min} and p_{max}, such that $p_0 > p_{0min}$, and $p(r) \leq p_{max}$ for all $r \in [0, R]$.

Remark: Assumption 1 is made mainly for the design of a tracking controller. Assumption 2 is common for nonlinear controller designs [55]. In Assumption 3,

a new parameter vector θ was defined for the convenience of further development. Basically, Assumption 3 implies that the ranges of the plant parameters, $a_i, i = 1...k$, are known in advance. This is a reasonable assumption on the prior knowledge of the system. As for Assumption 4, based on the properties of the density function $p(r)$, it is reasonable to set an upper bound p_{max} for $p(r)$. Here $p_{0min} > 0$ must be satisfied.

4.2. Controller Design

In presenting the developed robust adaptive control law, the following definitions are required:

$$\tilde{\theta}(t) = \hat{\theta}(t) - \theta, \tag{4.9}$$

$$\tilde{\phi}(t) = \hat{\phi}(t) - \phi, \tag{4.10}$$

$$\tilde{p}(t,r) = \hat{p}(t,r) - p(r), \quad for\ all\ r \in [0,R], \tag{4.11}$$

$\hat{\theta}$ is an estimate of θ as given in Assumption 3, $\hat{\phi}$ is an estimate of ϕ, which is defined as $\phi \triangleq (bp_0)^{-1}$. $\hat{p}(t,r)$ is an estimate of the density function $p(r)$. Let

$$B(v(t)) \triangleq \int_0^R p(r)\frac{|F_r[v](t)|}{p_{0min}}dr, \tag{4.12}$$

and the estimation $\hat{B}(t)$ is given by $\int_0^R \hat{p}(t,r)\frac{|F_r[v](t)|}{p_{0min}}dr$, which leads to

$$\tilde{B}(t) = \int_0^R (\hat{p}(t,r) - p(r))\frac{|F_r[v](t)|}{p_{0min}}dr. \tag{4.13}$$

Given the plant and hysteresis model subject to the assumptions described above, and noting that the term $d[v](t)$ in (4.3) is in the form of integral with the kernel $F_r[v](t)$, we propose the following control laws:

$$v(t) = -k_d s(t) + \hat{\phi}u_{fd}(t) + Y^T(\mathbf{x})\hat{\theta} + v_h(t) \tag{4.14}$$

with

$$u_{fd}(t) = x_d^{(n)}(t) - \Lambda_v^T \tilde{\mathbf{x}}(t); \tag{4.15}$$

$$v_h(t) = -sat(\frac{s}{\epsilon})\hat{B}(t); \tag{4.16}$$

where $k_d > 0$; $Y \triangleq [Y_1, ..., Y_k]^T \in \Re^k$; $\Lambda_v^T = [0, \lambda^{(n-1)}, (n-1)\lambda^{(n-2)}, ..., (n-1)\lambda]$, the parameters $\hat{\phi}$ and $\hat{\theta}$, and the function $\hat{B}(t)$ will be updated by the following adaptation laws

$$\dot{\hat{\theta}} = Proj(\hat{\theta}, -\gamma Y(\mathbf{x}) s_\epsilon), \tag{4.17}$$

$$\dot{\hat{\phi}} = Proj(\hat{\phi}, -\eta u_{fd} s_\epsilon), \tag{4.18}$$

$$\frac{\partial}{\partial t}\hat{p}(t,r) = Proj(\hat{p}(t,r), q\frac{|F_r[v](t)|}{p_{0min}}|s_\epsilon|), \quad for\ r \in [0, R], \tag{4.19}$$

where parameters γ, η and q are positive constants determining the rates of the adaptations, and $Proj(\cdot,\cdot)$ is a projection operator formulated as follows:

$$\{Proj(\hat{\theta}, -\gamma Y s_\epsilon)\}_i = \begin{cases} 0 & \text{if } \hat{\theta}_i = \theta_{imax} \text{ and } \gamma(Y s_\epsilon)_i < 0 \\ -\gamma(Y s_\epsilon)_i & \text{if } [\theta_{imin} < \hat{\theta}_i < \theta_{imax}] \\ & \text{or } [\hat{\theta}_i = \theta_{imax} \text{ and } \gamma(Y s_\epsilon)_i \geq 0] \\ & \text{or } [\hat{\theta}_i = \theta_{imin} \text{ and } \gamma(Y s_\epsilon)_i \leq 0] \\ 0 & \text{if } \hat{\theta}_i = \theta_{imin} \text{ and } \gamma(Y s_\epsilon)_i > 0 \end{cases} \tag{4.20}$$

$$Proj(\hat{\phi}, -\eta u_{fd} s_\epsilon) = \begin{cases} 0 & \text{if } \hat{\phi} = \phi_{max} \text{ and } \eta u_{fd} s_\epsilon < 0 \\ -\eta u_{fd} s_\epsilon & \text{if } [\phi_{min} < \hat{\phi} < \phi_{max}] \\ & \text{or } [\hat{\phi} = \phi_{max} \text{ and } \eta u_{fd} s_\epsilon \geq 0] \\ & \text{or } [\hat{\phi} = \phi_{min} \text{ and } \eta u_{fd} s_\epsilon \leq 0] \\ 0 & \text{if } \hat{\phi} = \phi_{min} \text{ and } \eta u_{fd} s_\epsilon > 0 \end{cases} \tag{4.21}$$

$$Proj(\hat{p}(t,r), q\frac{|F_r[v](t)|}{p_{0min}}|s_\epsilon|) = \begin{cases} 0 & \text{if } \hat{p}(t,r) = p_{max}; \\ q\frac{|F_r[v](t)|}{p_{0min}}|s_\epsilon| & \text{if } 0 \leq \hat{p}(t,r) < p_{max}\ . \end{cases} \tag{4.22}$$

Remarks: 1) Projection operator is used in the above control laws. It can be proved that the projection operator satisfies the following properties: (i) $\hat{z}(t) \in \Omega_z$ if $\hat{z}(0) \in \Omega_z$, where Ω_z is a compact set; (ii) $\|Proj(z,y)\| \leq \|y\|$; and (iii) $-(z-z^*)^T\Lambda Proj(z,y) \geq -(z-z^*)^T\Lambda y$, where Λ is a positive definite symmetric matrix.

2) The projection operators require the upper and lower bounds of the parameters θ, ϕ and $p(t,r)$. Assumptions 2)-4) are fundamental to this end. However, these parameters are only used to specify the ranges of the parameter changes for the projection operator. These ranges are not restricted as long as the estimated parameters are bounded.

3) The term $v_h(t)$ represents the compensation component for the function $d[v](t)$. Unlike traditional robust adaptive controller designs, where $d[v](t)$ is assumed to be bounded by either a constant or a known function, $d[v](t)$ is presented as an integral equation, and there is no assumption on its boundedness. Notice that the density function $p(r)$ is not a time function, we can thus treat this term as a parameter of the hysteresis model and develop an estimated law for it. This is crucial for the success of the adaptive law design.

4) For the calculation of $\hat{B}(t) = \int_0^R \hat{p}(r,t)\frac{|F_r[v](t)|}{p_{0min}}dr$ in the implementation, using numerical technique, we can simply replace the integration with the sum by dividing R into small intervals, i.e, $\hat{B}(t) = \sum_{l=0}^{N-1} \hat{p}(l\Delta r, t)\frac{|F_{l\Delta r}[v](t)|}{p_{0min}}\Delta r$, where N determines the size of the intervals as $\Delta r = R/N$. The selection of the size of the

intervals depends on the accuracy requirement. As will be shown in the simulation example, the size of the intervals may not necessarily be very small.

The stability of the closed-loop system described in (4.5), (4.14) and (4.17)-(4.19) is established in the following theorem:

Theorem: For the plant given in Equation (4.2) preceded by a hysteresis nonlinearity presented by Prandtl-Ishlinskii model (3.14) subject to Assumptions 1)-4) with

$$\Omega_\theta = \{\theta : \theta_{imin} \leq \theta_i \leq \theta_{imax}, \forall i \in \{1, ..., k\}\},$$

$$\Omega_\phi = \{\phi = \frac{1}{bp_0} : (b_{max}p_{0max})^{-1} \leq \phi \leq (b_{min}p_{0min})^{-1}\},$$

$$\Omega_p = \{\hat{p}(t,r) : 0 \leq \hat{p}(t,r) \leq p_{max},\ \forall r \in [0, R]\},$$

if $\hat{\theta}(t_0) \in \Omega_\theta$, $\hat{\phi}(t_0) \in \Omega_\phi$ and $\hat{p}(t_0, r) \in \Omega_p$, then the robust adaptive controller specified by Equations (4.14) and (4.17)-(4.19) ensures that all the closed-loop signals are bounded and the error of the state vector and the desired trajectory $\tilde{\mathbf{x}}(t)$ converges to $\Omega_\epsilon = \{\tilde{\mathbf{x}}(t) || \tilde{\mathbf{x}}_i | \leq 2^{i-1}\lambda^{i-n}\epsilon, i = 1, ..., n\}$ as $t \to \infty$.

Proof: Using the expression (4.5), the time derivative of the filtered error (4.7) can be written as:

$$\dot{s}(t) = -u_{fd}(t) - \sum_{i=1}^{k} a_i Y_i(\mathbf{x}(t)) + b\{p_0 v(t) - d[v](t)\}. \tag{4.23}$$

Using control laws (4.14)-(4.16), the above equation can be rewritten as

$$\begin{aligned} \dot{s}(t) &= -u_{fd}(t) - \sum_{i=1}^{k} a_i Y_i(\mathbf{x}(t)) - bd[v](t) \\ &\quad + bp_0[-k_d s(t) + \hat{\phi} u_{fd}(t) + Y^T(\mathbf{x})\hat{\theta} + v_h(t)]. \end{aligned} \tag{4.24}$$

To establish global boundedness, we define the following Lyapunov function candidate

$$V(t) = \frac{1}{2}[\frac{1}{bp_0}s_\epsilon^2 + \frac{1}{\gamma}(\hat{\theta} - \theta)^T(\hat{\theta} - \theta) + \frac{1}{\eta}(\hat{\phi} - \phi)^2 + \frac{1}{q}\int_0^R \tilde{p}^2(t,r)dr]. \tag{4.25}$$

Since the discontinuity at $|s| = \epsilon$ is of the first kind and $s_\epsilon = 0$ when $|s| \leq \epsilon$, the derivative $\dot{V}$ exists for all s, with

$$\dot{V}(t) = 0, \quad \text{for } |s| \leq \epsilon. \tag{4.26}$$

When $|s| > \epsilon$, using (4.24) and the fact that $s_\epsilon \dot{s}_\epsilon = s_\epsilon \dot{s}$, we have

$$\begin{aligned}
\dot{V}(t) &= \frac{1}{bp_0} s_\epsilon \dot{s} + \frac{1}{\gamma}(\hat{\theta} - \theta)^T \dot{\hat{\theta}} + \frac{1}{\eta}(\hat{\phi} - \phi)\dot{\hat{\phi}} \\
&\quad + \frac{1}{q}\int_0^R \tilde{p}(t,r)\frac{\partial}{\partial t}\tilde{p}(t,r)dr \\
&= -k_d s_\epsilon s + s_\epsilon[\hat{\phi} u_{fd}(t) + Y^T(\mathbf{x})\hat{\theta} + v_h(t) - d[v](t)] \\
&\quad + \frac{1}{bp_0} s_\epsilon[-u_{fd}(t) - \sum_{i=1}^{k} a_i Y_i(\mathbf{x}(t))] + \frac{1}{\gamma}(\hat{\theta} - \theta)^T \dot{\hat{\theta}} \\
&\quad + \frac{1}{\eta}(\hat{\phi} - \phi)\dot{\hat{\phi}} + \frac{1}{q}\int_0^R \tilde{p}(t,r)\frac{\partial}{\partial t}\tilde{p}(t,r)dr \\
&= -k_d s_\epsilon s + s_\epsilon[\hat{\phi} u_{fd}(t) + Y^T(\mathbf{x})\hat{\theta} + v_h(t) - d[v](t)] \\
&\quad + s_\epsilon[-\phi u_{fd}(t) - Y^T\theta] + \frac{1}{\gamma}(\hat{\theta} - \theta)^T \dot{\hat{\theta}} + \frac{1}{\eta}(\hat{\phi} - \phi)\dot{\hat{\phi}} \\
&\quad + \frac{1}{q}\int_0^R \tilde{p}(t,r)\frac{\partial}{\partial t}\tilde{p}(t,r)dr.
\end{aligned} \tag{4.27}$$

The above equation can be simplified, by the choice of s_ϵ, to

$$\begin{aligned}
\dot{V}(t) &\leq -k_d s_\epsilon^2 + s_\epsilon[\hat{\phi} u_{fd}(t) + Y^T(\mathbf{x})\hat{\theta} + v_h(t)] \\
&\quad + s_\epsilon[-\phi u_{fd}(t) - Y^T\theta - \frac{1}{p_0} d[v](t)] + \frac{1}{\gamma}(\hat{\theta} - \theta)^T \dot{\hat{\theta}} + \frac{1}{\eta}(\hat{\phi} - \phi)\dot{\hat{\phi}} \\
&\quad + \frac{1}{q}\int_0^R \tilde{p}(t,r)\frac{\partial}{\partial t}\tilde{p}(t,r)dr.
\end{aligned} \tag{4.28}$$

By using the adaptive laws given in (4.17)-(4.19) and the properties of

$$\frac{1}{\gamma}(\hat{\theta}-\theta)^T Proj(\hat{\theta}, -\gamma Y s_\epsilon) \leq -(\hat{\theta}-\theta)^T Y s_\epsilon$$

$$\frac{1}{\eta}(\hat{\phi}-\phi) Proj(\hat{\phi}, -\eta u_{fd} s_\epsilon) \leq -(\hat{\phi}-\phi) u_{fd} s_\epsilon,$$

we obtain

$$\begin{aligned}
\dot{V}(t) \leq\ & -k_d s_\epsilon^2 + s_\epsilon[\hat{\phi} u_{fd}(t) + Y^T(\mathbf{x})\hat{\theta} + v_h(t)] \\
& + s_\epsilon[-\phi u_{fd}(t) - Y^T\theta - \frac{1}{p_0} d[v](t)] - (\hat{\theta}-\theta)^T Y s_\epsilon - (\hat{\phi}-\phi) u_{fd} s_\epsilon \\
& + \frac{1}{q}\int_0^R \tilde{p}(t,r) Proj(\hat{p}(t,r), q\frac{|F_r[v](t)|}{p_{0min}}|s_\epsilon|) dr \\
\\
\leq\ & -k_d s_\epsilon^2 + v_h(t) s_\epsilon - \frac{1}{p_0} d[v](t) s_\epsilon \\
& + \frac{1}{q}\int_0^R \tilde{p}(t,r) Proj(\hat{p}(t,r), q\frac{|F_r[v](t)|}{p_{0min}}|s_\epsilon|) dr.
\end{aligned} \tag{4.29}$$

Now, we show that $\dot{V}(t) \leq -k_d s_\epsilon^2$. Since

$$\begin{aligned}
-\frac{1}{p_0} d[v](t) s_\epsilon + v_h(t) s_\epsilon &= -\frac{s_\epsilon}{p_0}\int_0^R p(r) F_r[v](t) dr - sat(\frac{s}{\epsilon}) s_\epsilon \int_0^R \hat{p}(t,r)\frac{|F_r[v](t)|}{p_{0min}} dr \\
&\leq +\frac{|s_\epsilon|}{p_0}\int_0^R p(r)|F_r[v](t)| dr - \frac{|s_\epsilon|}{p_{0min}}\int_0^R \hat{p}(t,r)|F_r[v](t)| dr \\
&\leq -\frac{|s_\epsilon|}{p_{0min}}\int_0^R \tilde{p}(t,r)|F_r[v](t)| dr,
\end{aligned} \tag{4.30}$$

let

$$\Re_{max} = \{r : \hat{p}(t,r) = p_{max}\} \subset [0, R] \tag{4.31}$$

$$\Re^c_{max} = \{r : \hat{p}(t,r) < p_{max}\} \subset [0, R] \tag{4.32}$$

from (4.22) and according to adaptation law (4.19), if r is in the subset $\Re_{max}$, we have $\tilde{p}(t,r) \geq 0$,

$$Proj(\hat{p}(t,r), q|F_r[v](t)s_\epsilon|/p_{0min}) = 0,$$

$$-\frac{|s_\epsilon|}{p_{0min}} \int_{\Re_{max}} \tilde{p}(t,r)|F_r[v](t)|dr + \frac{1}{q}\int_{\Re_{max}} \tilde{p}(t,r)Proj(\hat{p}(t,r), q\frac{|F_r[v](t)s_{|\epsilon|}}{p_{0min}})dr \leq 0$$

otherwise, we have $0 \leq \hat{p}(t,r) < p_{max}$ for $r \in \Re^c_{max}$, where $\Re^c_{max}$ is the complement of $\Re_{max}$ in $[0, R]$). By (4.22),

$$Proj(\hat{p}(t,r), q\frac{|F_r[v](t)s_\epsilon|}{p_{0min}}) = q\frac{|F_r[v](t)s_\epsilon|}{p_{0min}},$$

$$-\frac{|s_\epsilon|}{p_{0min}} \int_{\Re^c_{max}} \tilde{p}(t,r)|F_r[v](t)|dr + \frac{1}{q}\int_{\Re^c_{max}} \tilde{p}(t,r)q\frac{|F_r[v](t)|}{p_{0min}}|s_\epsilon|dr = 0$$

That is

$$\begin{aligned}
\dot{V}(t) &\leq -k_d s_\epsilon^2 + v_h(t)s_\epsilon - \frac{1}{p_0}d[v](t)s_\epsilon \\
&\quad + \frac{1}{q}\int_0^R \tilde{p}(t,r)Proj(\hat{p}(t,r), q\frac{|F_r[v](t)|}{p_{0min}}|s_\epsilon|)dr \\
&\leq -k_d s_\epsilon^2 - \frac{|s_\epsilon|}{p_{0min}}\int_0^R \tilde{p}(t,r)|F_r[v](t)|dr \\
&\quad + \frac{1}{q}\int_0^R \tilde{p}(t,r)Proj(\hat{p}(t,r), q\frac{|F_r[v](t)|}{p_{0min}}|s_\epsilon|)dr \\
&\leq -k_d s_\epsilon^2.
\end{aligned} \tag{4.33}$$

Equations (4.25), (4.26) and (4.33) imply that V is a Lyapunov function leading to global boundedness of variables s_ϵ, $(\hat{\theta}-\theta)$, $(\hat{\phi}-\phi)$, and $\hat{p}(t,r)-p(r)$. From the

definition of s_ϵ, $s(t)$ is bounded. It can be shown that if $\tilde{\mathbf{x}}(0)$ is bounded, then $\tilde{\mathbf{x}}(t)$ is also bounded for all $t \in [0, t_E]$. Since $\mathbf{x_d(t)}$ is bounded by design, $\mathbf{x(t)}$ must also be bounded. To complete the proof and establish an asymptotic convergence of the tracking error, it is necessary to show that $s_\epsilon \rightarrow 0$ as $t \rightarrow \infty$. This is accomplished by applying Barbalat's Lemma to the continuous, non-negative function:

$$\begin{aligned} V_1(t) &= V(t) - \int_0^t (\dot{V}(\tau) + k_d s_\epsilon^2(\tau))d\tau \text{ with} \\ \dot{V}_1(t) &= -k_d s_\epsilon^2(t) \end{aligned} \tag{4.34}$$

It can easily be shown that (4.23) is bounded. It should be mentioned that the term $b\{p_0 v(t) - d[v](t)\}$ is the Prandtl-Ishlinskii model defined by the play operator, which is equivalent to (3.13). Then, the boundedness of that term can be concluded from the Proposition given in Section 3.2.2. Hence $\dot{s}$ and $\dot{s}_\epsilon$ are bounded. This implies that $\dot{V}_1(t)$ is a uniformly continuous function of time. Since V_1 is bounded below by 0, and $\dot{V}_1(t) \leq 0$ for all t, using Barbalat's Lemma we can prove that $\dot{V}_1(t) \rightarrow 0$. Therefore, from (4.34), it can be shown that $s_\epsilon(t) \rightarrow 0$ as $t \rightarrow \infty$. The remark following Equation (4.7) indicates that $\tilde{\mathbf{x}}(t)$ will converge to Ω_ϵ.

$\triangle\triangle\triangle$

Remark: It is now clear that the developed control strategy to deal with the hysteresis nonlinearities can be applied to many systems and may not necessarily be limited to the system described by (4.2). However, it should be emphasized that our goal is to develop a control strategy in a simpler setting to reveal its essential features.

4.3. Simulation Studies

Consider a nonlinear system in the form of (4.2) given by

$$\dot{x} = a\frac{1 - e^{-x(t)}}{1 + e^{-x(t)}} + bw(t) \tag{4.35}$$

where $w(t)$ represents the output of the hysteresis operator described by the Prandtl-Ishlinskii model (3.14). Parameters a, b and the density function $p(r)$ are assumed unknown. The nominal values of $a = 1$, $b = 1$ and $p(r) = \alpha e^{-\beta(r-\sigma)^2}$ and $\psi(r) = 0.07$ for $r \in [0, 100]$, with $\alpha = 0.5, \beta = 0.00105$ and $\sigma = 2$ are used in the simulation. As mentioned before, $p(r)$ is expected to be identified from experimental data. Notice that when the control input $v(t) \equiv 0$ and $w(t) \equiv 0$, we can use basic analytical method to show that the system is unstable without control.

A sinusoidal desired trajectory of $x_d = 3sin(2t) + 0.1cos(6.7t)$ is used to illustrate the tracking capability of the proposed robust adaptive control. In the simulation, initial conditions are chosen as $\hat{p}(0, r) = 0$ for $r \in [0, R]$, $\hat{\theta}(0) = 1/4.41$, and $\hat{\phi}(0) = 1/2.32$. We also assume that $x(0) = -1$ and $v(0) = 0$. The approach to select their values was through iterative simulation. In this simulation, $k_d = 0.97$, $p_{0min} = 1.10 > 0$, $\gamma = 0.53$, $\eta = 0.91$, $q = 0.87$ and $\epsilon = 0.005$. The sampling time is 0.001. With these parameter values, the system responses are more sensitive to k_d, p_{0min} and q. It is obvious that p_{0min} and q are used to correct the errors caused by the hysteresis. As long as $0 < p_{0min} < p_0$ is satisfied, smaller p_{0min} and larger q (normally ≤ 1) will result in faster convergency of the tracking error and less smooth transient response of the control term $v_h(t)$. In this simulation, $0 < p_{0min} = 1.10 < p_0 = \int_0^{100} p(r)dr = 14.662$. To calculate $\hat{B}(t)$, the integration is replaced by the summation $\sum_0^N$, where $N = 4000$.

To illustrate the effectiveness of the proposed control scheme, the simulation is also conducted without controlling the effects of the hysteresis. This is done

by setting the component $v_h(t) = 0$ in the controller $v(t)$. Simulation results are shown in Figs.4.1-4.5. Fig.4.1 shows the tracking errors of the system state for the desired trajectory with and without controlling the effects of the hysteresis in the time spans of 1 second and 30 seconds, where the tracking error (solid line) is kept less than $\epsilon = 0.005$ after 0.2 seconds. In comparison, the tracking error for $v_h = 0$ is also shown by the dash-dot line. It is seen that the hysteresis in the system causes the tracking error at least 30 times higher than the desired level. It clearly demonstrates the excellent tracking performance of the proposed algorithm. Fig.4.2 gives the desired trajectory $x_d(t) = 3sin(2t) + 0.1cos(6.7t)$ and the system outputs $x(t)$ with control term $v_h \neq 0$ and $x(t)$ for $v_h = 0$. Figs.4.3 and 4.4 show the input control signal $v(t)$ and the hysteresis output $w(t)$.

It should be mentioned that simulations for several different desired trajectories with various parameter values and initial conditions have also been conducted. Results show that they all displayed similar behaviors as the one shown in this section. The simulation conducted with $N = 8000$, which resulted in smaller intervals, gives almost identical results. This further verifies that the developed control algorithm is repeatable and computationally implementable.

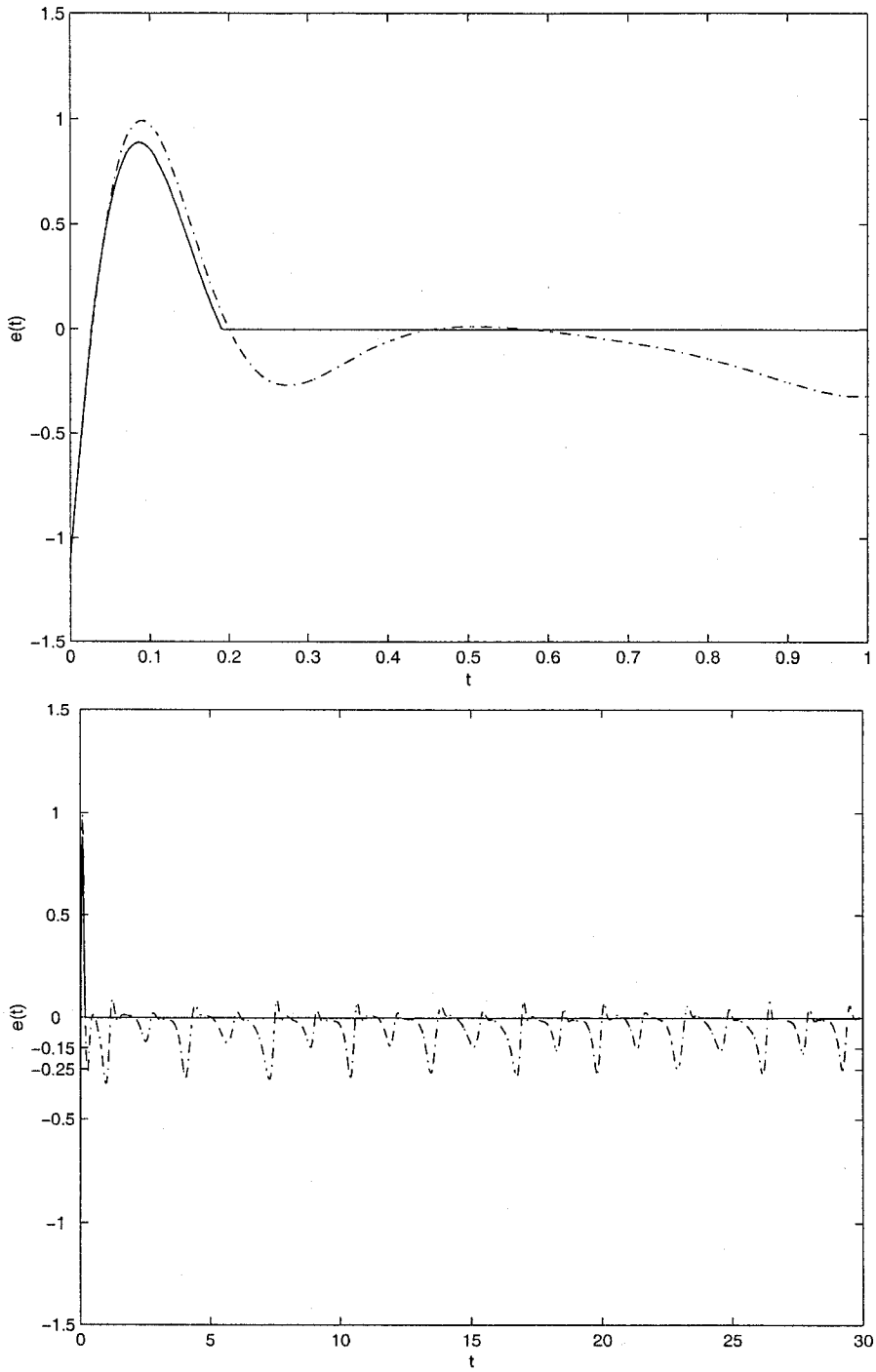

Figure 4.1: Tracking errors of the system state with control term $v_h \neq 0$ (solid line) and $v_h = 0$ ('-.-' line).

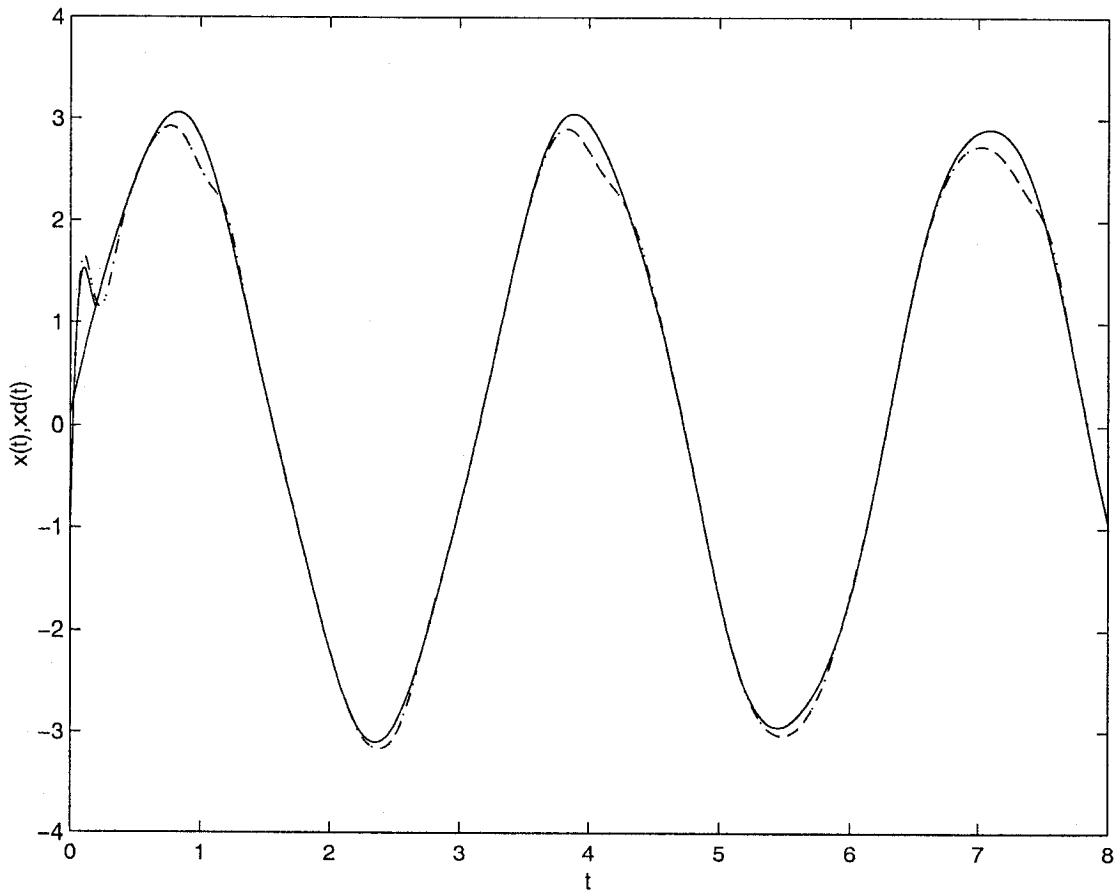

Figure 4.2: System outputs $x(t)$ with control term $v_h \neq 0$ (solid line) and $v_h = 0$ (dashed line).

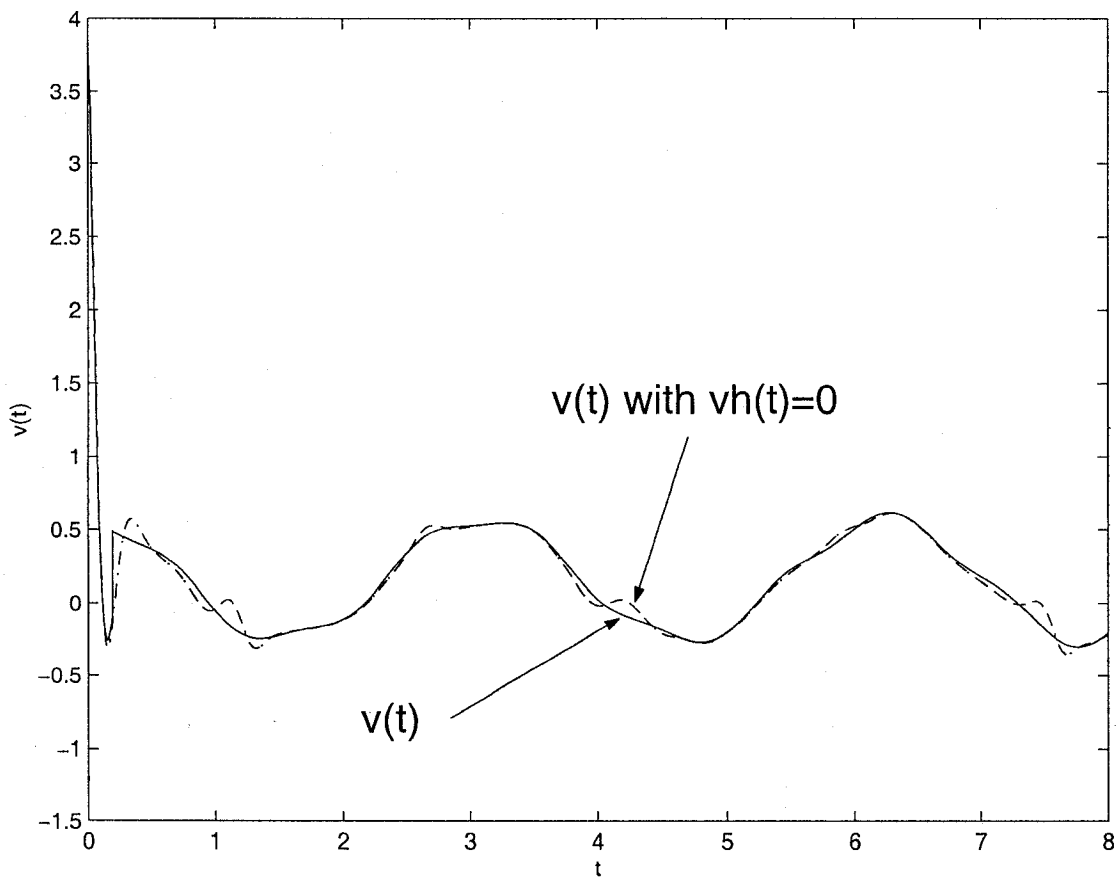

Figure 4.3: The control signals $v(t)$ with $v_h \neq 0$ (solid line) and $v_h = 0$ (broken line).

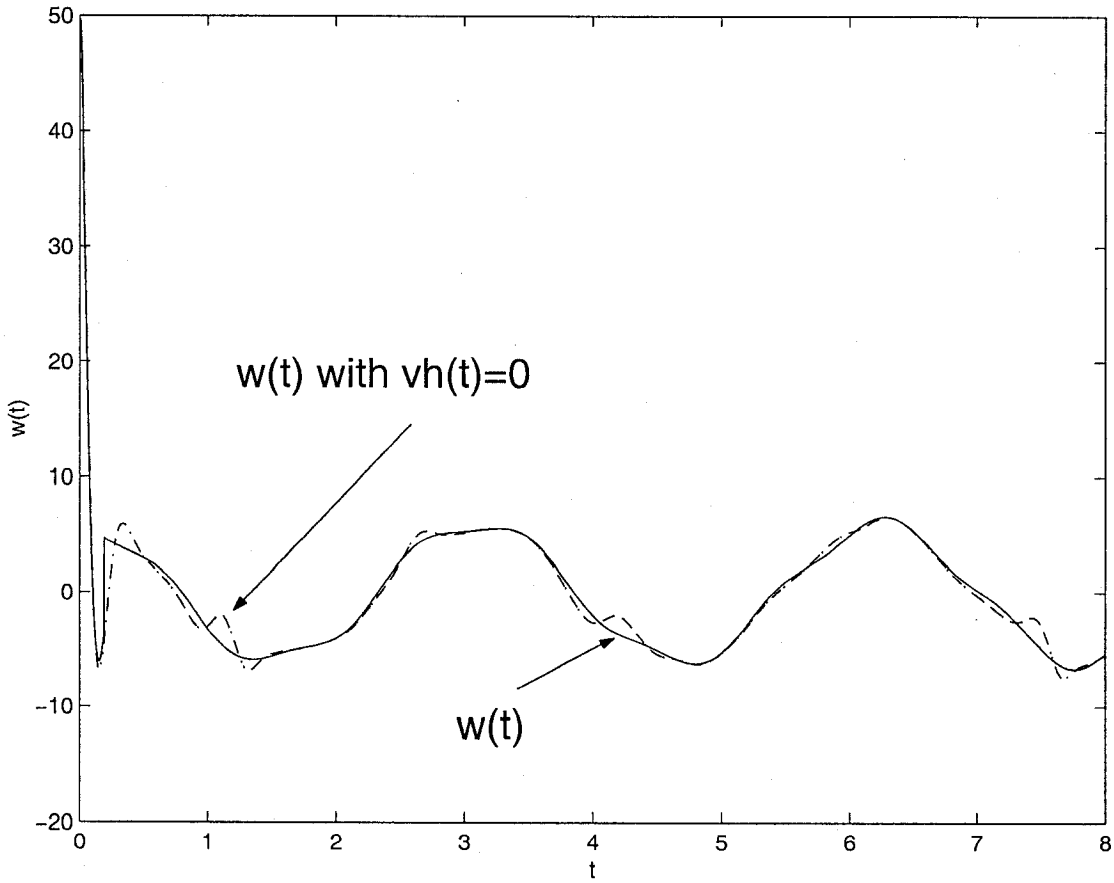

Figure 4.4: The hysteresis outputs $w(t)$ with $v_h \neq 0$ (solid line) and $v_h = 0$ (broken line).

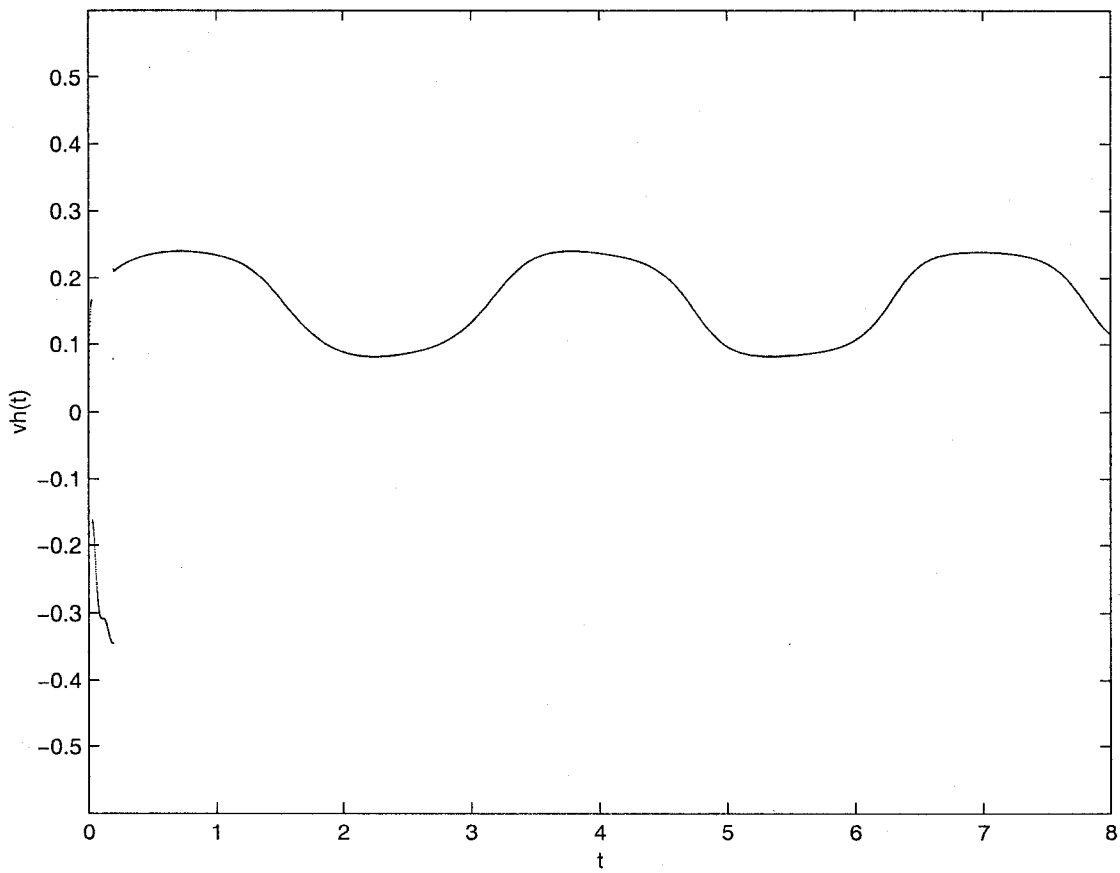

Figure 4.5: The signal v_h designed to reduce the tracking error caused by the hysteresis.

Chapter 5

Back-stepping Control Based Design

5.1. Problem Statement

In this chapter, for the similar class of nonlinear systems discussed in chapter 4, it is show that this approach can also be fused with adaptive back-stepping control design.

Consider the Prandtl-Ishlinskii model expressed by the play operator given in (3.14), the hysteresis output $w(t)$ can be expressed as

$$w(t) = p_0 v(t) - d[v](t), \tag{5.1}$$

where

$$d[v](t) = \int_0^R p(r) F_r[v](t) dr, \tag{5.2}$$

with $p_0 = \int_0^R p(r)dr$. For convenience, $F_r[v, \psi]$ is denoted by $F_r[v]$ for a given initial state $\psi \in \Psi$.

The nonlinear dynamic system being preceded by the above hysteresis is described in the canonical form as,

$$x^{(n)}(t) + \sum_{i=1}^{k} a_i Y_i(x(t), \dot{x}(t), ..., x^{(n-1)}(t)) = bw(t) \tag{5.3}$$

where Y_i are known continuous, linear or nonlinear functions. Parameters a_i and controller gain b are constants. It is a common assumption that the sign of b is known. Without losing generality, we assume that $b > 0$. It should be noted that more general classes of nonlinear systems can be transformed into this structure [32].

The control objective is to design a control law $v(t)$, to force state vector $\mathbf{x} = [\mathbf{x}, \dot{\mathbf{x}}, ..., \mathbf{x^{(n-1)}}]^{\mathbf{T}}$ to follow a desired trajectory $\mathbf{x_d} = [\mathbf{x_d}, \dot{\mathbf{x}}_\mathbf{d}, ..., \mathbf{x_d^{(n-1)}}]^{\mathbf{T}}$, i.e., $\mathbf{x} \rightarrow \mathbf{x_d}$ as $t \rightarrow \infty$.

5.2. Controller Design

Assumption : The desired trajectory $\mathbf{x_d} = [\mathbf{x_d}, \dot{\mathbf{x}}_\mathbf{d}, ..., \mathbf{x_d^{(n-1)}}]^{\mathbf{T}}$ is continuous and available. Furthermore, $[\mathbf{x_d^T}, \mathbf{x_d^{(n)}}]^{\mathbf{T}} \in \mathbf{\Omega_d} \subset \Re^{\mathbf{n+1}}$ with Ω_d a compact set.

Using the hysteresis model of (5.1), the nonlinear system dynamics described in (5.3) can be expressed as

$$x^{(n)}(t) + \sum_{i=1}^{k} a_i Y_i(x(t), \dot{x}(t), ..., x^{(n-1)}(t)) = b\{p_0 v(t) - d[v](t)\}, \tag{5.4}$$

which yields a linear relation to the input signal $v(t)$ together with a shifting term $bd[v]$.

Remark: As we mentioned in the previous section that the first term on the right-hand side of (5.4) is expressed as a linear function of the control signal $v(t)$. Such a structure would thus permit for the design of the adaptive variable structure

control algorithm. This particular aspect of the integration will become clear with the formulations presented later. Furthermore, the integrated model in (5.4) was also our primary motivation behind using the Prandtl-Ishlinskii model.

Equation (5.4) can be re-expressed as

$$\begin{aligned} \dot{x}_1 &= x_2 \\ &\vdots \\ \dot{x}_{n-1} &= x_n \\ \dot{x}_n &= \mathbf{a^T Y} + \mathbf{b_p v(t)} - \mathbf{d_b[v](t)} \end{aligned} \tag{5.5}$$

where $x_1(t) = x(t), x_2(t) = \dot{x}(t), \cdots, x_n(t) = x^{(n-1)}(t)$, $\mathbf{a} = [-\mathbf{a_1}, -\mathbf{a_2}, \cdots, -\mathbf{a_k}]^\mathbf{T}$, $Y = [Y_1, Y_2, \cdots, Y_k]^T$, $b_p = bp_0$, and

$$d_b[v](t) = \int_0^R p_b(r) F_r[v](t) dr \tag{5.6}$$

with $p_b(r) = bp(r)$.

We introduce the following new variables

$$\begin{aligned} z_1(t) &= x_1(t) - x_d(t) \\ z_i(t) &= x_i(t) - x_d^{(i-1)} - \alpha_{i-1}, \quad i = 2, 3, \cdots, n \\ \alpha_1(t) &= -c_1 z_1(t) \\ \alpha_i(t) &= -c_i z_i(t) - z_{i-1}(t) + \dot{\alpha}_{i-1}(x_1, \cdots, x_{i-1}, x_d, \cdots, x_d^{i-1}), \\ &\quad for \;\; i = 2, 3, \cdots, n-1 \end{aligned} \tag{5.7, 5.8}$$

where c_i, $i = 1, 2, \cdots, n-1$, are positive design parameters. The time derivative of z_1 is

$$\begin{aligned} \dot{z}_1(t) &= \dot{x}_1(t) - \dot{x}_d(t) \\ &= x_2(t) - \dot{x}_d(t) \end{aligned} \tag{5.9}$$

using the second and the third equations in (5.7)

$$\begin{aligned} \dot{z}_1(t) &= z_2(t) + \alpha_1(t) \\ &= z_2(t) - c_1 z_1(t) \end{aligned} \tag{5.10}$$

Similarly, for z_i, $i = 2, 3, \cdots, n-1$, we have

$$\begin{aligned} \dot{z}_i(t) &= \dot{x}_i(t) - x_d^{(i)}(t) - \dot{\alpha}_{i-1}(t) \\ &= -z_{i-1}(t) - c_i z_i(t) + z_{i+1}(t) \end{aligned} \tag{5.11}$$

Giving the following definitions

$$\tilde{\mathbf{a}}(t) = \mathbf{a} - \hat{\mathbf{a}}(\mathbf{t}), \tag{5.12}$$

$$\tilde{\phi}(t) = \phi - \hat{\phi}(t), \tag{5.13}$$

$$\tilde{p}_b(t, r) = p_b(r) - \hat{p}_b(t, r), \quad for\ all\ r \in [0, R], \tag{5.14}$$

$\hat{\mathbf{a}}$ is an estimate of $\mathbf{a}$, $\hat{\phi}$ is an estimate of ϕ, which is defined as $\phi \triangleq (b_p)^{-1}$, $\hat{p}_b(t, r)$ is an estimate of the density function $p_b(r)$,

$$B(v(t)) \triangleq \int_0^R p_b(r) |F_r[v](t)| dr, \tag{5.15}$$

and the estimation $\hat{B}(t)$ is given by $\int_0^R \hat{p}(t, r) |F_r[v](t)| dr$, which leads to

$$\tilde{B}(t) = \int_0^R (p_b(t, r) - \hat{p}_b(r)) |F_r[v](t)| dr, \tag{5.16}$$

and the time derivative of z_n is

$$\begin{aligned} \dot{z}_n(t) &= \dot{x}_n(t) - x_d^{(n)}(t) - \dot{\alpha}_{n-1}(t) \\ &= a^T Y + b_p v - d_b[v](t) - x_d^{(n)}(t) - \dot{\alpha}_{n-1} \end{aligned} \tag{5.17}$$

Subjected to the assumptions and definitions given above, the following control laws are proposed:

$$v(t) = \hat{\phi}(t) v_1(t) \tag{5.18}$$

with

$$v_1(t) = -c_n z_n - z_{n-1} - \hat{\mathbf{a}}^T Y + v_h(t) + x_d^{(n)} + \dot{\alpha}_{n-1} \tag{5.19}$$

$$v_h(t) = -sgn(z_n)\hat{B} \tag{5.20}$$

The parameters $\hat{\phi}$ and $\hat{\mathbf{a}}$, and function $\hat{B}(t)$ will be updated by the following adaptation laws

$$\dot{\hat{\mathbf{a}}} = \gamma Y z_n \tag{5.21}$$

$$\dot{\hat{\phi}} = -\eta v_1 z_n \tag{5.22}$$

$$\frac{\partial}{\partial t}\hat{p}_b(t,r) = q|F_r[v](t)||z_n|, \quad for\ r \in [0,R], \tag{5.23}$$

where parameters γ, η and q are positive constants determining the rates of the adaptations.

Remarks:

1) The term $v_h(t)$ represents the compensation component for the function $d[v](t)$. Unlike the traditional robust adaptive controller designs, where $d[v](t)$ is assumed to be bounded by either a constant or a known function, $d[v](t)$ is presented as an integral equation, and there is no assumption on its boundedness. Due to the fact that the density function $p(r)$ is not a time function, this term can thus be treated as a parameter of the hysteresis model and develop an estimated law for it. This is crucial for the success of the adaptive law design.

2) For the calculation of $\hat{B}(t) = \int_0^R \hat{p}_b(r,t)|F_r[v](t)|dr$ in the implementation, using numerical technique, we can simply replace the integration with the sum by dividing R into small intervals, i.e, $\hat{B}(t) = \sum_{l=0}^{N-1} \hat{p}_b(l\Delta r, t)|F_{l\Delta r}[v](t)|\Delta r$, where N determines the size of the intervals as $\Delta r = R/N$. The selection of the size of the intervals depends on the accuracy requirement. As will be shown in the simulation example, the size of the small intervals may not necessarily be very small, similar to that discussed in the previous chapter.

The stability of the closed-loop system described in (5.4), (5.18) and (5.21)-(5.23) is established in the following theorem:

Theorem: For the plant given in Equation (5.3) with the hysteresis (3.14), subject to the assumptions discussed above, the robust adaptive controller specified by Equations (5.18) and (5.21)-(5.23) ensures that all the closed-loop signals are bounded and the state vector $\mathbf{x(t)}$ converges to the desired trajectory $\mathbf{x_d} = [\mathbf{x_d}, \dot{\mathbf{x}}_\mathbf{d}, ..., \mathbf{x_d^{(n-1)}}]^\mathbf{T}$.

Proof: To establish the global boundedness, we define the following Lyapunov function candidate

$$V(t) = \sum_{i=1}^{n} \frac{1}{2} z_i^2 + \frac{1}{2\gamma} \tilde{\mathbf{a}}^T \tilde{\mathbf{a}} + \frac{b_p}{2\eta} \tilde{\phi}^2 + \frac{1}{2q} \int_0^R \tilde{p}_b^2(t,r) dr \tag{5.24}$$

The derivative $\dot{V}$ is

$$\dot{V}(t) = \sum_{i=1}^{n} z_i \dot{z}_i + \frac{1}{\gamma} \tilde{\mathbf{a}}^T \dot{\tilde{\mathbf{a}}} + \frac{b_p}{\eta} \tilde{\phi} \dot{\tilde{\phi}} + \frac{1}{q} \int_0^R \tilde{p}_b(t,r) \frac{\partial}{\partial t} \tilde{p}_b(t,r) dr \tag{5.25}$$

Multiply (5.10) by z_1 and (5.11) by z_i , we have

$$\begin{aligned} z_1 \dot{z}_1 &= -c_1 z_1^2 + z_1 z_2 \\ z_i \dot{z}_i &= -z_{i-1} z_i - c_i z_i^2 + z_i z_{i+1}, \quad i = 2, 3, \cdots, n-1 \end{aligned} \tag{5.26}$$

noticing that

$$\begin{aligned} b_p v(t) &= b_p \hat{\phi} v_1(t) \\ &= v_1(t) - b_p \tilde{\phi} v_1(t) \end{aligned} \tag{5.27}$$

substitute (5.27) into (5.17), we have

$$\dot{z}_n = -c_n z_n - z_{n-1} + \tilde{\mathbf{a}}^T Y - sign(z_n) \hat{B} - d_b[v](t) - b_p \tilde{\phi} v_1(t) \tag{5.28}$$

$$\begin{aligned}
\dot{V}(t) &= (-c_1 z_1^2 + z_1 z_2) + (-z_1 z_2 - c_2 z_2^2 + z_2 z_3) \\
&\quad + \cdots + (-z_{n-2} z_{n-1} - c_{n-1} z_{n-1}^2 + z_{n-1} z_n) + z_n \dot{z}_n \\
&\quad + \frac{1}{\gamma} \tilde{\mathbf{a}}^T \dot{\tilde{\mathbf{a}}} + \frac{b_p}{\eta} \tilde{\phi} \dot{\tilde{\phi}} + \frac{1}{q} \int_0^R \tilde{p}_b(t,r) \frac{\partial}{\partial t} \tilde{p}_b(t,r) dr \\
&= -\sum_{i=1}^{n} c_i z_i^2 + \tilde{\mathbf{a}}^T Y z_n - b_p \tilde{\phi} v_1(t) z_n - |z_n| \hat{B} - d_b[v](t) z_n \\
&\quad + \frac{1}{\gamma} \tilde{\mathbf{a}}^T \dot{\tilde{\mathbf{a}}} + \frac{b_p}{\eta} \tilde{\phi} \dot{\tilde{\phi}} + \frac{1}{q} \int_0^R \tilde{p}_b(t,r) \frac{\partial}{\partial t} \tilde{p}_b(t,r) dr
\end{aligned} \tag{5.29}$$

as defined in (5.6) and (5.15)

$$d_b[v](t) = \int_0^R p_b(r) F_r[v](t) dr \tag{5.30}$$

$$B(v(t)) = \int_0^R p_b(r) |F_r[v](t)| dr, \tag{5.31}$$

we have

$$\begin{aligned}
\dot{V}(t) &\leq -\sum_{i=1}^{n} c_i z_i^2 + \frac{1}{\gamma} \tilde{\mathbf{a}}^T (\dot{\tilde{\mathbf{a}}} + \gamma Y z_n) + \frac{b_p}{\eta} \tilde{\phi} (\dot{\tilde{\phi}} - \eta v_1 z_n) - |z_n| \hat{B} + |d_b[v](t)||z_n| \\
&\quad + \int_0^R \tilde{p}_b(t,r) |F_r[v](t)||z_n| dr \\
&\leq -\sum_{i=1}^{n} c_i z_i^2 + \frac{1}{\gamma} \tilde{\mathbf{a}}^T (\dot{\tilde{\mathbf{a}}} + \gamma Y z_n) + \frac{b_p}{\eta} \tilde{\phi} (\dot{\tilde{\phi}} - \eta v_1 z_n) - |z_n| \tilde{B} \\
&\quad + \int_0^R \tilde{p}_b(t,r) |F_r[v](t)||z_n| dr
\end{aligned} \tag{5.32}$$

by adaptation laws (5.21), (5.22) and (5.23)

$$\dot{V}(t) \leq -\sum_{i=1}^{n} c_i z_i^2 \tag{5.33}$$

Equations (5.24) and (5.33) imply that V is a non-increasing function. Hence, $z_1, \cdots, z_n$, $\hat{\mathbf{a}}$, $\hat{\phi}(t)$, and $\hat{p}_b(t,r)$ are bounded. Notice that

$$-\int_{t_0}^{\infty} \dot{V}(t) = V(t_0) - v(\infty) < \infty \quad \forall t_0 \geq 0 \tag{5.34}$$

implies

$$0 \leq \int_{t_0}^{\infty} \sum_{i=1}^{n} c_i z_i^2 < \infty \quad \forall t_0 \geq 0 \tag{5.35}$$

since c_i are positive constants, $z_i \in L^2$, for $i = 1, \cdots, n$. If we can show that $\dot{z}_i$ is bounded, then from Barbalat Lemma (see Appendix), we will have $z_i \to 0$ as $t \to \infty$ for $i = 1, 2, \cdots, n$. Furthermore, we want to show that $x_i \to x_d^{i-1}$ as $t \to \infty$ for $i = 1, 2, \cdots, n$.

For $i = 1$:

$$\dot{z}_1(t) = z_2(t) - c_1 z_1(t) \tag{5.36}$$

since z_1 and z_2 are bounded, $\dot{z}_1(t)$ is bounded, from Barbalat Lemma, $z_1 \to 0$.

$$z_1(t) = x_1(t) - x_d(t) \tag{5.37}$$

we have $x_1 \to x_d$ as $t \to \infty$.

When $i = 2, \cdots, n-1$:

$$\dot{z}_i(t) = -z_{i-1}(t) - c_i z_i(t) + z_{i+1}(t) \tag{5.38}$$

we have $z_i \to 0$ as $t \to \infty$. From definition

$$z_i(t) = x_i(t) - x_d^{(i-1)}(t) - \alpha_{i-1}$$

$$\begin{aligned}\alpha_1(t) &= -c_1 z_1(t) \\ \alpha_i(t) &= -c_i z_i(t) - z_{i-1}(t) + \dot{\alpha}_{i-1}(x_1, \cdots, x_{i-1}, x_d, \cdots, x_d^{i-1}), \\ & \quad for \;\; i = 2, 3, \cdots, n-1 \end{aligned} \tag{5.39}$$

where α_{i-1} is the function of $z_1(t), \cdots, z_{i-1}(t)$, by conduction, $\alpha_{i-1} \to 0$. Thus, we have $x_1 \to x_d$ as $t \to \infty$.

When $i = n$:

$$\dot{z}_n(t) = a^T Y + b_p v - d_b[v](t) - x_d^{(n)}(t) - \dot{\alpha}_{n-1} \tag{5.40}$$

It can be shown that the right hand side of the above equation is bounded. $\dot{\alpha}_{n-1}$ is bounded because its definition and the facts that $z_i, i = 1, \cdots, n$ are bounded. The $b_p v - d_b[v](t)$ boundedness is proved in the previous section. From the assumption of continuity of Y and boundedness of all other variables, $\dot{z}_n(t)$ is bounded. By Barbalat Lemma, $z_n \to 0$. Using the same argument as for $i < n$, we conclude that $x_n \to x_d^{n-1}$ as $t \to \infty$.

$\triangle\triangle\triangle$

5.3. Simulation Studies

In this section, we illustrate the methodology based on the adaptive back-stepping control design presented in the previous sections using the same nonlinear system described by

$$\dot{x} = a\frac{1 - e^{-x(t)}}{1 + e^{-x(t)}} + bw(t) \tag{5.41}$$

where $w(t)$ represents the output of the hysteresis. The hysteresis is given as

$$w(t) = p_0 v(t) - \int_0^R p(r) F_r[v](t) dr. \tag{5.42}$$

The actual parameter values are $b = 1$ and $a = 1$. Without control, i.e., $v(t) = 0$, so $w(t) = 0$, we can use basic analytical method to show that the system in (5.41) is unstable. The objective is to control the system state x to follow the desired trajectory.

The simulations are conducted under two sets of parameters. Both show that the proposed robust controller demonstrates excellent tracking performance. In Case 1), we consider the desired trajectory as $x_d = 5sin(2t) + cos(3.2t)$, the hysteresis density function is $p(r) = \alpha e^{-\beta(r-\sigma)^2}$ for $r \in [0, 100]$, with parameters $\alpha = 0.5, \beta = 0.0014$, and $\sigma = 1$. In the simulation, the robust adaptive control laws (5.21)-(5.23) are used with $c_1 = 0.9368$. In the adaptation laws, we choose $\gamma = 0.13$, $\eta = 0.05$ and $q = 0.437$ with the initial parameters values being $\hat{a}(0) = 0.13$, $\hat{\phi}(0) = 0.431$, and $\hat{p}_b(0, r) = 0$. The initial state is chosen as $x(0) = 2.05$, sampling time is 0.002. To avoid the vibration caused by the discontinuity of the sign function, we use saturate function $sat(s/\epsilon) = s/\epsilon$ instead of the sign function $sign(s)$ in the simulation. The proof is valid except in a small neighborhood of $(-\epsilon, \epsilon])$, and in this example we choose $\epsilon = 0.01$. We also assume that the hysteresis internal state was $\psi(r) = 0.07$ for $r \in [0, R]$ before $v(0)$ is applied. For the calculation of $\hat{B}(t)$, we replace the integration by the sum $\sum_0^N$. In the simulation, we choose $N = 4000$.

To illustrate the effectiveness of the proposed control scheme, the simulation are also conducted without controlling the effects of hysteresis, which is implemented by setting $v_h(t) = 0$ in the controller $v(t)$. This implies that the control compensation for the hysteresis nonlinearity is ignored. Simulation results are shown in Figs.5.1 - 5.4 for the system (5.4) to track the desired trajectory $x_d(t) = 5sin(2t) + cos(3.2t)$. Figs.5.1 and 5.2 show the state trajectories and tracking errors for the desired trajectory with and without considering the effects of hysteresis, where the solid line is the results for $v_h(t) \neq 0$ and the dotted line is for $v_h(t) = 0$. From Figs.5.1 and 5.2,

we see that the proposed robust controller clearly demonstrates excellent tracking performance and the developed control algorithm can overcome the effects of the hysteresis. We should mention that we also conducted the simulations for $N = 6000$, which results in smaller intervals. The simulation results were almost identical to those presented above. This further verifies that the developed control algorithm is computationally implementable.

In case 2), we consider the desired trajectory $x_d = 3sin(2t) + 0.1cos(6.7t)$, which is the same desired trajectory used in the previous chapter. The hysteresis density function $p(r) = \alpha e^{-\beta(r-\sigma)^2}$ for $r \in [0, 100]$, with parameters $\alpha = 0.5, \beta = 0.00105$, and $\sigma = 1$, we use the robust adaptive control laws given by (5.21)-(5.23) with $c_1 = 0.37$. In this case, we choose $\gamma = 0.33$, $\eta = 0.41$ and $q = 0.573$ with the initial conditions $\hat{a}(0) = 1/4.41$, $\hat{\phi}(0) = 1/2.32$, and $\hat{p}_b(0, r) = 0$. The initial state is chosen as $x(0) = 2.05$, sampling time is 0.01, and $\epsilon = 0.05$. We also assume that the hysteresis internal state was $\psi(r) = 0.07$ for $r \in [0, R]$ before $v(0)$ is applied. For the calculation of $\hat{B}(t)$, we replace the integration by the sum $\sum_0^N$ with $N = 4000$. Figs.5.5 - 5.9 show the simulation results. Also we point out that, under the above assumptions, if we do not control the hysteresis effect, i.e. let $v_h(t) = 0$, the system state will not follow the desired trajectory, $x(t) - x_d(t)$ is divergent as $t \to \infty$.

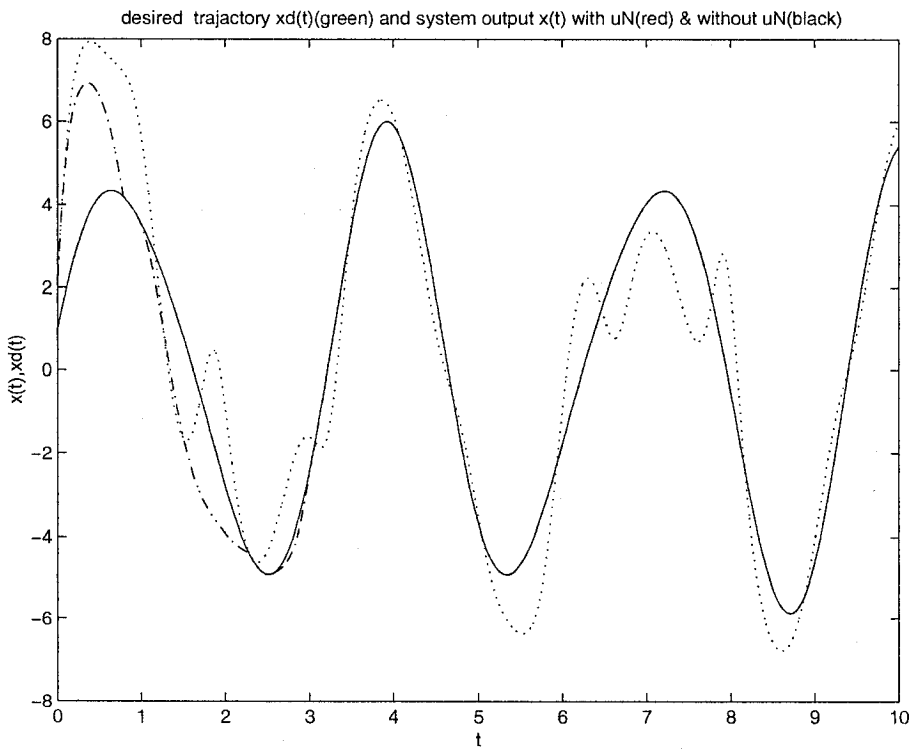

Figure 5.1: Case 1): Desired trajectory $x_d(t) = 5sin(2t) + cos(3.2t)$, *system outputs* $x(t)$ *with control term* v_h *(-.) and* $v_h = 0$ *(dotted line)*

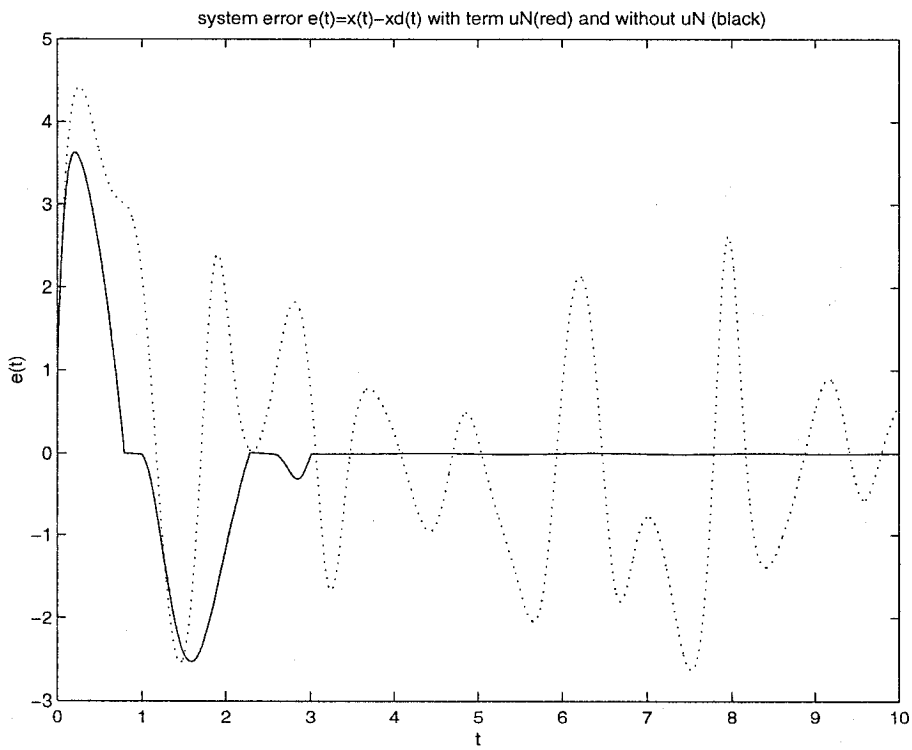

Figure 5.2: Case 1): Tracking errors $x(t) - x_d(t)$ *for* $x_d(t) = 5sin(2t) + cos(3.2t)$ *with control term* v_h *and* $v_h = 0$ *(dotted line)*

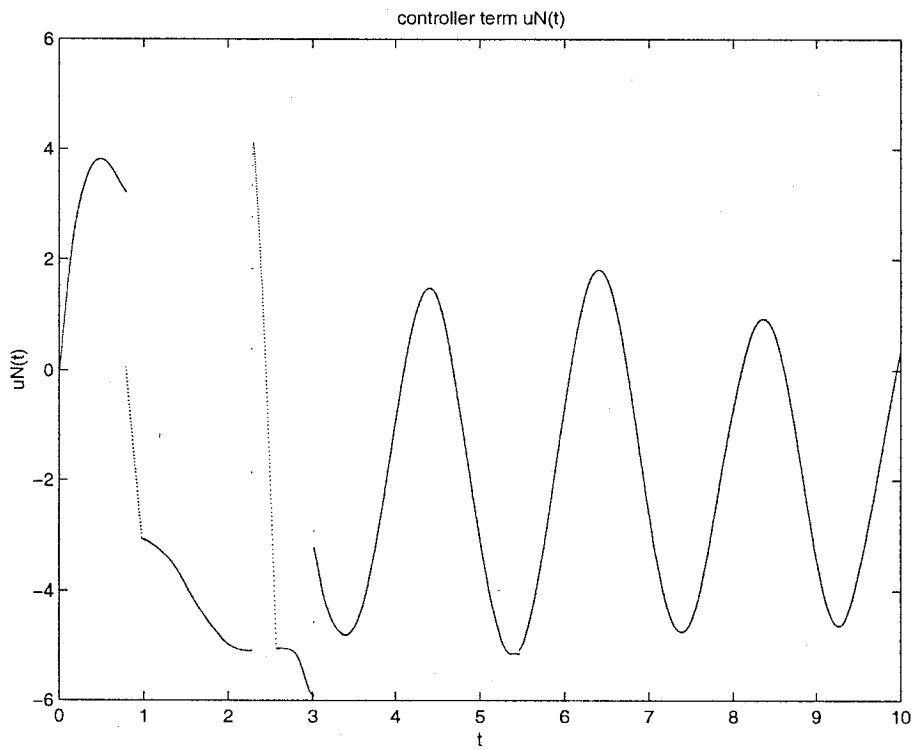

Figure 5.3: Case 1): Signal v_h designed to reduce the tracking error caused by the hysteresis when $x_d(t) = 5sin(2t) + cos(3.2t)$

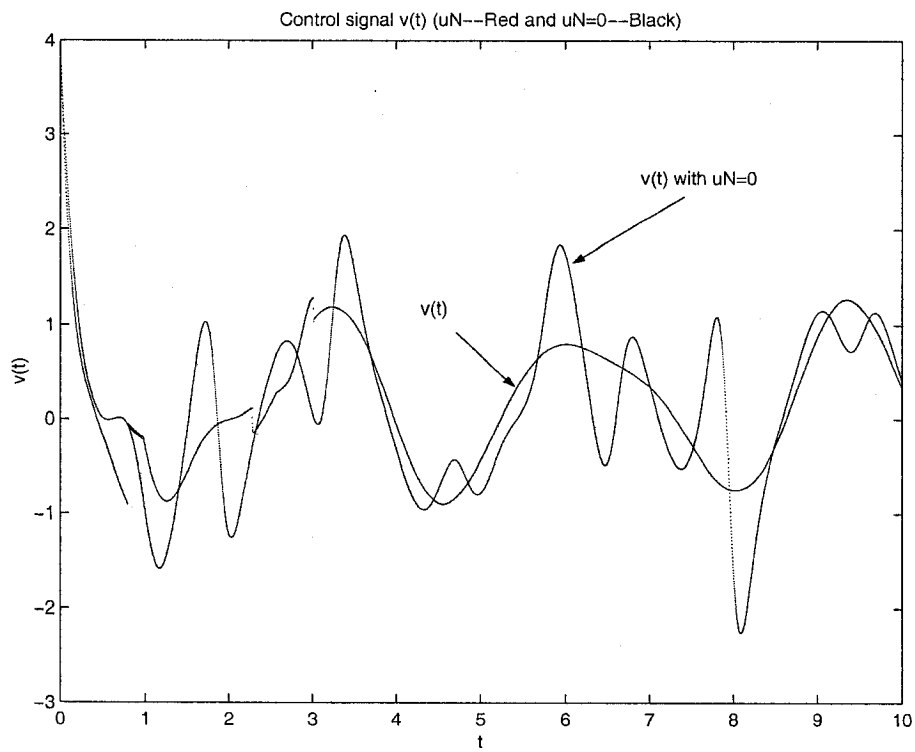

Figure 5.4: Case 1): Control signal $v(t)$ and the hysteresis output $w(t)$ when $x_d(t) = 5sin(2t) + cos(3.2t)$

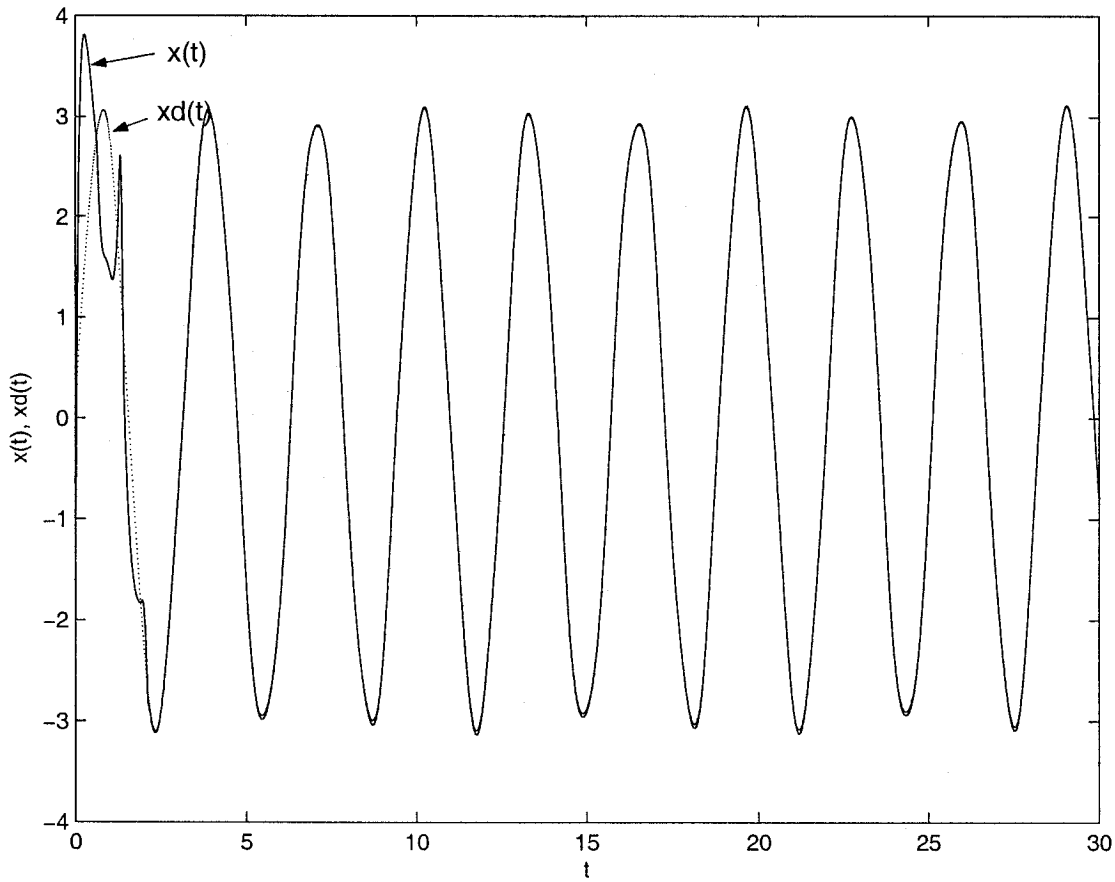

Figure 5.5: Case 2): System state $x(t)$ and the desired trajectory $x_d(t) = 3sin(2t) + 0.1cos(6.7t)$

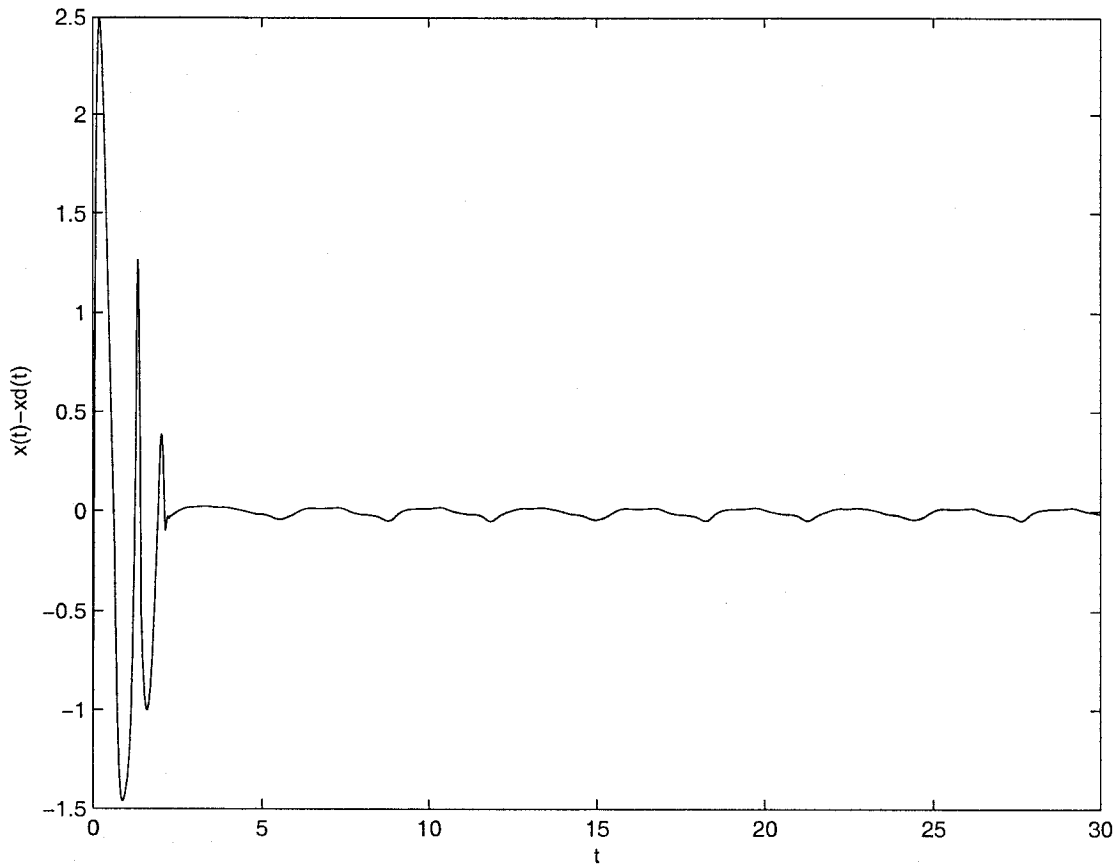

Figure 5.6: Case 2): Tracking errors $x(t) - x_d(t)$ *for* $x_d(t) = 3sin(2t) + 0.1cos(6.7t)$

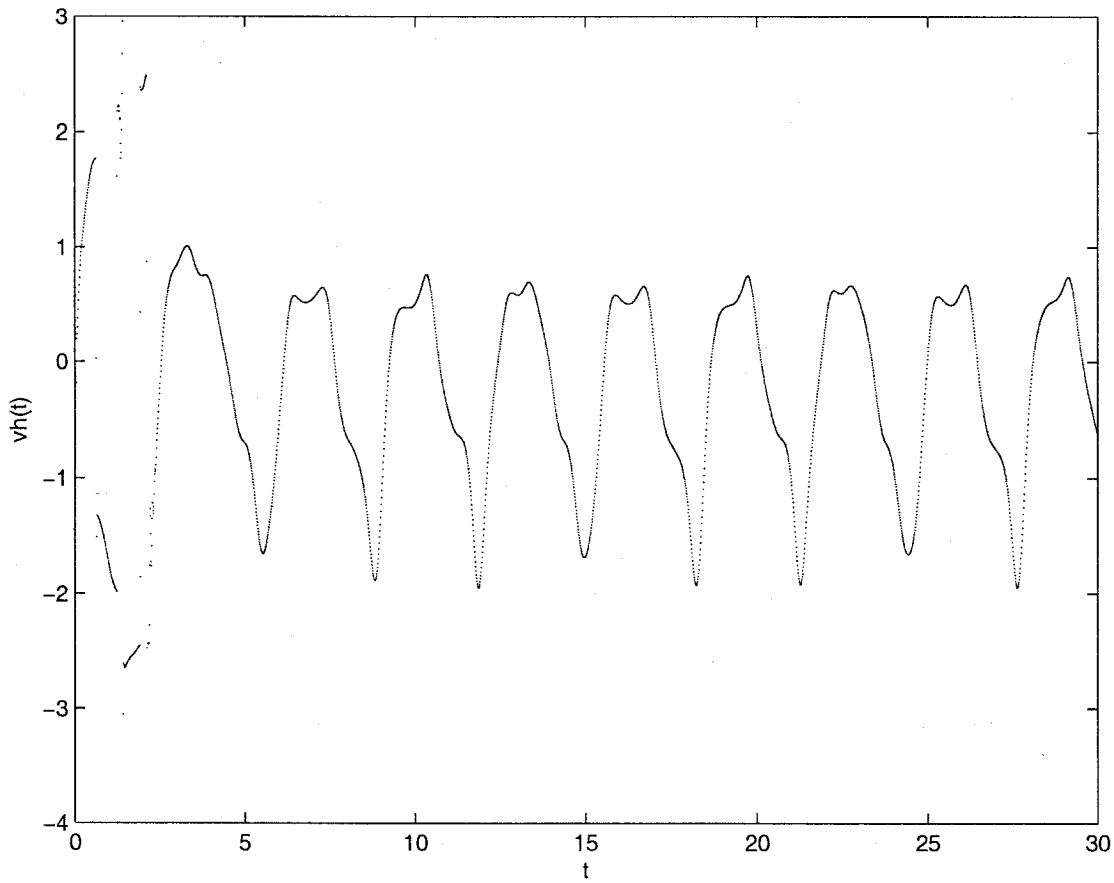

Figure 5.7: Case 2): Signal v_h designed to reduce the tracking error caused by the hysteresis when $x_d(t) = 3sin(2t) + 0.1cos(6.7t)$

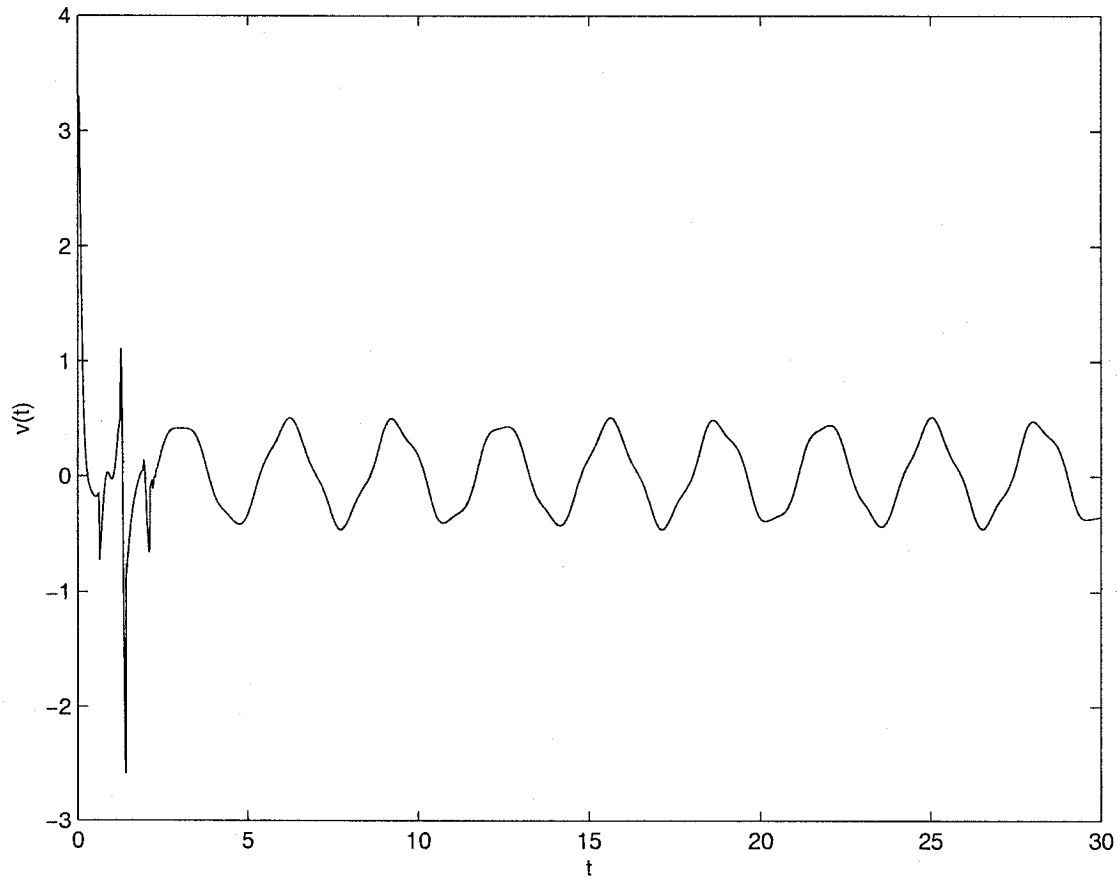

Figure 5.8: Case 2): Control signal $v(t)$ when $x_d(t) = 3sin(2t) + 0.1cos(6.7t)$

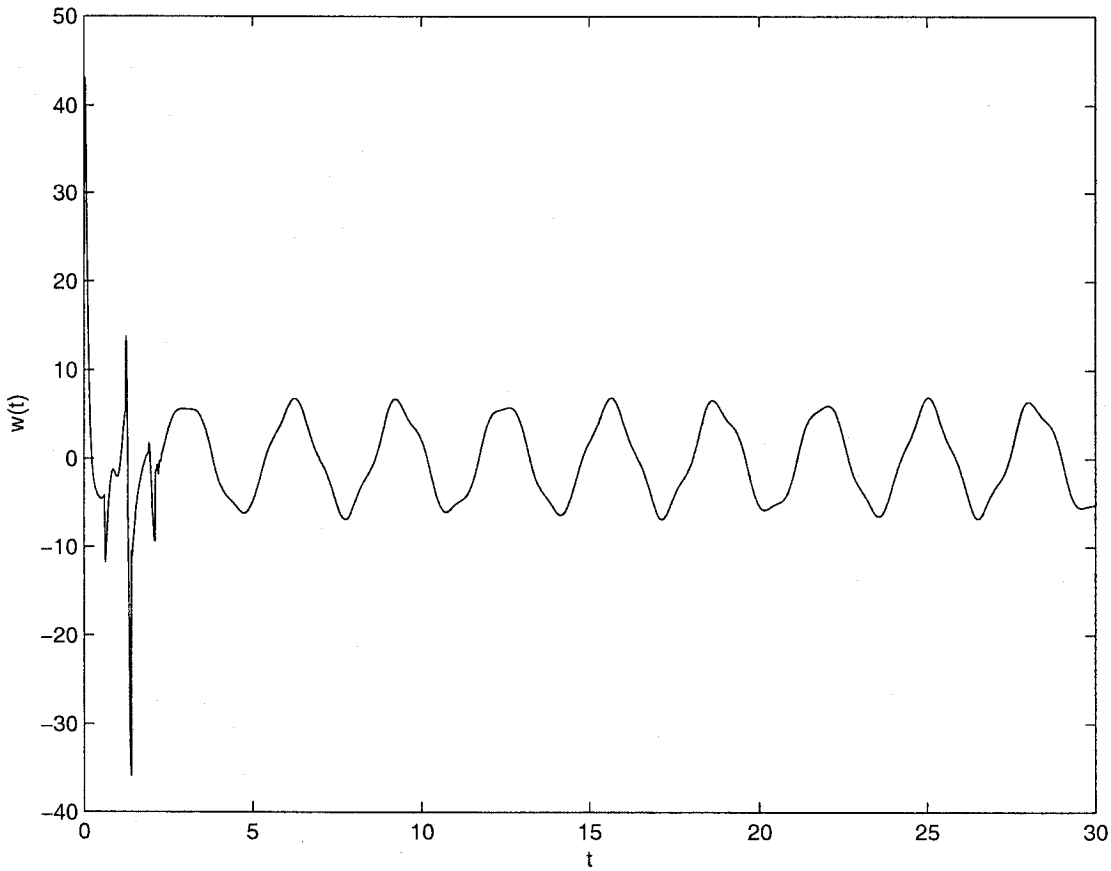

Figure 5.9: Case 2): Hysteresis output $w(t)$ when $x_d(t) = 3sin(2t) + 0.1cos(6.7t)$

Chapter 6

Controller Design Based on Neural Network Adaptive Control

6.1. Problem Statement

Consider an SISO nonlinear system with the hysteresis presented as an input

$$\begin{aligned} \dot{x}_i &= x_{i+1}, \qquad i = 1, 2, \cdots, n-1 \\ \dot{x}_n &= a(x) + b(x)w(t) + d_e(t) \\ y &= x_1 \end{aligned} \tag{6.1}$$

where $x = [x_1, x_2, \cdots, x_n]^T \in \Re^n$ is the system state; $a(x)$ and $b(x)$ are unknown smooth functions; $d_e(t)$ represents the system uncertainties such as the external disturbances and modelling errors bounded by a known constant $d_0 > 0$, i.e., $|d_e(t)| \leq d_0$. $w(t)$ is the hysteresis operator given by

$$w(t) = p_0 v(t) - d[v](t) \tag{6.2}$$

$$d[v](t) = \int_0^R p(r) F_r[v](t) dr \tag{6.3}$$

where $p_0 = \int_0^R p(r)dr$. For convenience, $F_r[v, \psi_1]$ is denoted by $F_r[v]$ for any given hysteresis initial state $\psi_1 \in \Psi$. By using this hysteresis model, system (6.1) becomes

$$\begin{aligned} \dot{x}_i &= x_{i+1}, \qquad i = 1, 2, \cdots, n-1 \\ \dot{x}_n &= a(x) + b(x)p_0 v(t) - b(x)d[v](t) + d_e(t) \\ y &= x_1 \end{aligned} \tag{6.4}$$

In this chapter, the study is focused on the adaptive control problem of the physical plants operating in bounded regions and the state variable belongs to a compact set $\Omega_x \subset \Re^n$. The objective is to design a stable control law $v(t)$ to force the state vector $x = [x_1, x_2, \cdots, x_n]^T \in \Omega_x$ to follow a specified and desired trajectory $\mathbf{x_d} = [\mathbf{x_d}, \dot{\mathbf{x}}_\mathbf{d}, ..., \mathbf{x}_\mathbf{d}^{(\mathbf{n-1})}]^\mathbf{T}$ as close as possible.

For the considered systems the following assumptions are made:

Assumption 1: The sign of $b(x)$ is known and there exists a constant $b_0 > 0$, $b_0 < |b(x)|$, $\forall x \in \Omega_x$. Since the sign of $b(x)$ is known and $b(x)$ is not equal to zero, we may assume that $b(x) > 0$.

Assumption 2: There exists a smooth function $\bar{b}(x)$ such that $|b(x)| \leq \bar{b}(x)$ and $b(x)/\bar{b}(x)$ is independent of the state x_n, $\forall x \in \Omega_x \subset \Re^n$.

Assumption 3: The desired trajectory $\mathbf{x_d} \in \mathbf{C^{(n)}(R)}$ is available and $\mathbf{x_d} \in \mathbf{\Omega_d} \subset \Re^\mathbf{n}$ with Ω_d being a compact set.

Assumption 4: There exist a known constant $p_{0min} > 0$ and a known function $p_{max}(r)$, such that $p_0 > p_{0min}$ and $p(r) \leq p_{max}(r)$ for all $r \in [0, R]$.

Remark: Assumptions 1 and 3 are generally adopted for the design of a tracking controller. As mentioned in [19], Assumption 2 imposes an additional restriction on the class of systems. However, many physical systems possess such a property. Examples of such systems include pendulum plants, magnetic levitation systems and single link robots with flexible joints. As for Assumption 4, based on the properties

of the density function $p(r)$, it is reasonable to set an upper bound p_{max} for $p(r)$. Here $p_{0min} > 0$ must be satisfied, otherwise $p_0 = 0$ implies $w(t) = 0$.

To simplify the notification, let

$$g(x) = b(x)p_0/\bar{b}(x)p_{0max}$$

where $p_{0max} = \int_0^R p_{max}(r)dr$. From Assumptions 1, 2 and 3, $g(x)$ is independent of x_n and $0 < g(x) \leq 1$.

Define the tracking error vector $\tilde{\mathbf{x}}$ as

$$\tilde{\mathbf{x}} = \mathbf{x} - \mathbf{x_d},$$

and a filtered tracking error as

$$s(t) = (\frac{d}{dt} + \lambda)^{(n-1)}\tilde{x}_1(t), \qquad \lambda > 0 \tag{6.5}$$

$s(t)$ can be rewritten as $s(t) = [\Lambda^T 1]\tilde{\mathbf{x}}(t)$ with $\Lambda^T = [\lambda^{(n-1)}, (n-1)\lambda^{(n-2)}, ..., (n-1)\lambda]$.

It has been shown in [55] that the definition given in (6.5) has following properties: (i) the equation $s(t) = 0$ defines a time-varying hyperplane in $\Re^n$ on which the tracking error vector $\tilde{\mathbf{x}}(t)$ decays exponentially to zero, (ii) if $\tilde{\mathbf{x}}(0) = 0$ and $|s(t)| \leq \epsilon$, where ϵ is a constant, then $\tilde{\mathbf{x}}(t) \in \Omega_\epsilon \triangleq \{\tilde{\mathbf{x}}(t) \mid |\tilde{\mathbf{x}}_i| \leq 2^{i-1}\lambda^{i-n}\epsilon, i = 1, ..., n\}$ for $\forall t \geq 0$, and (iii) if $\tilde{\mathbf{x}}(0) \neq 0$ and $|s(t)| \leq \epsilon$, then $\tilde{\mathbf{x}}(t)$ will converge to Ω_ϵ within a time-constant $(n-1)/\lambda$.

6.2. Controller Design

In this section, we first assume that the nonlinear functions $a(x)$ and $b(x)$ are known, the hysteresis weight function $p(r)$ is available, and the system uncertainty $d_e(t) = 0$. Notice that the Prandtl-Ishlinskii model (6.2) decomposes the hysteresis behavior

into two terms: the linear reversible component $p_0 v(t)$ and the nonlinear hysteretic component $d[v](t)$. If $d[v](t) = 0$, then the system input is $w(t) = p_0 v(t)$, there exists an ideal feedback control v^* as suggested in [19]. Under this control the state vector $\mathbf{x}$ will follow the desired trajectory $\mathbf{x_d}$ asymptotically.

Consider the state feedback control

$$v^*(t) = \frac{1}{\overline{b}(x)p_{0max}} v_n^*(t) \tag{6.6}$$

with

$$v_n^*(t) = -\frac{1}{g(x)}[a(x) + \mu] - s[\frac{1}{\delta g(x)} + \frac{1}{\delta g^2(x)} - \frac{\dot{g}(x)}{2g^2(x)}], \tag{6.7}$$

where $\delta > 0$ is a constant and

$$\mu = (0, \Lambda^T)\tilde{\mathbf{x}} - y_d^{(n)}$$

By definition (6.5), the time derivative of s with the input $v^*(t)$ for the system (6.4) can be written as

$$\dot{s}(t) = -[\frac{1}{\delta} + \frac{1}{\delta g(x)} - \frac{\dot{g}(x)}{2g(x)}]s. \tag{6.8}$$

Define a Lyapunov function candidate $V_1 = \frac{1}{2g(x)}s^2$, the time derivative of V_1 along (6.8) equals

$$\dot{V}_1(t) = -\frac{2}{\delta}[1 + \frac{1}{g(x)}]\frac{1}{2g(x)}s^2. \tag{6.9}$$

Since $0 < g(x) \leq 1$, it follows that

$$\dot{V}_1(t) \leq -\frac{4}{\delta}V_1. \tag{6.10}$$

the solution of the above inequality satisfies

$$V_1(t) \leq e^{-\frac{4}{\delta}(t-t_0)}V_1(t_0), \quad \forall \ t \geq t_0 \tag{6.11}$$

$|b(x)| \geq b_0 > 0$, $\lim_{t\to\infty} V_1(t) = 0$ implies that $\lim_{t\to\infty} s = 0$. Furthermore, using the properties of s, $\lim_{t\to\infty} \|\tilde{\mathbf{x}}\| = 0$.

It is proved that when functions $a(x)$ and $b(x)$ are known and the hysteresis weight function $p(r)$ is available, then using the control input v^* defined in (6.6), the tracking error vector $\tilde{\mathbf{x}} = \mathbf{x} - \mathbf{x_d}$ converges asymptotically to zero if $d[v](t) = 0$ and the system uncertainty $d_e(t) = 0$.

When $a(x)$, $b(x)$ and $p(r)$ are unknown, the controller v^* given in (6.6) cannot be implemented. A reasonable approach is to use an estimated v to approximate $v^*(t)$. From the previous discussion, v_n^* does exist. Under Assumptions 1 and 2, $a(x)$ and $b(x)$ are continuous functions of x and v_n^* is continuous with respect to $x(t)$ and $\mathbf{x_d}$. It has been assumed that $\mathbf{x_d}$ is continuous on the compact set Ω_d and $x(t)$ takes values in compact set Ω_x. We can see that all conditions for the Universal Approximation Theorem are satisfied. Therefore, function approximation methods such as neural networks or fuzzy systems can be applied. In the following discussion, neural networks will be used to approximate v_n^*.

Let $z = (x^T, s, s/\delta, \mu)^T$, z belongs to a compact set

$$\Omega_z = \{(x^T, s, s/\delta, \mu) | x \in \Omega_x, x_d \in \Omega_d\}$$

v_n^* is a function of z. As mentioned in [19], s and s/δ are in different scales when a small δ is chosen. Feeding the neural networks with both s and s/δ will improve the approximation accuracy. For any arbitrary constant ϵ_0, there exists an integer l^*, such that for all $l \geq l^*$, the following approximation holds:

$$v_n^*(t) = \theta^{*T}\Phi(z) + \epsilon_l \qquad \forall z \in \Omega_z \tag{6.12}$$

where l is number of nodes of the neural network, $\Phi(z) \in \Re^l$ is the basis function vector and the approximation error ϵ_l satisfies $|\epsilon_l| \leq \epsilon_0$. θ^* is the ideal weight defined

by

$$\theta^* = arg\ min_{\theta \in \Re^l}\{sup_{z \in \Omega_z}|\theta^T \Phi(z) - v_n^*(t)|\} \tag{6.13}$$

Now, the unknown nonlinearity problem is transformed to a problem of estimating the ideal parameter vector θ^*. Let $\hat{\theta}$ be an estimate of the ideal neural network weight θ^*, and the controller $v_n(t)$ is chosen as

$$v_n(t) = \hat{\theta}^T \Phi(z) \tag{6.14}$$

with the adaptation law

$$\dot{\hat{\theta}} = -\Gamma[\Phi(z)s + \sigma\hat{\theta}] \tag{6.15}$$

where $\Gamma, \sigma > 0$ are adaptive gains.

In order to cancel the effect caused by term $d[v](t)$, we notice that $d[v](t)$ is determined by the weight function $p(r)$, which is not a function of t. So it can be considered as a parameter for each fixed $r \in [0, R]$ and adjusted by the adaptation law. Let $\hat{p}(t, r)$ be the estimate of $p(r)$ at any $r \in [0, R]$. Define

$$v_h(t) = \int_0^R \frac{\hat{p}(t,r)}{p_{0min}} |F_r[v](t)| dr sign(s) \tag{6.16}$$

with the adaptation law

$$\frac{\partial}{\partial t}\hat{p}(t,r) = -\gamma\eta\hat{p}(t,r) + \eta\frac{\bar{b}(x)p_{0max}}{p_{0min}}|F_r[v](t)||s| \tag{6.17}$$

where $\gamma > 0$ and $\eta > 0$ are adaptive parameters.

The adaptive controller is then defined as following

$$v(t) = \frac{1}{\bar{b}(x)p_{0max}} v_n(t) + v_h(t) \tag{6.18}$$

where v_n and v_h are given by (6.14) and (6.16). Substituting $v(t)$ into system (6.4), the time derivative of s can be rewritten as

$$\begin{aligned} \dot{s}(t) &= [a(x) + \mu] + g(x)v_n + b(x)p_0 v_h(t) \\ &\quad -b(x)\int_0^R p(r)F_r[v](t)dr + d_e(t) \end{aligned} \tag{6.19}$$

To establish the global boundedness, let

$$\tilde{\theta} = \hat{\theta} - \theta^*, \tag{6.20}$$

$$\tilde{p}(t,r) = \hat{p}(t,r) - p(r), \quad \forall\, r \in [0,R]. \tag{6.21}$$

We choose the Lyapunov function candidate as

$$V(t) = \frac{1}{2g(x)}s^2 + \frac{1}{2}\tilde{\theta}^T\Gamma^{-1}\tilde{\theta} + \frac{1}{2\eta}\int_0^R \tilde{p}^2(t,r)dr \tag{6.22}$$

The time derivative of V is

$$\begin{aligned}\dot{V}(t) &= -[\frac{1}{\delta g(x)} + \frac{1}{\delta g^2(x)}]s^2 - \epsilon_l s + \frac{d_e(t)}{g(x)}s \\ &\quad +\tilde{\theta}^T[\Phi(z)s + \Gamma^{-1}\dot{\hat{\theta}}] + \frac{1}{\eta}\int_0^R \tilde{p}(t,r)\frac{\partial}{\partial t}\tilde{p}(t,r)dr \\ &\quad +\bar{b}(x)p_{0max}s[v_h(t) - \int_0^R \frac{p(r)}{p_0}F_r[v](t)dr]\end{aligned} \tag{6.23}$$

Utilizing the adaptation law (6.15),

$$\tilde{\theta}^T[\Phi(z)s + \Gamma^{-1}\dot{\hat{\theta}}] = -\sigma\tilde{\theta}^T\hat{\theta}. \tag{6.24}$$

To simplify the last three terms in (6.23), from definition (6.16), we have

$$\begin{aligned}&\bar{b}(x)p_{0max}s[v_h(t) - \frac{1}{p_0}\int_0^R p(r)F_r[v](t)dr] \\ &\quad +\frac{1}{\eta}\int_0^R \tilde{p}(t,r)\frac{\partial}{\partial t}\tilde{p}(t,r)dr \\ &= \bar{b}(x)p_{0max}s[-\frac{sign(s)}{p_{0min}}\int_0^R t,\hat{p}(r)|F_r[v](t)|dr \\ &\quad -\frac{1}{p_0}\int_0^R p(r)F_r[v](t)dr] \\ &\quad +\frac{1}{\eta}\int_0^R \tilde{p}(t,r)\frac{\partial}{\partial t}\tilde{p}(t,r)dr\end{aligned} \tag{6.25}$$

$$\leq \bar{b}(x)p_{0max}[-\frac{|s|}{p_{0min}}\int_0^R \hat{p}(t,r)|F_r[v](t)|dr + \frac{|s|}{p_0}\int_0^R p(r)|F_r[v](t)|dr] + \frac{1}{\eta}\int_0^R \tilde{p}(t,r)\frac{\partial}{\partial t}\tilde{p}(t,r)dr \tag{6.26}$$

$$\leq \frac{\bar{b}(x)p_{0max}|s|}{p_{0min}}[-\int_0^R (\hat{p}(t,r)-p(r))|F_r[v](t)|dr] + \frac{1}{\eta}\int_0^R \tilde{p}(t,r)\frac{\partial}{\partial t}\tilde{p}(t,r)dr \tag{6.27}$$

Noticing that $\tilde{p}(t,r) = \hat{p}(r) - p(r)$, and substituting (6.17) into the above equation, we have

$$\frac{\bar{b}(x)p_{0max}|s|}{p_{0min}}[-\int_0^R (\hat{p}(t,r)-p(r))|F_r[v](t)|dr] + \frac{1}{\eta}\int_0^R \tilde{p}(t,r)\frac{\partial}{\partial t}\tilde{p}(t,r)dr \tag{6.28}$$

$$\begin{aligned} &\leq -\frac{\bar{b}(x)p_{0max}|s|}{p_{0min}}\int_0^R \tilde{p}(t,r)|F_r[v](t)|dr \\ &\quad +\frac{1}{\eta}\int_0^R \tilde{p}(t,r)[-\gamma\eta\hat{p}(t,r) + \eta\frac{\bar{b}(x)p_{0max}}{p_{0min}}|F_r[v](t)||s|]dr \\ &\leq -\gamma\int_0^R \tilde{p}(t,r)\hat{p}(t,r)dr \end{aligned} \tag{6.29}$$

Therefore,

$$\begin{aligned} \dot{V}(t) \;\leq\; & -[\frac{1}{\delta g(x)} + \frac{1}{\delta g^2(x)}]s^2 - \epsilon_l s + \frac{d_e(t)}{g(x)}s \\ & -\sigma\tilde{\theta}^T\hat{\theta} - \gamma\int_0^R \tilde{p}(t,r)\hat{p}(t,r)dr \end{aligned} \tag{6.30}$$

Furthermore, using the following inequalities

$$-\sigma\tilde{\theta}^T\hat{\theta} \leq -\frac{\sigma}{2}\|\tilde{\theta}\|^2 + \frac{\sigma}{2}\|\theta^*\|^2 \tag{6.31}$$

$$|\epsilon_l s| \leq \sqrt{2}|\epsilon_l s| \leq \frac{1}{\delta g(x)}s^2 + \frac{\delta g(x)}{2}\epsilon_l^2 \tag{6.32}$$

$$|\frac{d_e(t)}{g(x)}s| \leq \frac{1}{2\delta g^2(x)}s^2 + \frac{\delta}{2}d_e^2(t) \tag{6.33}$$

$$-\tilde{p}(t,r)\hat{p}(t,r) \leq -\frac{1}{2}\tilde{p}^2(t,r) + \frac{1}{2}p^2(r) \tag{6.34}$$

and noticing that $0 < g(x) \leq 1$, $|\epsilon_l| \leq \epsilon_0$, and $|d_e(t)| \leq d_0$,

$$\begin{aligned}\dot{V}(t) \leq & -\frac{1}{2\delta g(x)}s^2 - \frac{\sigma}{2}\|\tilde{\theta}\|^2 - \frac{\gamma}{2}\int_0^R \tilde{p}^2(t,r)dr \\ & +\frac{\delta}{2}\epsilon_0^2 + \frac{\delta}{2}d_0^2 + \frac{\sigma}{2}\|\theta^*\|^2 + \frac{\gamma}{2}\int_0^R p^2(r)dr\end{aligned} \tag{6.35}$$

let

$$\tau = min(\frac{1}{\delta}, \frac{\sigma}{\lambda_{max}}, \gamma\eta) \tag{6.36}$$

where λ_{max} is the largest eigenvalue of Γ^{-1}. The above inequality satisfies

$$\dot{V}(t) \leq -\tau V + \frac{c}{2} \tag{6.37}$$

with

$$c = \delta\epsilon_0^2 + \delta d_0^2 + \sigma\|\theta^*\|^2 + \gamma\int_0^R p^2(r)dr \tag{6.38}$$

and we have

$$V(t) \leq e^{-\tau(t-t_0)}V(t_0) + \frac{c}{2\tau} \tag{6.39}$$

From the definition of V, we conclude that s, $\tilde{\theta}$, and $\tilde{p}$ are bounded. Especially,

$$|s(t)| \leq \sqrt{2V(t)} \leq \sqrt{2V(t_0)}e^{-\frac{\tau(t-t_0)}{2}} + \sqrt{\frac{c}{\tau}} \tag{6.40}$$

Noticing that the bound for the filtered tracking error in (6.40) is a function of t and depends on the initial value $V(t_0)$. Using the same method as in [55], we can prove that the tracking error vector $\tilde{\mathbf{x}}$ converges to a set, which is not depend on the initial condition $V(t_0)$. Let $p = d/dt$ be the Laplace operator,

$$\begin{aligned}y_1(p) &= \frac{1}{p+\lambda}s(p) \\ y_i(p) &= \frac{1}{p+\lambda}y_{i-1}, \qquad i = 1, 2, \cdots, n-1\end{aligned} \tag{6.41}$$

From (6.40), $y_1(t)$ is bounded by

$$
\begin{aligned}
|y_1(t)| &\leq \int_{t_0}^{t} e^{-\lambda(t-\alpha)}|s(\alpha)|d\alpha \\
&\leq \begin{cases} \frac{1}{\lambda}\sqrt{\frac{c}{\tau}} & +\sqrt{2V(t_0)}e^{-\lambda(t-t_0)}(t-t_0) \\ & \text{if } \lambda = \tau/2; \\ \frac{1}{\lambda}\sqrt{\frac{c}{\tau}} & +\frac{2\sqrt{2V(t_0)}}{2\lambda-\tau}\{e^{-\frac{\tau}{2}(t-t_0)} - e^{-\lambda(t-t_0)}\} \\ & \text{otherwise} \end{cases}
\end{aligned} \tag{6.42}
$$

By integrating inequality $|y_i(t)| \leq \int_{t_0}^{t} e^{-\lambda(t-\alpha)}|y_{i-1}(t)|d\alpha$ from $i = 2$ to $i = n-1$, for $n \geq 3$, we have

$$
|y_{n-1}(t)| \leq \int_{t_0}^{t} e^{-\lambda(t-\alpha)}|y_{n-2}(t)|d\alpha \tag{6.43}
$$

$$
\leq \begin{cases} \frac{1}{\lambda^{n-1}}\sqrt{\frac{c}{\tau}} & +\frac{\sqrt{2V(t_0)}}{(n-1)!}(t-t_0)^{n-1}e^{-\lambda(t-t_0)} \\ & \text{if } \lambda = \tau/2; \\ \frac{1}{\lambda^{n-1}}\sqrt{\frac{c}{\tau}} & +\sqrt{2V(t_0)}\{(\frac{2}{2\lambda-\tau})^{n-1}e^{-\frac{\tau}{2}(t-t_0)} \\ -\sum_{i=1}^{n-1} & (\frac{2}{2\lambda-\tau})^{n-i}\frac{(t-t_0)^{i-1}}{(i-1)!}e^{-\lambda(t-t_0)}\} \\ & \text{otherwise} \end{cases} \tag{6.44}
$$

Since $\tilde{x}_1(t) = y_{n-1}(t)$ and $\tilde{x}_1(t)$ satisfies the above inequality, and $\lim_{t\to\infty}\tilde{x}_1(t) = \frac{1}{\lambda^{n-1}}\sqrt{\frac{c}{\tau}}$, where c and τ are existing constants given in (6.36) and (6.38). The upper bounds for $|\tilde{x}_1(t)|$ and $\forall t \geq t_0$ are also given as

$$
|\tilde{x}_1(t)| \leq \begin{cases} \frac{1}{\lambda^{n-1}}\sqrt{\frac{c}{\tau}} & +\frac{\sqrt{2V(t_0)}}{(n-1)!}(\frac{n-1}{\lambda})^{n-1}e^{-(n-1)} \\ & \text{if } \lambda = \tau/2; \\ \frac{1}{\lambda^{n-1}}\sqrt{\frac{c}{\tau}} & +\sqrt{2V(t_0)}\{(\frac{2}{2\lambda-\tau})^{n-1}e^{-\frac{\tau}{2\lambda}(i-1)} \\ -\sum_{i=1}^{n-1} & (\frac{2}{2\lambda-\tau})^{n-i}\frac{(i-1)^{i-1}}{(i-1)!\lambda^{i-1}}e^{-(i-1)}\} \\ & \text{otherwise} \end{cases} \tag{6.45}
$$

They are reached at $t = \frac{n-1}{\lambda} + t_0$ for $\lambda = \tau/2$, and $t = \frac{i-1}{\lambda} + t_0$ otherwise.

Similarly, for $\tilde{x}_i(t), i = 2, \cdots, n-1$, let

$$\begin{aligned} y_1(p) &= \frac{1}{p+\lambda} s(p) \\ y_j(p) &= \frac{1}{p+\lambda} y_{j-1}(p), \qquad j = 1, 2, \cdots, n-i-1 \\ z_1(p) &= y_{n-i-1}(p) \\ z_j(p) &= \frac{s}{s+\lambda} z_{j-1}(p), \qquad j = 2, \cdots, i \end{aligned} \tag{6.46}$$

Since $\tilde{x}_i(t) = z_i(t)$, using previous results we can prove that

$$\lim_{t\to\infty} \tilde{x}_i(t) = \lim_{t\to\infty} z_i(t) = 2^{i-1}\lambda^{i-n}\sqrt{c/\tau}$$

As a conclusion, we summarize the above discussion in the following theorem:

Theorem: Consider a nonlinear system (6.1) with the hysteresis as an input represented by the Prandtl-Ishlinskii model satisfying Assumptions 1)-4, if the robust adaptive controller is specified by (6.18) with adaptation laws (6.15) and (6.17), then for any bounded initial conditions, all closed-loop signals are bounded and the state vector $x(t)$ converges to

$$\Omega_\epsilon = \{x(t) |\ |\tilde{x}_i| \leq 2^{i-1}\lambda^{i-n}\sqrt{c/\tau}, i = 1, ..., n\}$$

where τ and c are constants given in (6.36) and (6.38).

Remark : We point out that, in the above theorem, the bound for the converging set Ω_ϵ is determined by τ and c. Since τ is a constant decided by controller parameters δ, σ, λ_{max}, γ, and η. c depends on the controller parameters and the properties of the plant such as the weight function of the hysteresis $p(r)$, the bound of disturbances d_0, and the approximator to be used to estimate the unknown nonlinear functions $a(x)$ and $b(x)$. The bound of the converging set Ω_ϵ can be adjusted by choosing suitable parameters of system properties such as ϵ_0, d_0, θ^*, and $p(r)$.

6.3. Simulation Studies

To illustrate the proposed robust adaptive control algorithm, we use the same example given in [19]. Consider a variable length $l(\phi)$ pendulum as shown in Fig.6.1. ϕ is the angle subtended by the rod and the vertical axis, and w is a torque applied to the pendulum. The plant dynamics can be expressed in the following form

$$\begin{aligned} \dot{x}_i &= x_{i+1}, \qquad i = 1, 2, \cdots, n-1 \\ \dot{x}_n &= a(x) + b(x)w(t) + d_e(t) \\ y &= x_1 \end{aligned} \tag{6.47}$$

If the parameters satisfy $l(\phi) = l_0 + l_1 cos(\phi)$, $l_1/l_0 = 0.5$, $g/l_0 = 10$ and $ml_0^2 = 1$, we have

$$\begin{aligned} a(x) &= \frac{0.5 sinx_1(1 + 0.5 cosx_1)x_2^2 - 10 sinx_1(1 + cosx_1)}{0.25(2 + cosx_1)^2} \\ b(x) &= \frac{1}{0.25(2 + cosx_1)^2} \\ d_e(t) &= d_1(t) cosx_1 \qquad with \quad d_1(t) = cos(3t) \end{aligned} \tag{6.48}$$

where $x = [x_1, x_2]^T = [\phi, \dot{\phi}]^T$. The state variables belong to the compact set

$$\Omega_x = \{(x_1, x_2)|\ |x_1| \leq \pi/2,\ |x_2| \leq 4\pi\} \tag{6.49}$$

We can verify that $4/9 \leq b(x) \leq 1$ for all $x \in \Omega_x$ and Assumptions 1 and 2 are satisfied. We set $\bar{b}(x) = 1$. The reference signal is given as $x_d = sin(2t)$. Initial states are assumed to be $[x_1(0), x_2(0)]^T = [0, 0]^T$ and $\lambda = 5$.

In (6.47), the torque $w(t)$ is the output of the hysteresis operator expressed by the Prandtl-Ishlinskii model

$$w(t) = p_0 v(t) - \int_0^R p(r) F_r[v](t) dr, \tag{6.50}$$

where $p(r) = \alpha e^{-\beta(r-0.5)^2}$ for $r \in [0, 100]$, with $\alpha = 0.45, \beta = 0.009$. $p_0 = 5.379$, $p_{0max} = 6.379$ and $p_{0min} = 4.379$. We also assume that the internal state of hysteresis was $\psi(r) = 0.15$ for $r \in [0, 100]$ before $v(0)$ was applied. For the calculation of $\hat{B}(t)$, we replace the integration by the summation $\sum_0^N$. In the simulation, we choose $N = 4000$. The sampling time is 0.005. To avoid the vibration caused by the discontinuity of the sign function, we use saturate function $sat(s/\epsilon) = s/\epsilon$ instead of the sign function $sign(s)$ in the simulation. The proof is valid except in a small neighborhood of $(-\epsilon, \epsilon]$).

In this example, a two-order neural network with 20 nodes ($l = 20$) is selected as

$$f_n(\theta, z) = \hat{\theta}^T \Phi(z) \qquad \forall z \in \Omega_z \tag{6.51}$$

where $z = [x_1, x_2, s, s/\delta, \mu]$, and θ is the vector of the weight parameters. Let

$$\Phi(z) = [\phi_1(z), \phi_2(z), \ldots, \phi_{20}(z)]^T \tag{6.52}$$

If we choose $\phi(z_j)$ as the hyperbolic tangent functions

$$\phi(z_j) = \frac{e^{z_j} - e^{-z_j}}{e^{z_j} + e^{-z_j}}, \qquad j = 1, \ldots, 5 \tag{6.53}$$

then $\phi_i(z)$ are the possible combinations of $\phi(z_j)^{d_{i,1}} \phi(z_k)^{d_{i,2}}$ for $j, k = 1, \ldots, 5$, for example, denoting as following

$$\phi_1(z) = \phi(z_1)^{d_{1,1}}\phi(z_2)^{d_{1,2}};$$
$$\phi_2(z) = \phi(z_2)^{d_{2,1}}\phi(z_2)^{d_{2,2}};$$
$$\phi_3(z) = \phi(z_1)^{d_{3,1}}\phi(z_3)^{d_{3,2}};$$
$$\phi_4(z) = \phi(z_3)^{d_{4,1}}\phi(z_1)^{d_{4,2}};$$
$$\phi_5(z) = \phi(z_1)^{d_{5,1}}\phi(z_4)^{d_{5,2}};$$
$$\phi_6(z) = \phi(z_4)^{d_{6,1}}\phi(z_1)^{d_{6,2}};$$
$$\phi_7(z) = \phi(z_1)^{d_{7,1}}\phi(z_5)^{d_{7,2}};$$
$$\phi_8(z) = \phi(z_5)^{d_{8,1}}\phi(z_1)^{d_{8,2}};$$
$$\phi_9(z) = \phi(z_2)^{d_{9,1}}\phi(z_3)^{d_{9,2}};$$
$$\phi_{10}(z) = \phi(z_3)^{d_{10,1}}\phi(z_2)^{d_{10,2}};$$
$$\phi_{11}(z) = \phi(z_2)^{d_{11,1}}\phi(z_4)^{d_{11,2}};$$
$$\phi_{12}(z) = \phi(z_4)^{d_{12,1}}\phi(z_2)^{d_{12,2}};$$
$$\phi_{13}(z) = \phi(z_2)^{d_{13,1}}\phi(z_5)^{d_{13,2}};$$
$$\phi_{14}(z) = \phi(z_5)^{d_{14,1}}\phi(z_2)^{d_{14,2}};$$
$$\phi_{15}(z) = \phi(z_3)^{d_{15,1}}\phi(z_4)^{d_{15,2}};$$
$$\phi_{16}(z) = \phi(z_4)^{d_{16,1}}\phi(z_3)^{d_{16,2}};$$
$$\phi_{17}(z) = \phi(z_3)^{d_{17,1}}\phi(z_5)^{d_{17,2}};$$
$$\phi_{18}(z) = \phi(z_5)^{d_{18,1}}\phi(z_3)^{d_{18,2}};$$
$$\phi_{19}(z) = \phi(z_4)^{d_{19,1}}\phi(z_5)^{d_{19,2}};$$
$$\phi_{20}(z) = \phi(z_5)^{d_{20,1}}\phi(z_4)^{d_{20,2}};$$

where $d_{i,1}$ and $d_{i,2}$ are non-negative integers. $\phi_i(z)$ are called basis functions of the neural network, and they are dependent on $d_{i,1}$ and $d_{i,2}$. In the following, we conducted simulations in two cases. First, we chose all $d_{i,1}$ and $d_{i,2}$ equal to 1. Under this condition, simulation results are given for three sets of neural network and hysteresis adaptation parameters for the same initial conditions. Then, for the

different neural network basis functions defined by given different values of $d_{i,1}$ or $d_{i,2}$, we show that the system states still converge to the neighborhood of zero.

Case 1) Let $d_{i,1} = 1$ and $d_{i,2} = 1$ for all $i = 1, \cdots, 20$, i.e.

$$\begin{pmatrix} d_{1,1} & d_{1,2} \\ d_{2,1} & d_{2,2} \\ d_{3,1} & d_{3,2} \\ d_{4,1} & d_{4,2} \\ d_{5,1} & d_{5,2} \\ d_{6,1} & d_{6,2} \\ d_{7,1} & d_{7,2} \\ d_{8,1} & d_{8,2} \\ d_{9,1} & d_{9,2} \\ d_{10,1} & d_{10,2} \\ d_{11,1} & d_{11,2} \\ d_{12,1} & d_{12,2} \\ d_{13,1} & d_{13,2} \\ d_{14,1} & d_{14,2} \\ d_{15,1} & d_{15,2} \\ d_{16,1} & d_{16,2} \\ d_{17,1} & d_{17,2} \\ d_{18,1} & d_{18,2} \\ d_{19,1} & d_{19,2} \\ d_{20,1} & d_{20,2} \end{pmatrix} = \begin{pmatrix} 1 & 1 \\ 1 & 1 \\ 1 & 1 \\ 1 & 1 \\ 1 & 1 \\ 1 & 1 \\ 1 & 1 \\ 1 & 1 \\ 1 & 1 \\ 1 & 1 \\ 1 & 1 \\ 1 & 1 \\ 1 & 1 \\ 1 & 1 \\ 1 & 1 \\ 1 & 1 \\ 1 & 1 \\ 1 & 1 \\ 1 & 1 \\ 1 & 1 \end{pmatrix}$$

Under the basis functions defined as above, we give two sets of parameters to study the system performances for different designed parameters.

1.1) For the neural network initial weight vector $\theta = 0$, we set the neural network adaptation gains as $\Gamma = diag\{35\}$, $\sigma = 0.1$, and $\delta = 0.05$. For the adaptation laws of hysteresis, we choose adaptive parameters $\gamma = 0.11$ and $\eta = 0.15$. Simulation results for $\epsilon = 0.1$ are shown in Fig.6.2 to Fig.6.7. Figs.6.2 and 6.3 show the tracking errors of the system states for the desired trajectory. It can be seen that with the term $v_h(t) \neq 0$ designed to reduce the effects of hysteresis, system state errors $\tilde{x}_1 = x_1 - x_d$ and $\tilde{x}_2 = x_2 - \dot{x}_d$ converge to a small region after 2 seconds. The transient performances are shown in the detailed Figure (b) in the time spans of 10. Fig.6.4 shows system outputs $x(t)$. In Fig.6.5, the norm of the estimated neural network weight parameters $\|\hat{\theta}\|$ is bounded. The control input $v(t)$ and the term $v_h(t)$ designed to reduce the hysteresis effect are given in Fig.6.7 and Fig.6.6. To illustrate the effectiveness of the proposed control scheme, simulation was also conducted without controlling the effects of hysteresis. This was implemented by setting $v_h(t) = 0$ in the controller $v(t)$. This implies that the control compensation for the hysteresis nonlinearity was ignored. The results are presented in the figures with dashed lines. We can see that the proposed controller clearly demonstrates robust tracking performance and the developed control algorithm can overcome the effects of the hysteresis.

1.2) For the same neural network initial weight vector $\theta = 0$, if we reduce the neural network adaptation gain Γ from $\Gamma = diag\{35\}$ to $\Gamma = diag\{3.5\}$, and keep $\sigma = 0.1$. Then we have to increase $\delta = 0.25$. For the adaptation laws of hysteresis, we reduce the adaptive parameters to $\gamma = 0.0081$ and $\eta = 0.078$. Simulation results for $\epsilon = 0.1$ are shown in Fig.6.8. In this case, it takes longer time for the system to converge.

1.3) If we reduce ϵ from $\epsilon = 0.1$ to $\epsilon = 0.01$, and keep the rest of the parameters the same as in the case 1.1), tracking errors of the system states $\tilde{x}_1 = x_1 - x_d$,

$\tilde{x}_2 = x_2 - \dot{x}_d$ and control input $v(t)$ are shown in Fig.6.12 to 6.14.

Case 2) If we change neural network basis functions by taking $d_{i,j}$, for $i = 1, \cdots, 20$ and $j = 1, 2$, as following

$$\begin{pmatrix} d_{1,1} & d_{1,2} \\ d_{2,1} & d_{2,2} \\ d_{3,1} & d_{3,2} \\ d_{4,1} & d_{4,2} \\ d_{5,1} & d_{5,2} \\ d_{6,1} & d_{6,2} \\ d_{7,1} & d_{7,2} \\ d_{8,1} & d_{8,2} \\ d_{9,1} & d_{9,2} \\ d_{10,1} & d_{10,2} \\ d_{11,1} & d_{11,2} \\ d_{12,1} & d_{12,2} \\ d_{13,1} & d_{13,2} \\ d_{14,1} & d_{14,2} \\ d_{15,1} & d_{15,2} \\ d_{16,1} & d_{16,2} \\ d_{17,1} & d_{17,2} \\ d_{18,1} & d_{18,2} \\ d_{19,1} & d_{19,2} \\ d_{20,1} & d_{20,2} \end{pmatrix} = \begin{pmatrix} 1 & 1 \\ 1 & 0 \\ 1 & 0 \\ 1 & 1 \\ 1 & 1 \\ 1 & 2 \\ 1 & 2 \\ 1 & 1 \\ 1 & 1 \\ 1 & 1 \\ 1 & 1 \\ 1 & 1 \\ 1 & 1 \\ 1 & 1 \\ 1 & 1 \\ 1 & 1 \\ 1 & 1 \\ 1 & 1 \\ 1 & 1 \\ 1 & 1 \end{pmatrix}$$

and keep all the other parameters the same as in case 1.1): $\theta = 0$, $\Gamma = diag\{35\}$, $\sigma = 0.1$, $\delta = 0.05$, $\gamma = 0.11$ and $\eta = 0.15$. Simulation results for $\epsilon = 0.1$ are shown in Fig.6.15 to Fig.6.18.

The simulation results show that the proposed control methodology effectively reduces the tracking errors of the system states. The estimated weight parameters of the neural network are bounded. The system shows robust performances for the neural network basis functions and the system parameters.

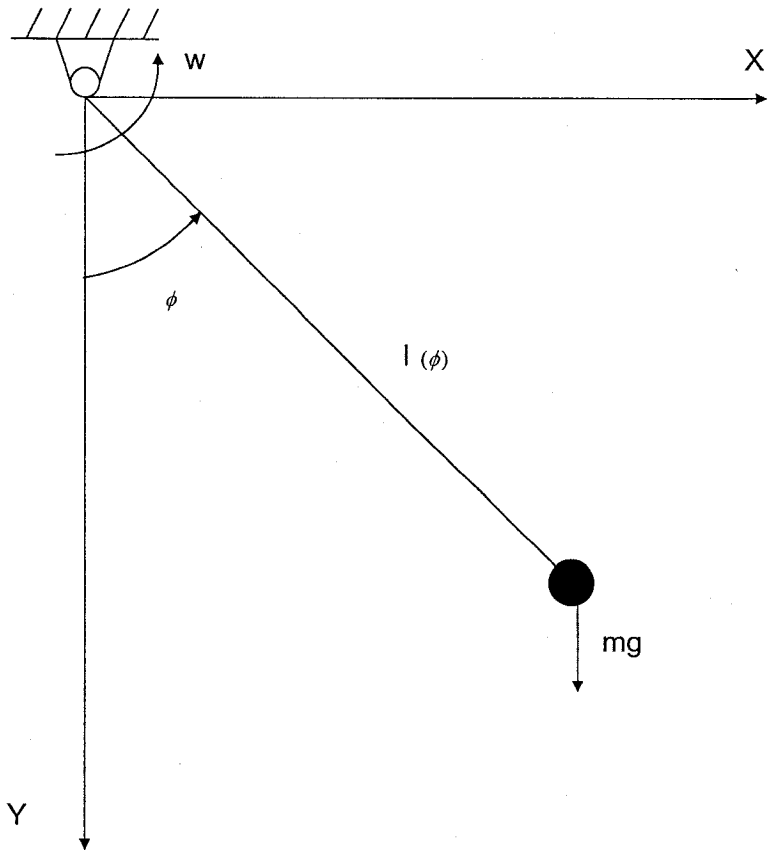

Figure 6.1: Variable length pendulum with $l(\phi) = l_0 + l_1 cos(\phi), l_1/l_0 = 0.5, g/l_0 = 10$ *and* $ml_0^2 = 1$.

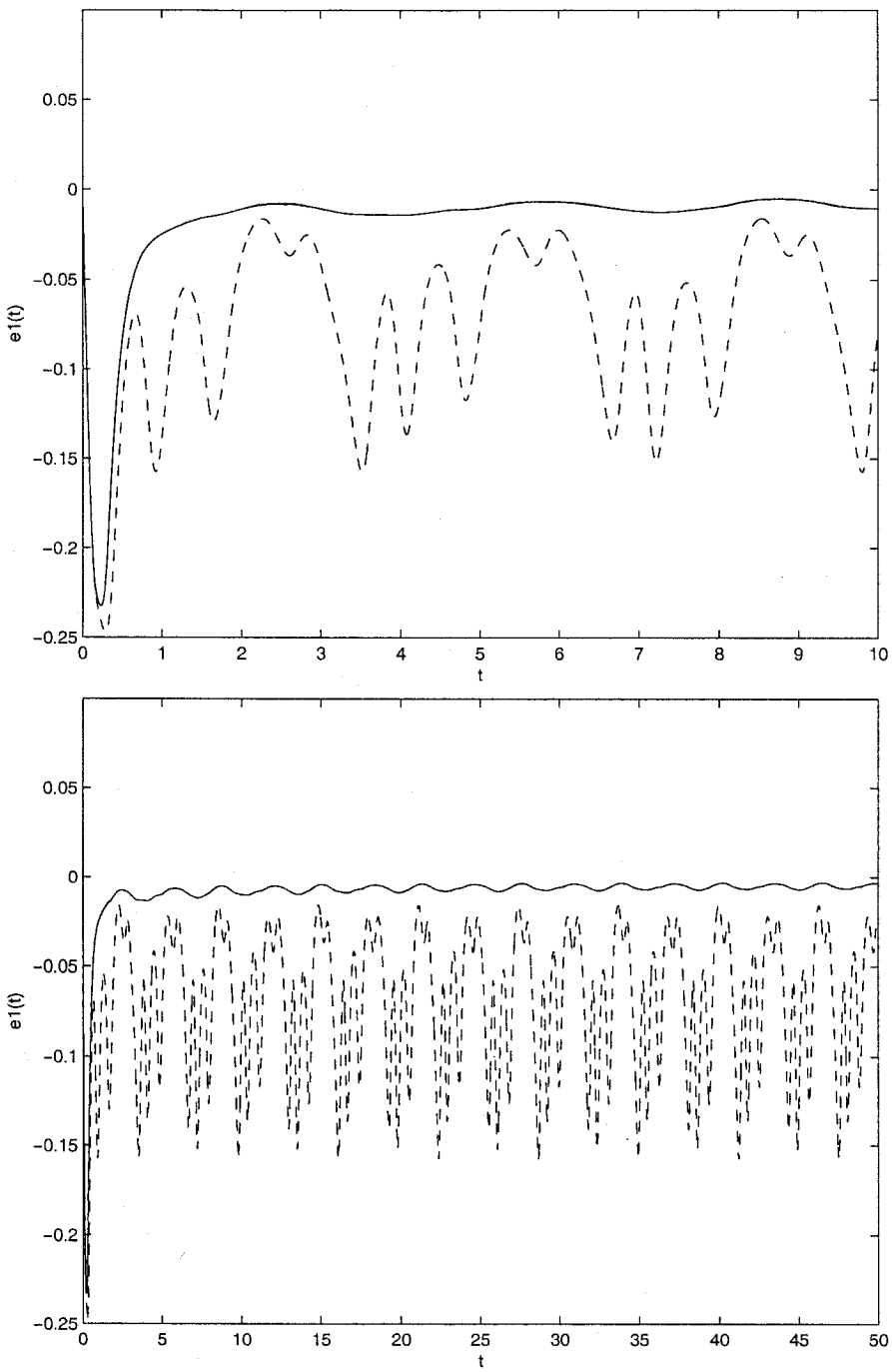

Figure 6.2: Case 1.1): Tracking errors of the system state for the desired trajectory $\tilde{x}_1 = x_1 - x_d$ *in the time spans of* 10 *seconds and* 50 *seconds with* $\Gamma = diag\{35\}$, $\sigma = 0.1$, $\delta = 0.05$, $\gamma = 0.11$, $\eta = 0.15$ *and* $\epsilon = 0.1$. *Where solid lines represent the result with control term* $v_h \neq 0$ *and dashed lines with* $v_h = 0$.

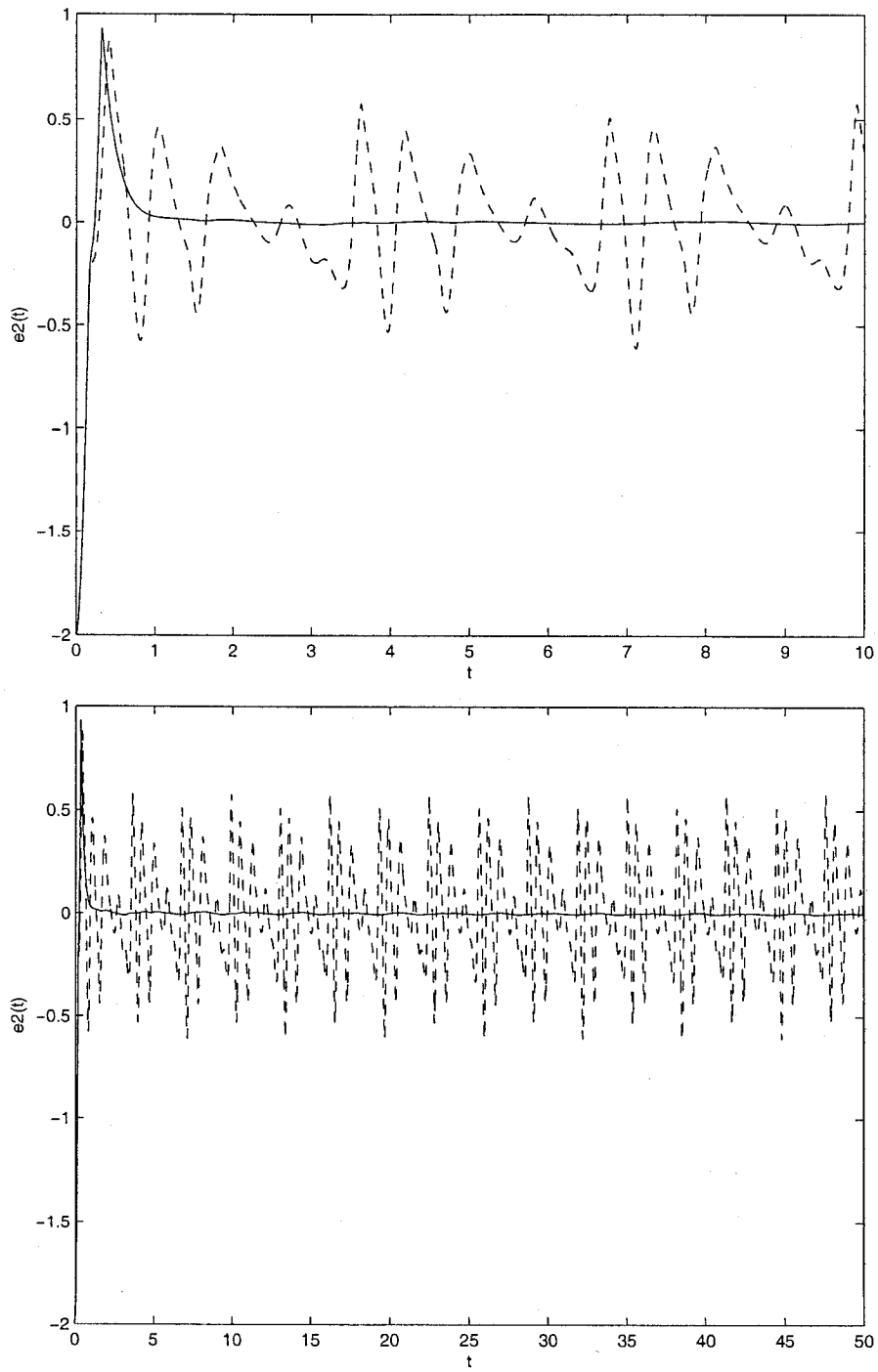

Figure 6.3: Case 1.1): Tracking errors of the system state for the desired trajectory $\tilde{x}_2 = x_2 - \dot{x}_d$ *in the time spans of* 10 *seconds and* 50 *seconds with* $\Gamma = diag\{35\}$, $\sigma = 0.1$, $\delta = 0.05$, $\gamma = 0.11$, $\eta = 0.15$ *and* $\epsilon = 0.1$. *Where solid lines represent the result with control term* $v_h \neq 0$ *and dashed lines with* $v_h = 0$.

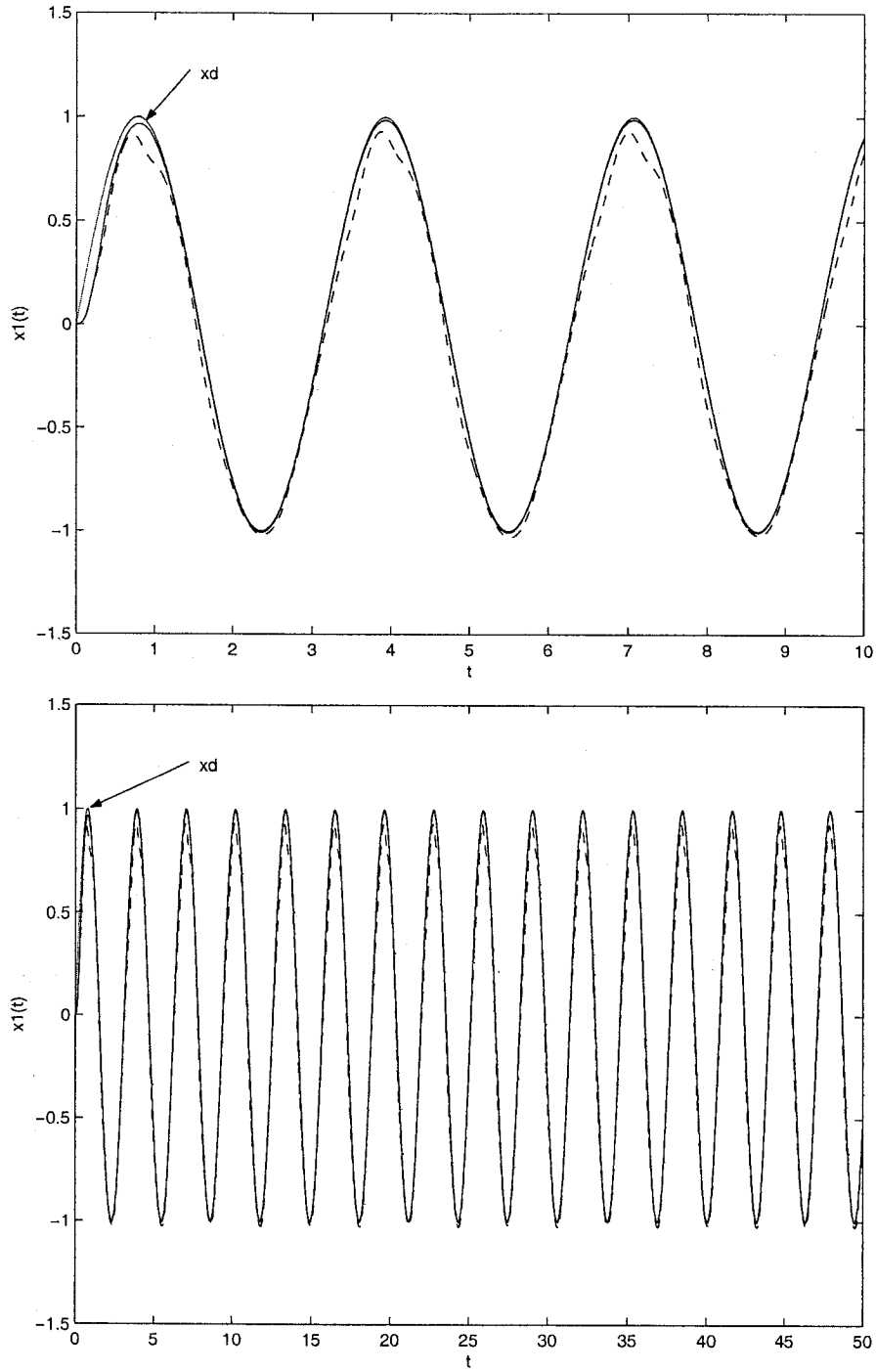

Figure 6.4: Case 1.1): System outputs $x(t)$ in the time spans of 10 seconds and 50 seconds with $\Gamma = diag\{35\}$, $\sigma = 0.1$, $\delta = 0.05$, $\gamma = 0.11$, $\eta = 0.15$ and $\epsilon = 0.1$. Where solid lines represent the result with control term $v_h \neq 0$ and dashed lines with $v_h = 0$.

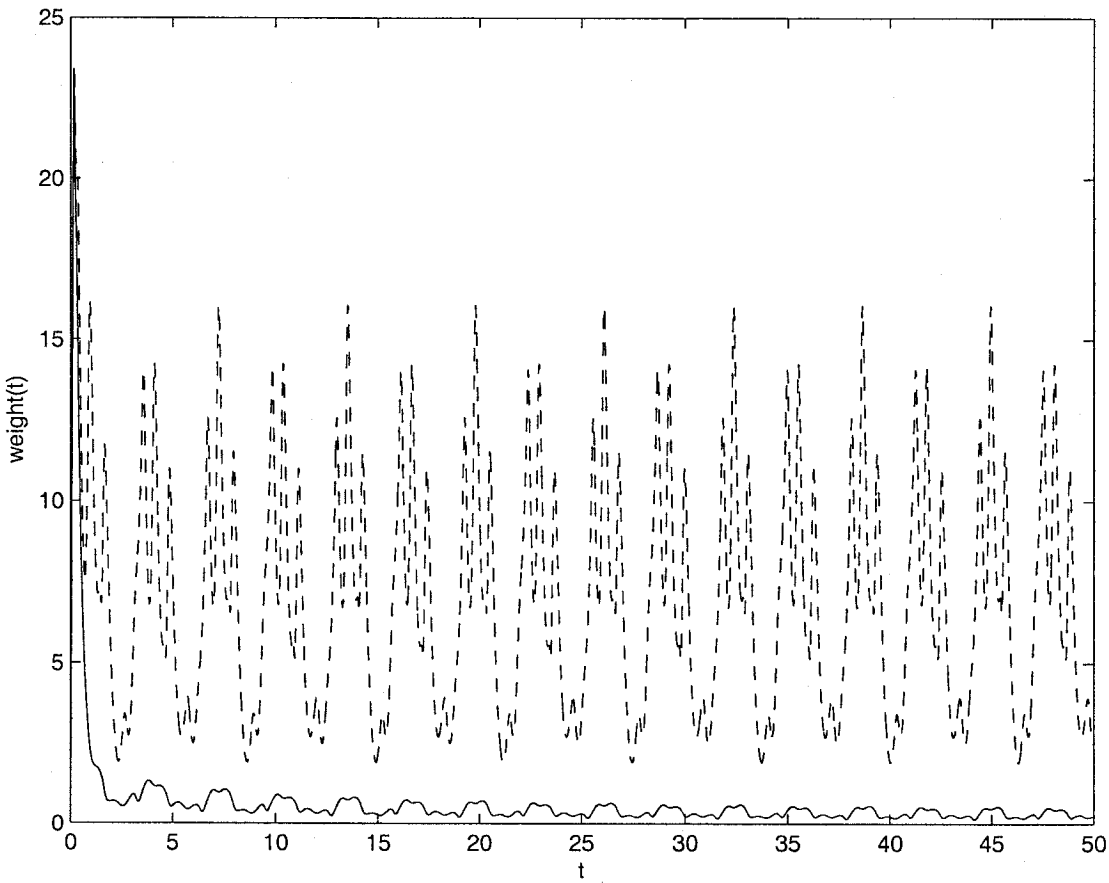

Figure 6.5: Case 1.1): Neural network weight $\|\hat{\theta}\|$ *with* $\Gamma = diag\{35\}$, $\sigma = 0.1$, $\delta = 0.05$, $\gamma = 0.11$, $\eta = 0.15$ *and* $\epsilon = 0.1$. *Where solid line represents the result with control term* $v_h \neq 0$ *and dashed line with* $v_h = 0$.

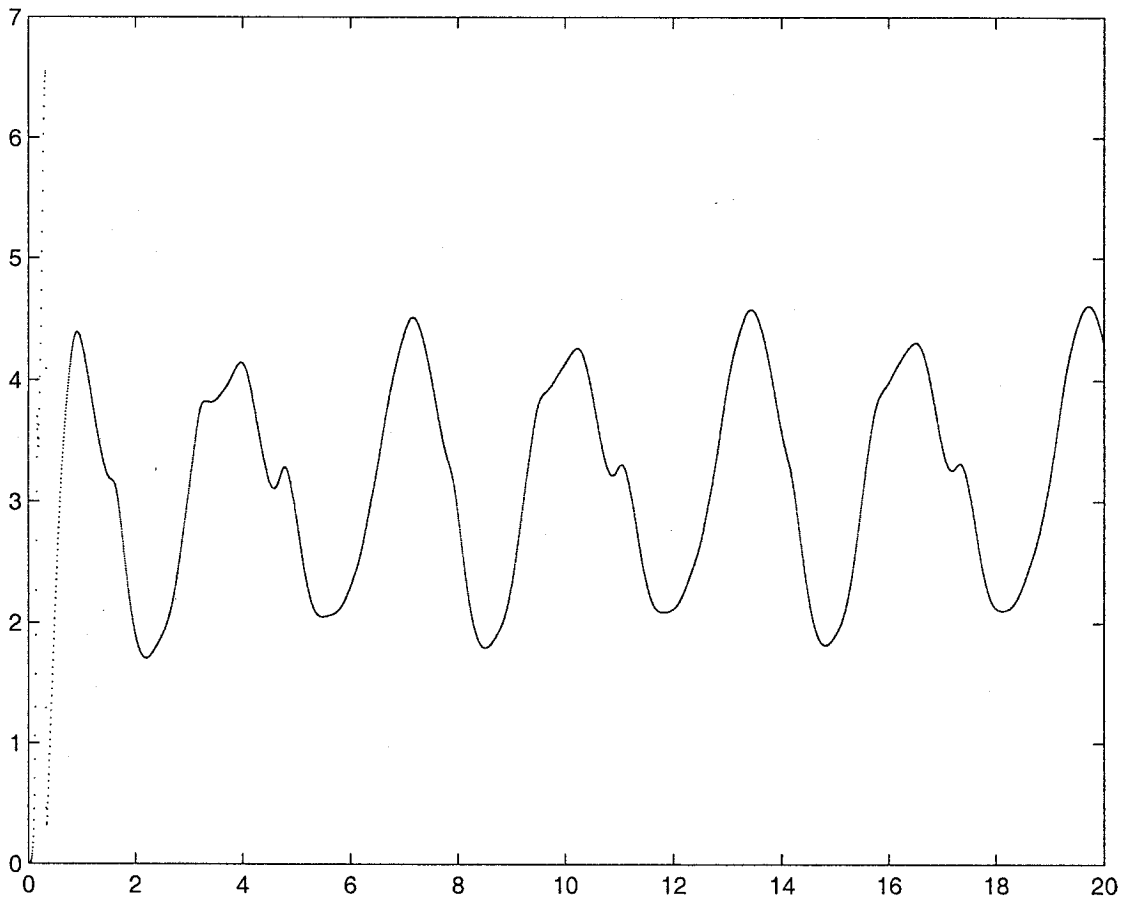

Figure 6.6: Case 1.1): Signal v_h designed to reduce the tracking error caused by the hysteresis with $\Gamma = diag\{35\}$, $\sigma = 0.1$, $\delta = 0.05$, $\gamma = 0.11$, $\eta = 0.15$ and $\epsilon = 0.1$.

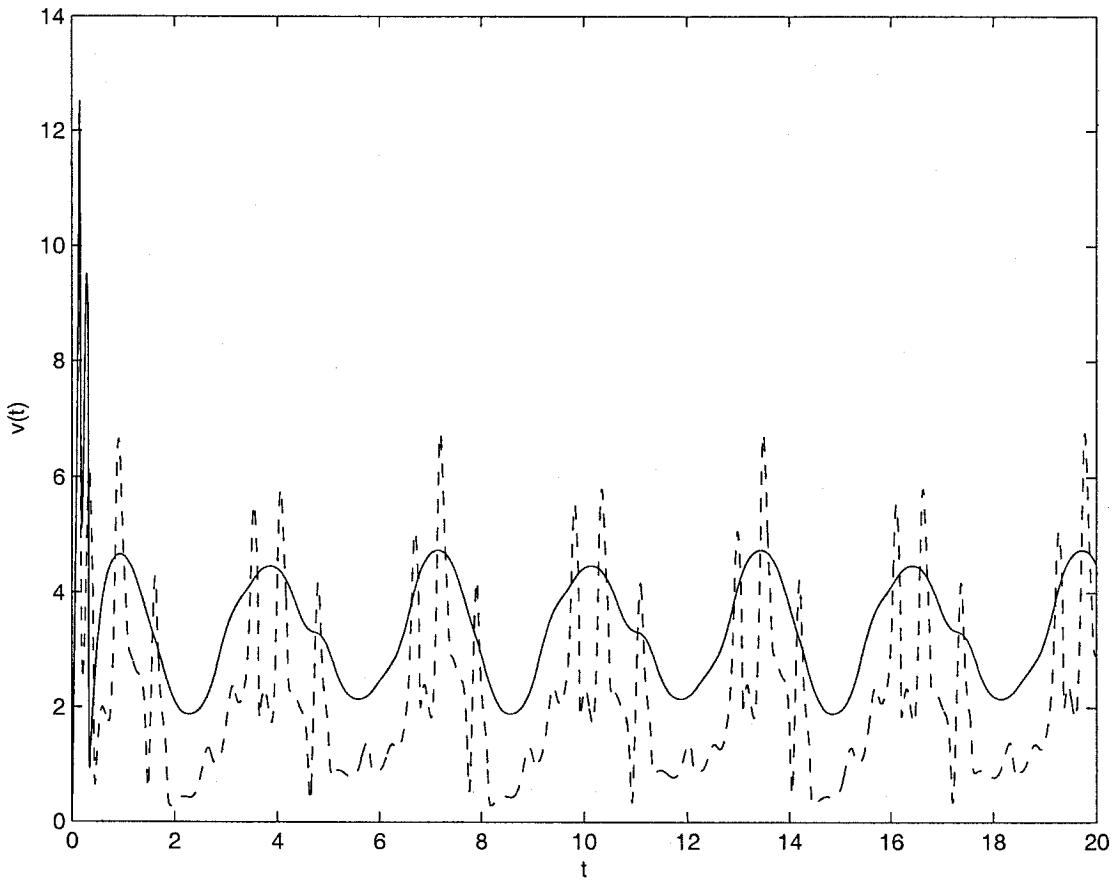

Figure 6.7: Case 1.1): The control input $v(t)$ *with* $\Gamma = diag\{35\}$, $\sigma = 0.1$, $\delta = 0.05$, $\gamma = 0.11$, $\eta = 0.15$ *and* $\epsilon = 0.1$. *Where solid line represents the result with control term* $v_h \neq 0$ *and dashed line with* $v_h = 0$.

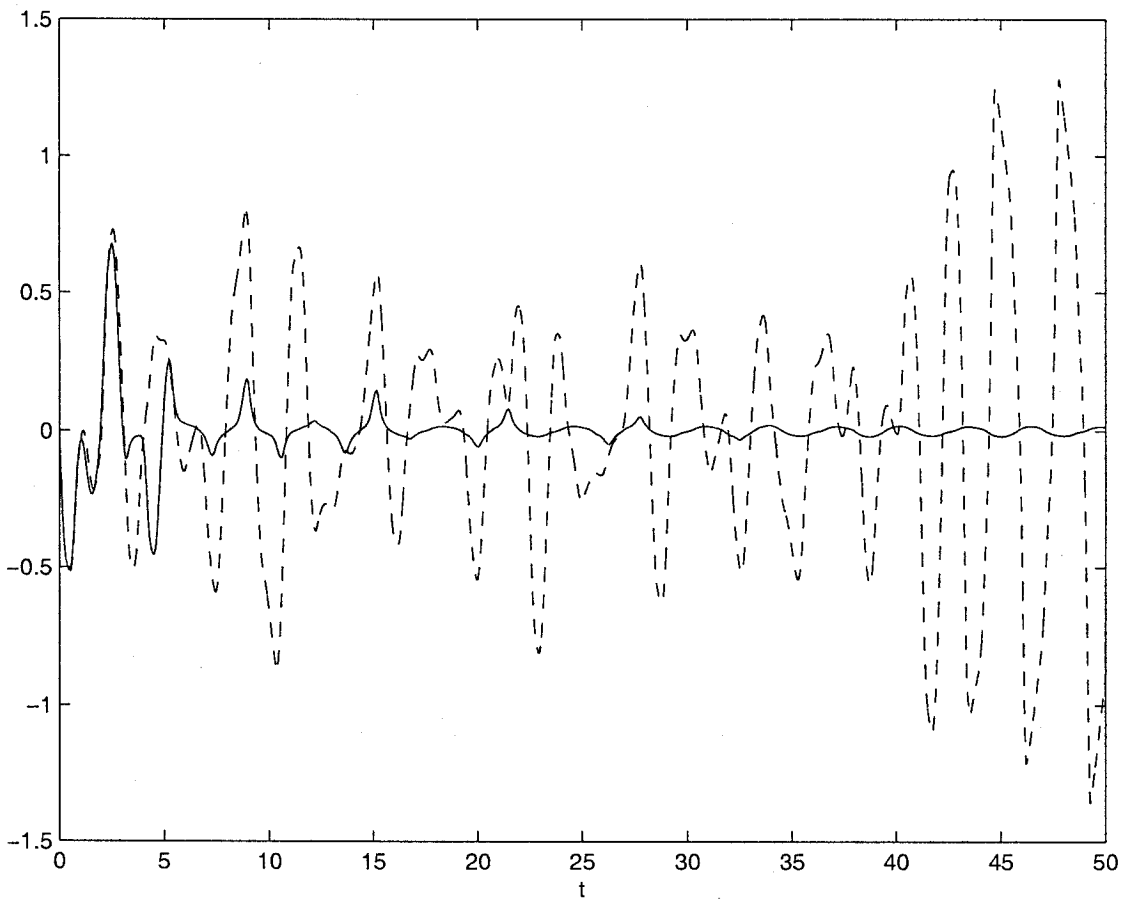

Figure 6.8: Case 1.2): Tracking error of the system state for the desired trajectory $\tilde{x}_1 = x_1 - x_d$ *with* $\Gamma = diag\{3.5\}$, $\sigma = 0.1$, $\delta = 0.25$, $\gamma = 0.0081$, $\eta = 0.078$ *and* $\epsilon = 0.1$. *Where solid line represents the result with control term* $v_h \neq 0$ *and dashed line with* $v_h = 0$.

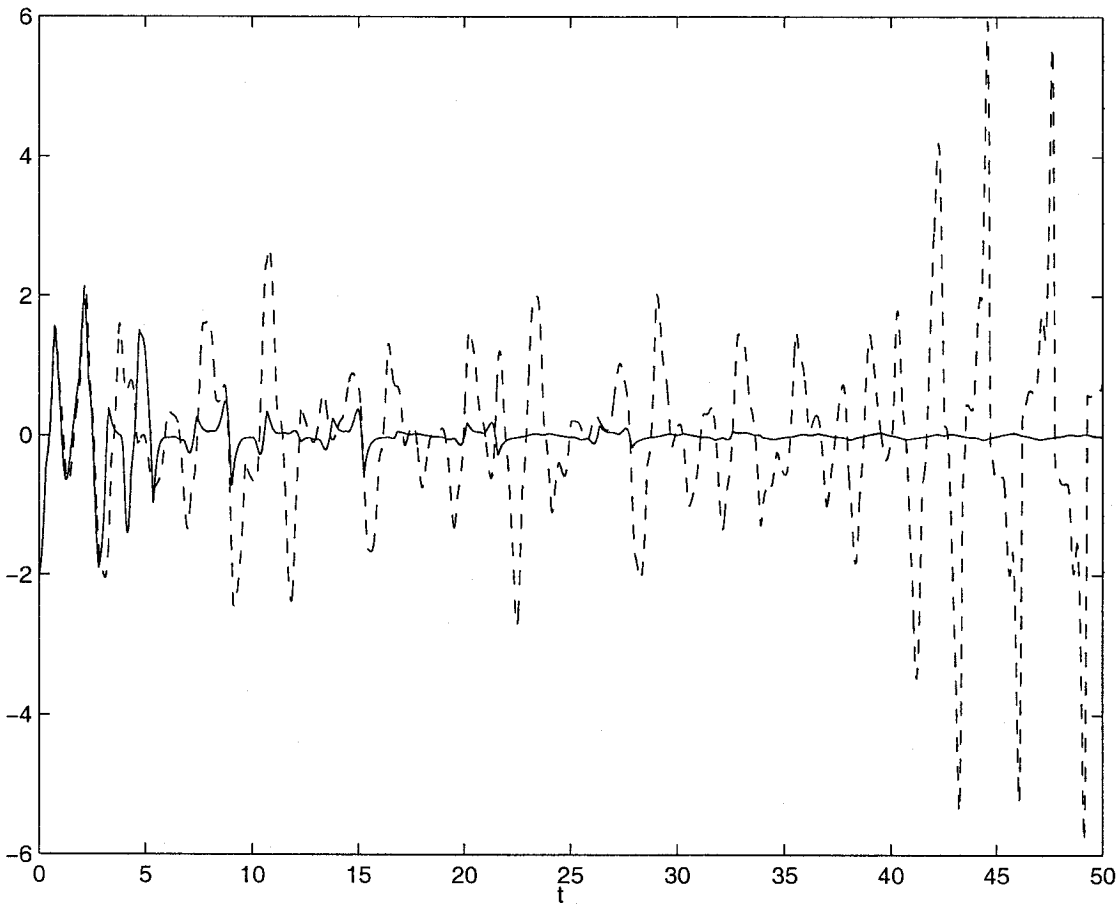

Figure 6.9: Case 1.2): Tracking error of the system state for the desired trajectory $\tilde{x}_2 = x_2 - \dot{x}_d$ *with* $\Gamma = diag\{3.5\}$, $\sigma = 0.1$, $\delta = 0.25$, $\gamma = 0.0081$, $\eta = 0.078$ *and* $\epsilon = 0.1$. *Where solid line represents the result with control term* $v_h \neq 0$ *and dashed line with* $v_h = 0$.

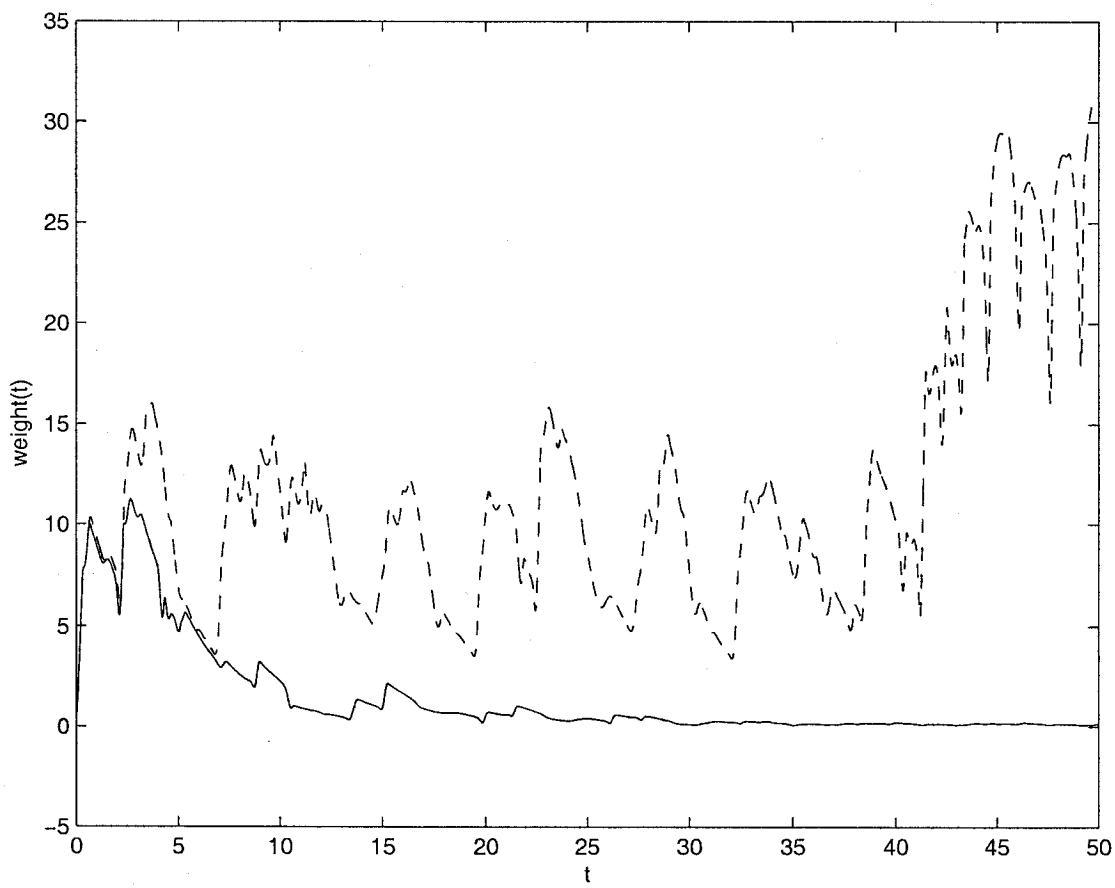

Figure 6.10: Case 1.2): Neural network weight $\|\hat{\theta}\|$ *with* $\Gamma = diag\{3.5\}$, $\sigma = 0.1$, $\delta = 0.25$, $\gamma = 0.0081$, $\eta = 0.078$ *and* $\epsilon = 0.1$. *Where solid line represents the result with control term* $v_h \neq 0$ *and dashed line with* $v_h = 0$.

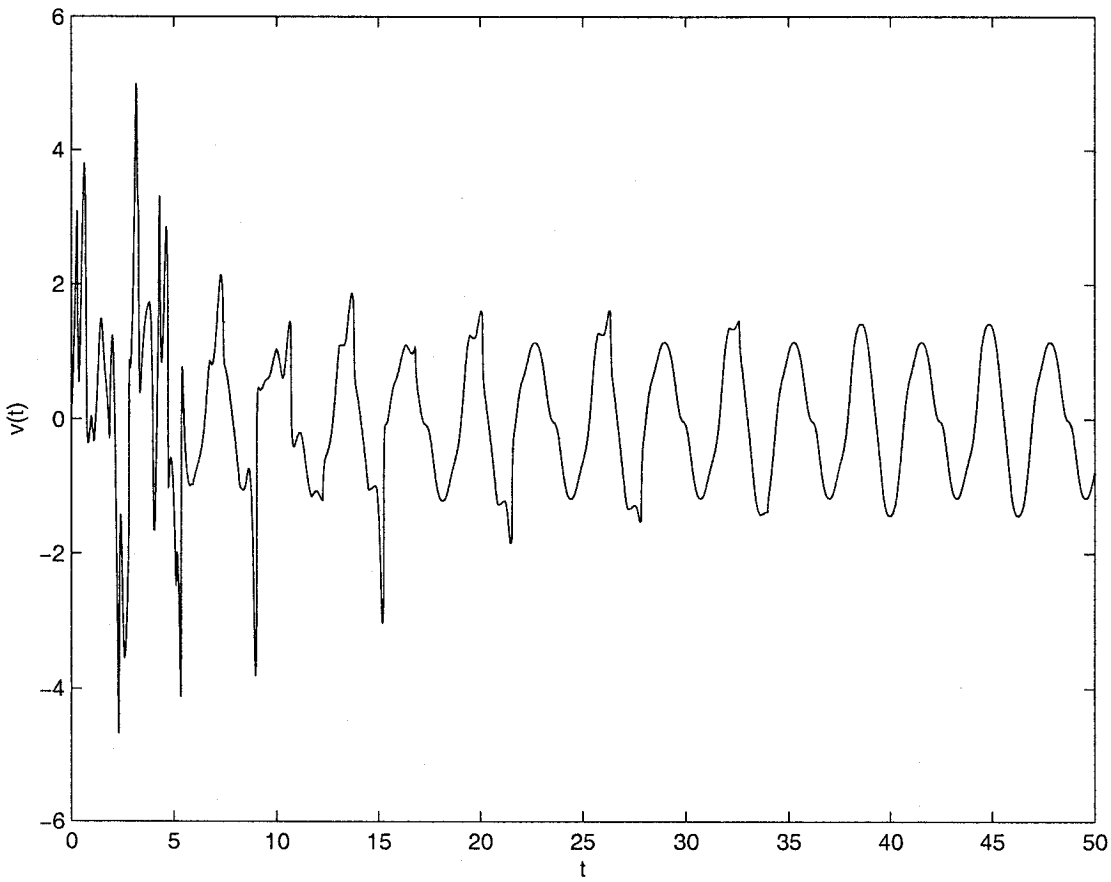

Figure 6.11: Case 1.2): The control input $v(t)$ *with* $\Gamma = diag\{3.5\}$, $\sigma = 0.1$, $\delta = 0.25$, $\gamma = 0.0081$, $\eta = 0.078$ *and* $\epsilon = 0.1$.

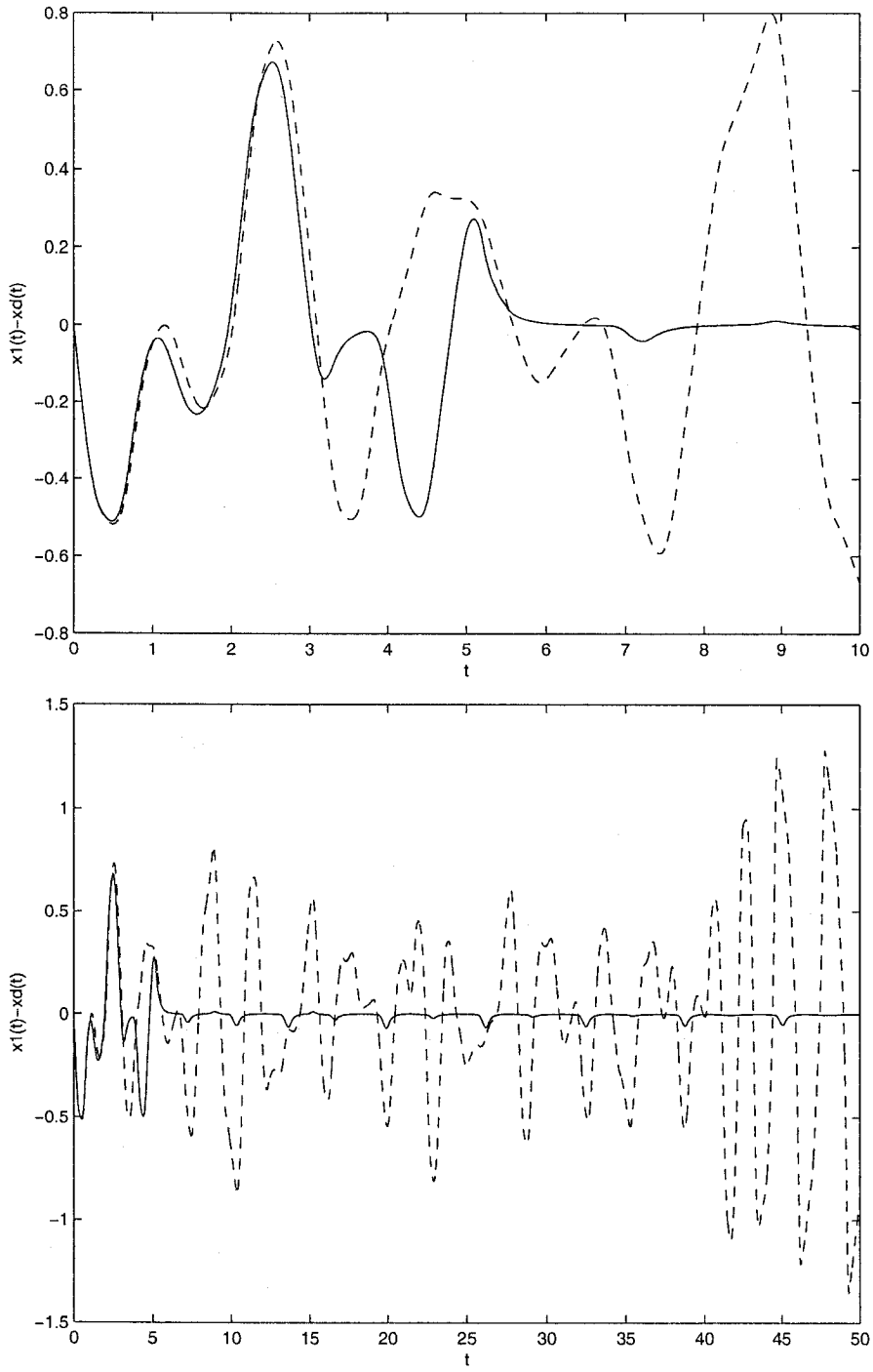

Figure 6.12: Case 1.3): Tracking errors of the system state for the desired trajectory $\tilde{x}_1 = x_1 - x_d$ *in the time spans of* 10 *seconds and* 50 *seconds with* $\Gamma = diag\{35\}$, $\sigma = 0.1$, $\delta = 0.05$, $\gamma = 0.11$, $\eta = 0.15$ *and* $\epsilon = 0.01$. *Where solid lines represent the result with control term* $v_h \neq 0$ *and dashed lines with* $v_h = 0$.

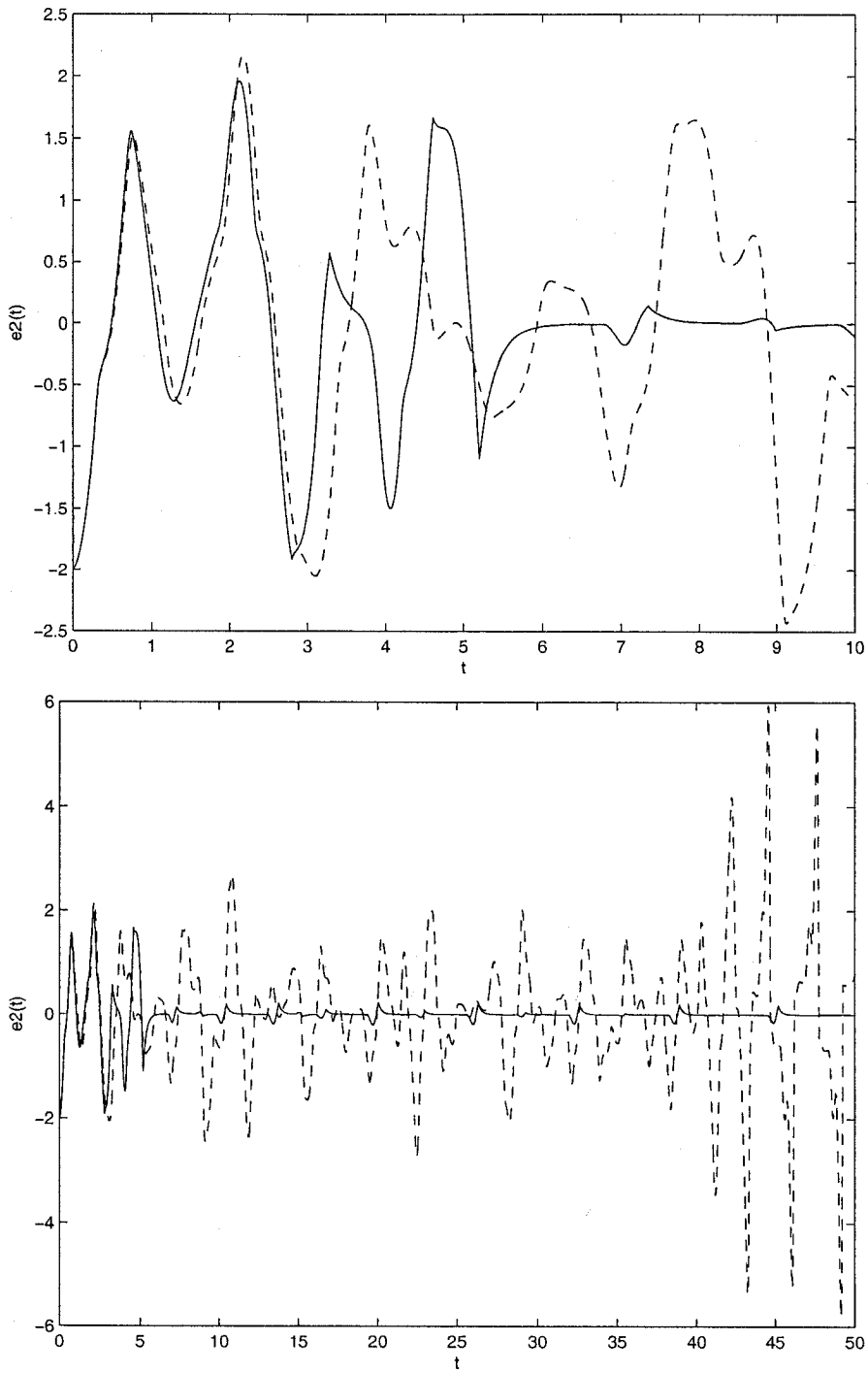

Figure 6.13: Case 1.3): Tracking errors of the system state for the desired trajectory $\tilde{x}_2 = x_2 - \dot{x}_d$ *in the time spans of* 10 *seconds and* 50 *seconds with* $\Gamma = diag\{35\}$, $\sigma = 0.1$, $\delta = 0.05$, $\gamma = 0.11$, $\eta = 0.15$ *and* $\epsilon = 0.01$. *Where solid lines represent the result with control term* $v_h \neq 0$ *and dashed lines with* $v_h = 0$.

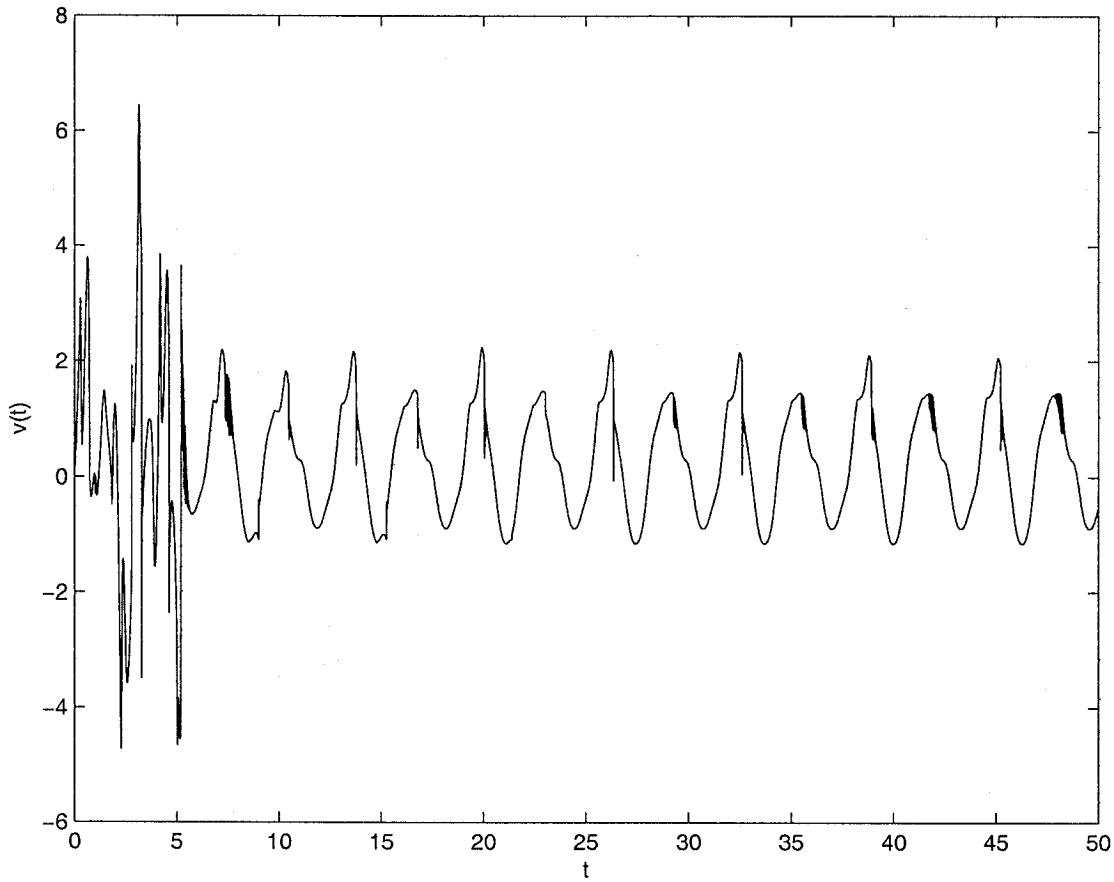

Figure 6.14: Case 1.3): The control input $v(t)$ with $\Gamma = diag\{35\}$, $\sigma = 0.1$, $\delta = 0.05$, $\gamma = 0.11$, $\eta = 0.15$ and $\epsilon = 0.01$. Where solid line represents the result with control term $v_h \neq 0$ and dashed line with $v_h = 0$.

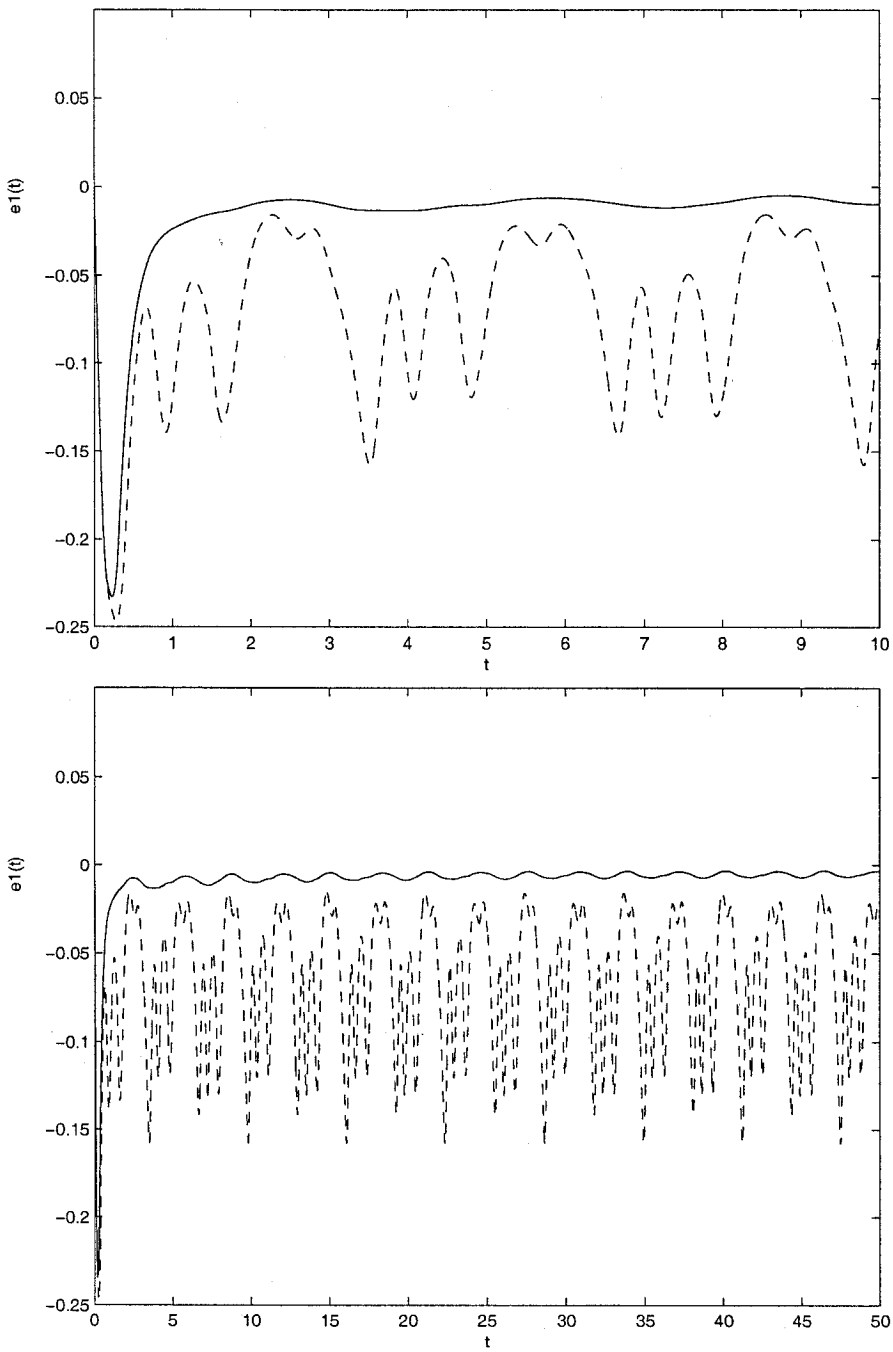

Figure 6.15: Case 2): Tracking errors of the system state for the desired trajectory $\tilde{x}_1 = x_1 - x_d$ *in the time spans of* 10 *seconds and* 50 *seconds with* $\Gamma = diag\{35\}$, $\sigma = 0.1$, $\delta = 0.05$, $\gamma = 0.11$, $\eta = 0.15$ *and* $\epsilon = 0.1$. *Where solid lines represent the result with control term* $v_h \neq 0$ *and dashed lines with* $v_h = 0$.

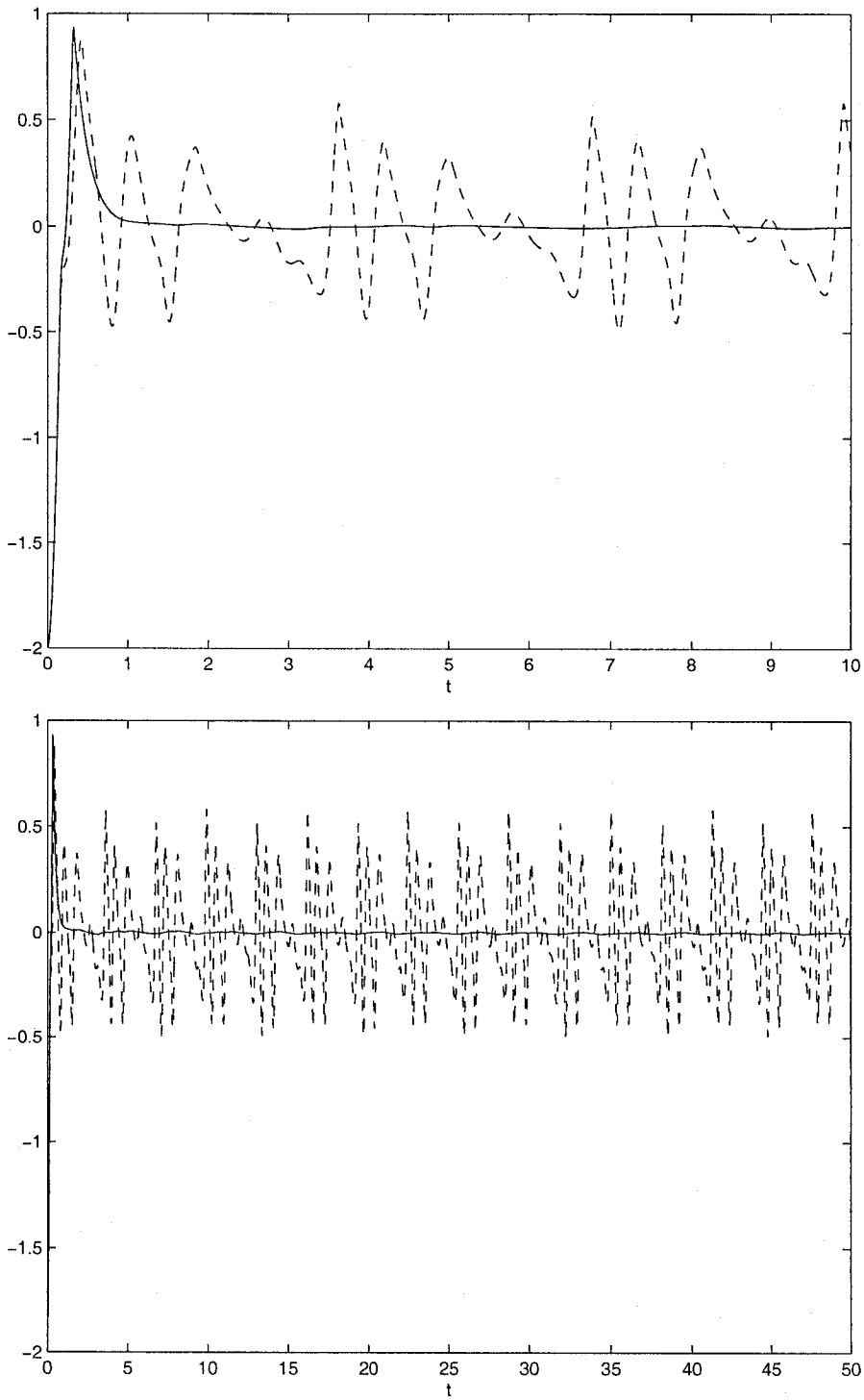

Figure 6.16: Case 2): Tracking errors of the system state for the desired trajectory $\tilde{x}_2 = x_2 - \dot{x}_d$ *in the time spans of* 10 *seconds and* 50 *seconds with* $\Gamma = diag\{35\}$, $\sigma = 0.1$, $\delta = 0.05$, $\gamma = 0.11$, $\eta = 0.15$ *and* $\epsilon = 0.1$. *Where solid lines represent the result with control term* $v_h \neq 0$ *and dashed lines with* $v_h = 0$.

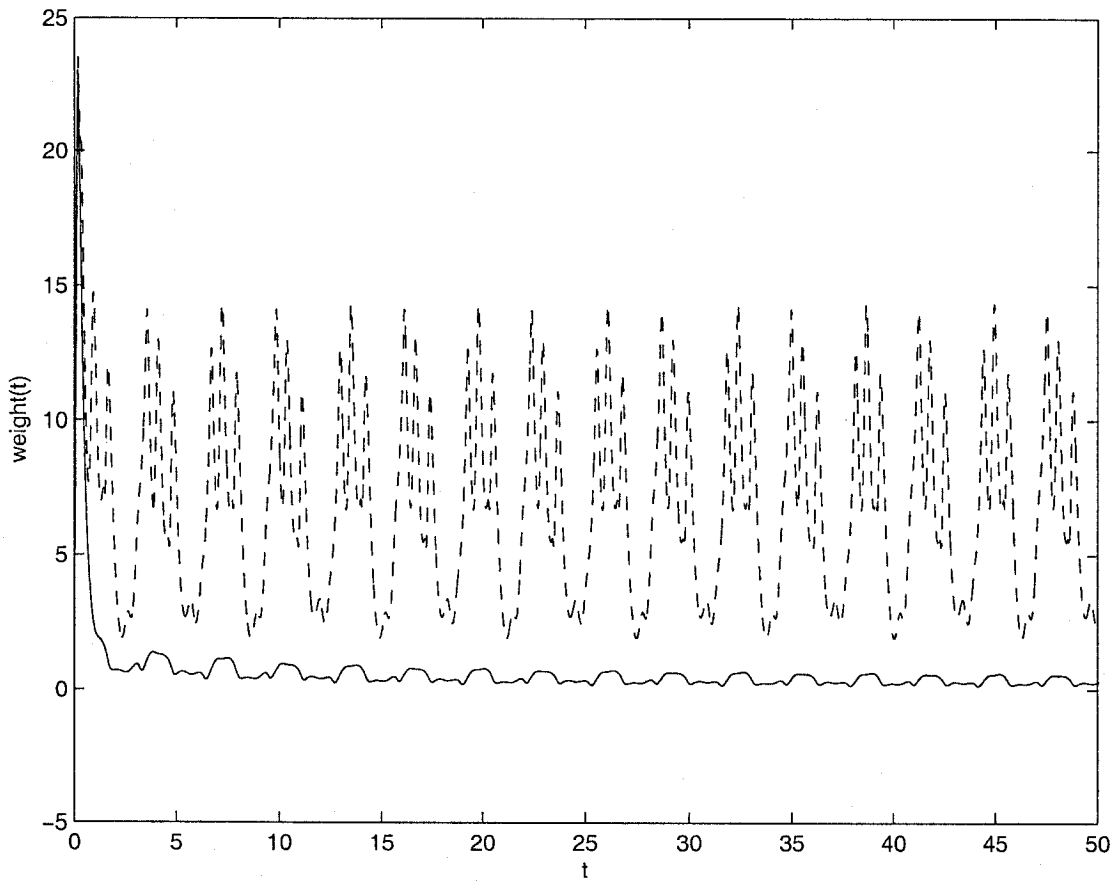

Figure 6.17: Case 2): Neural network weight $\|\hat{\theta}\|$ *with* $\Gamma = diag\{35\}$, $\sigma = 0.1$, $\delta = 0.05$, $\gamma = 0.11$, $\eta = 0.15$ *and* $\epsilon = 0.1$. *Where solid line represents the result with control term* $v_h \neq 0$ *and dashed line with* $v_h = 0$.

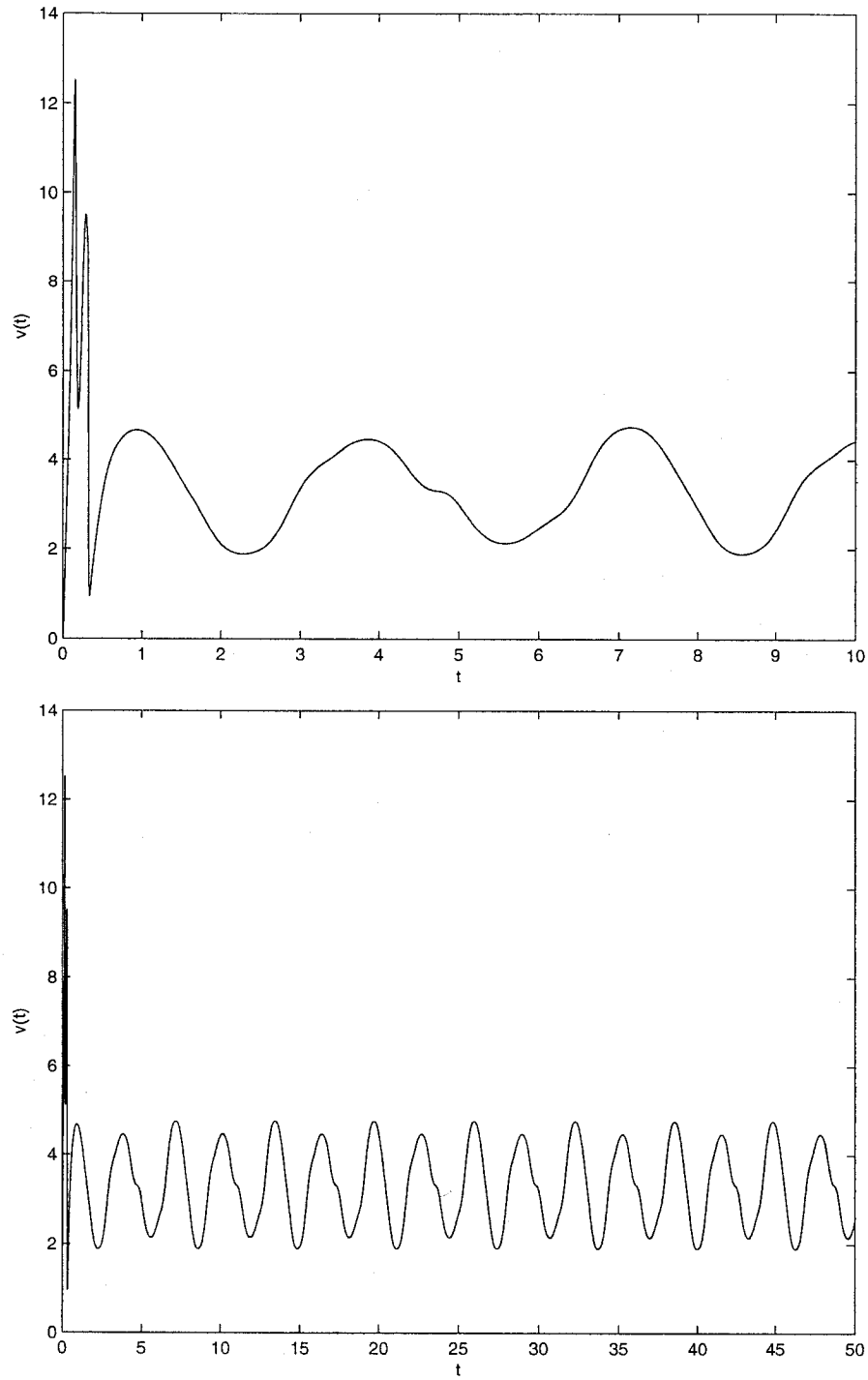

Figure 6.18: Case 2): The control input $v(t)$ *with* $\Gamma = diag\{35\}$, $\sigma = 0.1$, $\delta = 0.05$, $\gamma = 0.11$, $\eta = 0.15$ *and* $\epsilon = 0.1$ *in the time spans of* 10 *seconds and* 50 *seconds.*

Chapter 7

Conclusions and Future Work

7.1. Concluding Remarks

In practical control systems, especially for accurate control of positioning systems, hysteresis nonlinearity with unknown parameters in physical components may severely limit the controlled system performances. By using the Prandtl-Ishlinskii model with a play operator, a robust adaptive control scheme is developed to reduce hysteresis effect. This scheme is first combined with sliding mode control technique for a class of continuous-time nonlinear dynamic systems with unknown parameters and preceded by a hysteresis nonlinearity. It is proved that the proposed control laws can ensure global stability of the entire system and achieve both stabilization and tracking within a desired precision. Then, for the similar class of systems with less requirements for the design parameters, it is proved that the scheme can also be integrated with back-stepping control technique and lead to the same results. Simulations based on both methods were performed on an unstable nonlinear system. The results illustrate and further validate the effectiveness of the proposed approaches.

In this research, the developed method is also extended to a more general class of systems. The systems are in the presence of parametric uncertainties, unknown nonlinear functions, bounded disturbances caused by the system uncertainties such as external disturbances and modelling errors, and unknown hysteresis nonlinearities preceded by the plant. We combined our technique designed to reduce hysteresis effects with neural network adaptation control method given in [19] and proved that, if the system states defined in a bounded domain, then for any bounded initial conditions, all closed-loop signals are bounded and the state vector $x(t)$ converges to a neighborhood of the desired trajectory. To illustrate this robust adaptive control method, simulations are conducted on a variable length pendulum plant. The results show that the developed method is effective and robust under different set of parameters.

It is now clear that the developed control strategy to deal with hysteresis nonlinearities can be applied to many systems and may not necessarily be limited to the system described by (4.2) or (6.1). However, the goal of this research is to develop a control strategy in a simpler setting that reveals its essential features. The primary purpose of this research is to explore new avenues to fuse the models of hysteresis nonlinearities with available adaptive controller design methodologies without constructing a hysteresis inverse. This goal is achieved with very promising results. The results presented in this thesis can be considered as a stepping stone to be used towards the development of a general control framework for systems with hysteresis behavior.

7.2. Future Work

The following future research topics in this area will be of academic and practical interests and can be conducted in extending the current research presented in this thesis:

- Generalized Prandtl-Ishlinskii models: In our research the Prandtl-Ishlinskii model is based on the stop operators and takes the form of

$$w(t) = p_0 v(t) - \int_0^R p(r) F_r[v](t) dr, \tag{7.1}$$

with $p_0 = \int_0^R p(r)dr$. As we mentioned in section 3.4, the Prandtl-Ishlinskii model can be defined in a more general form, see reference [10]. Notice that in the above model, hysteresis loops are created by the integration of the weighted play operators. By changing the coefficients of the two terms on the right hand side of $w(t)$, the shape and direction of the hysteresis branches or loops can be impacted. Research results based on the more general form, therefore, should be suitable for broader applications.

- Rate-dependent hysteresis models: Rate-independent property is one of the characteristics of the Preisach type hysteresis models. Under certain conditions, it approximates hysteresis exhibited in many materials. It is possible and useful to further develop and extend the current research to rate-dependent circumstances.

- Practical controller development and implementations for industrial and other system control: Theoretical results and with supporting simulation studies presented in this thesis can be implemented for real system and process control in manufacturing, automation, robotics, aerospace and other applications

where hysteresis is a critical issue. Such implementation can be done through further software and/or hardware development. It will be a challenging task since many factors such as real time response, tolerances, computer interface, compatibility with existing systems, etc. are involved.

7.3. Publications from This Thesis Research

Several papers reporting results of this thesis research have been published in journals and well known international conferences as listed below. These papers were written under the guidance of my supervisor, Dr. C.-Y. Su. Other co-authors of some of the papers contributed partially through extensive discussions with important recommendations, initial computing codes and simulations, or the combinations of the above.

- C.-Y. Su, Q. Wang, X. Chen, and S. Rakheja, "Adaptive Variable Structure Control of a Class of Nonlinear Systems with Unknown Prandtl-Ishlinskii Hysteresis", *IEEE Transactions on Automatic Control*, Vol. 50, No. 12, pp2069-2074, 2005. (Chapter 5)

- Q. Wang and C.-Y. Su, "Robust Adaptive Control of a Class of Nonlinear Systems Including Actuator Hysteresis with Prandtl-Ishlinskii Presentations", *Automatica*, Vol. 42, pp859-867, 2006. (Chapter 4)

- Q. Wang, C.-Y. Su, Y. Tan, "On the Control of Plants with Hysteresis: Overview and a Prandtl-Ishlinskii Hysteresis Based Control Approach", *Acta Automatica Sinica*, Vol.31, No.1, pp92-104, 2005. (Chapter 2)

- Q. Wang, C.-Y. Su, S. Ge, "A Direct Method for Robust Adaptive Nonlinear Control with Unknown Hysteresis " *Proceedings of the Joint 44th IEEE*

Conference on Decision and Control and European Control Conference (CDC-ECC'05), Seville, Spain, December 12-15,2005. Full version will be submitted to *International Journal of Control.* (Chapter 6)

APPENDIX

Definition A.1 A function $f : \Re^n \rightarrow \Re^m$ is said to be continuous at a point x if, given $\epsilon > 0$, there is $\delta > 0$ such that for any y satisfies

$$\|x - y\| < \delta \tag{1}$$

implies

$$\|f(x) - f(y)\| < \epsilon \tag{2}$$

A function f is continuous on a set S if it is continuous at every point of S. A function f is uniformly continuous on a set S if, given $\epsilon > 0$, there is $\delta > 0$ dependent only on ϵ such that the inequality (2) holds for all $x, y \in S$. Note that uniform continuity is defined on a set, the same constant δ works for all points in the set.

Definition A.2 A function $f(x,t)$ is said to be Lipschitz in x if there exists a positive constant L such that

$$\|f(x,t) - f(y,t)\| \leq L\|x - y\| \tag{3}$$

for all (x,t) and (y,t) in some neighborhood of (x_0, t_0).

A function $f(x,t)$ is said to be locally Lipschitz in x on $D \times [a,b] \subset \Re^n \times \Re$, where D is an open and connected set, if each point $x \in D$ has a neighborhood D_0 such that f satisfies (3) on $D_0 \times [a,b]$ with some Lipschitz constant L_0. A function $f(x,t)$ is Lipschitz in x on $W \times [a,b]$ if it satisfies (3) on for all $t \in [a,b]$ and all points in W, with the same Lipschitz constant L.

Consider the non-autonomous system

$$\dot{x} = f(x,t) \tag{4}$$

where $f : \Re^n \times \Re_+ \rightarrow \Re^n$ is locally Lipschitz in x and piecewise continuous in t.

Definition A.3 The origin $x = 0$ is the equilibrium point for (4) if

$$f(0,t) = 0 \quad \forall t \geq 0 \tag{5}$$

Definition A.4 A continuous function $\gamma : [0,a) \rightarrow \Re_+$ is said to belong to class K if it is strictly increasing and $\gamma(0) = 0$. It is said to belong to class K_∞ if $a = \infty$ and $\gamma(r) \rightarrow \infty$ as $r \rightarrow \infty$.

Lemma (Barbalat)

Consider the function $\phi : \Re^+ \rightarrow \Re$. If ϕ is uniformly continuous and $\lim_{t\rightarrow\infty} \int_0^\infty \phi(r)dr$ exists and is finite, then

$$\lim_{t\rightarrow\infty} \phi(t) = 0.$$

Corollary

Consider the function $\phi : \Re^+ \rightarrow \Re$. If $\phi, \dot{\phi} \in L_\infty$, and $\phi \in L_p$ for some $p \in [1,\infty)$, then

$$\lim_{t\rightarrow\infty} \phi(t) = 0.$$

Bibliography

[1] Han J. M. T. A. Adriaens, W. L. de Koning and R. Banning, "Modeling piezoelectric actuators," *IEEE/ASME Trans. Mechatron.*, vol. 5, pp. 331-341, 2000.

[2] N. Ahmad and F. Khorrami "Adaptive control of systems with backlash hysteresis at the input," *Proc. American Control Conf.*, San Diego, California, pp.3018-3022, June 1999.

[3] H. T. Banks, A. Kurdila and G. Webb, "Identification of hysteretic control influence operators representing smart actuators part 1: Formulation," *Tech. Rep.*, Center for Research in Scientific Computation, Department of Mathematics, North Carolina State University, Raleigh, NC 27695-8205 and the Department of Aerospace Engineering, Department of Mathematics, Texas A and M University, College Station, TX 77843, 1996.

[4] H. T. Banks, A. Kurdila, and G. Webb, "Identification of hysteretic control influence operators representing smart actuators: Convergent approximation," *Tech. Rep.*, Center for Research in Scientific Computation, Department of Mathematics, North Carolina State University, Raleigh, NC 27695-8205 and the Department of Aerospace Engineering, Department of Mathematics, Texas A and M University, College Station, TX 77843, 1997.

[5] H. T. Banks and R. C. Smith, "Hysteresis modeling in smart material systems," *Journal of Applied Mechanics and Engineering*, vol. 5, pp. 31-45, 2000.

[6] R. Banning, W. L. de Koning and Han J. M. A. Adriaens, "State-space analysis and identification for a class of hysteretic systems," *Automatica*, vol. 37, pp. 1883-1892, 2001.

[7] S. A. Belbas and I. D. Mayergoyz, "Optimal control of dynamical systems with Preisach hysteresis," *International Journal of Non-Linear Mechanics*, vol. 37, pp. 1351-1361, 2002.

[8] Y. Bernard, E. Mendes and F. Bouillault, "Dynamic hysteresis modeling based on Preisach model," *IEEE Trans. on Magnetics*, vol.38, pp.885-888, 2002.

[9] M. Brokate, "Some BV properties of the Preisach model for hysteresis," *Appl. Anal.*, 32, pp.229-252, 1989.

[10] M. Brokate and J. Sprekels, *Hysteresis and Phase Transitions* , New York: Springer-Verlag, 1996.

[11] L. O. Chua and S. C. Bass, "A generalized hysteresis model," *IEEE Trans. Circuit Theory*, vol. CT-19, pp. 36-48, 1972.

[12] B. D. Coleman and M. L. Hodgdon, "A constitutive relation for rate-independent hysteresis in ferromagnetically soft materials," *Int. J. Engrg. Sci.*, vol. 24, pp. 897-919, 1986.

[13] B. D. Coleman and M. L. Hodgdon, "On a class of constitutive relations for ferromagnetic hysteresis," *Arch. Rational Mech. Anal.*, vol. 402, pp. 375-396, 1989.

[14] D. Croft, G. Shed and S. Devasia, "Creep, hysteresis, and vibration compensation for piezoactuators: Atomic force microscopy application," *J. of Dynamic Systems, Measurement, and Control*, vol.123, pp.35-43, 2001.

[15] C. A. Dickinson, D. Hughes and J.T. Wen, "Hysteresis in shape memory alloy actuators: The control issues," *Proc. SPIE 2715, V. V. Varandan and J. Chandra, Eds.,* pp. 494-506, 1996.

[16] D. G. Fertis and C. T. Lee, "Inelastic response of variable stiffness members under cyclic loading," *J. Engineering Mechanics,* vol.118, pp. 1406-1446, 1992.

[17] W. S. Galinaitis, "Two methods for modeling scalar hysteresis and their use in controlling actuators with hysteresis," *Ph.D. Thesis*, Blacksburg, Virginia, USA, 1999.

[18] P. Ge, and M. Jouaneh "Tracking control of a piezoceramic actuator," *IEEE Trans. on Control Systems Technology*, Vol.4, pp.209-216, 1996.

[19] S. S. Ge, C.C. Hang and T. Zhang, "A direct method for robust adaptive nonlinear control with guaranteed transient performance" *Systems & Control Letters*, vol. 37, pp. 275-284, 1999.

[20] J. Getpreecharsawas and E. Lyshevski, "Modeling and analysis of flexible beams with surface-mounted PZT actuators," *Proc. of the 41st IEEE conference on Decision and control*, Las Vegas, Nevada, USA, Dec. 2002.

[21] M. Goldfarb and N. Celanovic, "Modeling piezoelectric stack actuators for control of micromanipulation," *IEEE Control Systems Magazine*, vol.17, issue 3, pp. 69-79, 1997.

[22] R. B. Gorbet, "Control of hysteresis systems with Preisach representations," *Ph.D. Thesis*, Waterloo, Ontario, Canada, 1997.

[23] R. B. Gorbet, K. A. Morris and D. W. L. Wang "Passivity-based stability and control of hysteresis in smart actuators," *IEEE Trans. on Control Systems Technology*, vol.9, pp.5-16, 2001.

[24] M. L. Hodgdon, " Applications of a theory of ferromagnetic hysteresis," *IEEE Trans. Magn.*, MAG-24, pp. 218-221, 1988.

[25] M. L. Hodgdon, "Mathematical theory and calculations of magnetic hysteresis curves," *IEEE Trans. Magn.*, MAG-24, pp. 3120-3122, 1988.

[26] H. Hu and R. B. Mrad, "On the classical Preisach model for hysteresis in piezoceramic actuators," *Mechatronics*, vol. 13, pp. 85-94, 2003.

[27] D. Hughes and J.T. Wen, "Preisach modeling of piezoceramic and shape memory alloy hysteresis," *Smart Materials and Structures*, vol. 6, pp. 287300, 1997.

[28] C-L. Hwang and C. Jan, "A reinforcement discrete neuro-adaptive control for unknown piezoelectric actuator systems with dominant hysteresis," *IEEE Trans. Neural Networks*, vol. 14, no.1, pp. 66-78, 2003.

[29] C-L. Hwang, C. Jan and Y-H. Chen, "Piezomechanics using intelligent variable-structure control," *IEEE Trans. Industrial Electronics*, vol.48, pp. 47-59, 2001.

[30] P. A. Ioannou and J. Sun, *Robust adaptive control*, Prentice Hall PTR, 1996.

[31] A. Y. Ishlinskii, "Some applications of statistical methods to describing deformations of bodies," *Izv. AN SSSR, Techn. Ser.,*, no. 9, pp. 580-590, 1944 (in Russian).

[32] A. Isidori, *Nonlinear Control Systems: An Introduction*, 2nd ed. Berlin, Germany: Springer-Verlag, 1989.

[33] D.C. Jiles, "Modelling the effects of eddy current losses on frequency dependent hysteresis in electrically conducting media", *IEEE Transactions on Magnetics*, vol 30, pp. 4326-4328, 1994.

[34] D. C. Jiles and D. L. Atherton, Theory of ferromagnetic hysteresis, J. Magn. Magn. Mater., vol. 61, pp. 48-60, 1986.

[35] D.C. Jiles and J.B.Thoelke, "Theory of ferromagnetic hysteresis: determination of model parameters from experimental hysteresis loops," *IEEE Transactions on Magnetics*, vol. 25, pp.3928 - 3930, 1989.

[36] A. Kojic, C. Cao and A. M. Annaswamy, "Parameter Convergence in systems with Convex/Concave Parameterization," *Proceedings of the 2000 American Control Conference,* pp. 2240-2244, 2000.

[37] M. A. Krasnosekl'skii and A. V. Pokrovskii, *Systems with Hysteresis*, Nauka, Moscow, 1983.

[38] P. Krejci and K. Kuhnen, "Inverse control of systems with hysteresis and creep," *IEE Proc.-Control Theory Appl.*, vol. 148, pp. 185-192, 2001.

[39] K. Kuhnen and H. Janocha, "Complex hysteresis modeling of a broad class of hysteretic actuator nonlinearities" *Proc. of the 8th Int. Conf. on New Actuators*, Bremen, pp.10-12, June 2002

[40] J.V. Leite, N. Sadowski, P. Kuo-Peng, N.J. Batistela and J.P.A. Bastos, "The inverse Jiles-Atherton model parameters identification ", *IEEE Transactions on Magnetics*, vol. 39, pp. 1397 - 1400, 2003.

[41] A-P Loh, A. M. Annaswamy and F. P. Skantze, "Adaptation in the Presence of a General Nonlinear Parameterization: An Error Model Approach," *IEEE Trans. on Automatic Control,* vol.44, pp. 1634-1652, 1999.

[42] Tianshun Lu, Y. H. Tan, and Chun-Yi Su, "Pole placement control of discrete time systems preceded with hysteresis via dynamic neural network compensator intelligent control," *Proc. of the 2002 IEEE International Symposium*, 2002.

[43] J. W. Macki, P. Nistri and P. Zecca, "Mathematical models for hysteresis," *SIAM Review*, vol. 35, pp. 94-123, 1993.

[44] D. Makaveev, L. Dupre, M. De Wulf and J. Melkebeek, "Dynamic hysteresis modelling using feed-forward neural networks," *J. of Magnetism and Magnetic Materials*, vol. 254-255, pp. 256-258, 2003.

[45] I. D. Mayergoyz, *Mathematical Models of Hysteresis*, Berlin: Springer-Verlag, 1991.

[46] S. Mittal and C-H. Meng, "Hysteresis compensation in electromagnetic actuators through Preisach model inverse," *IEEE/ASME Trans. Mechatron.*, vol. 5, pp. 394-409, 2000.

[47] T. Nakaguchi, S. Isome, K. Jin'no, and M. Tanaka "Box Puzzling Problem Solver by Hysteresis Neural Networks," *IEICE Trans. Fundamentals*, vol.E84-A, pp. 2173-2181, 2001.

[48] T. E. Pare "Robust stability and performance analysis of systems with hysteresis nonlinearities," *Proc. of American Control Conference*, Philadelphia, Pennsylvania, pp.1904-1908, June 1998.

[49] D. A. Philips , L. R. Dupre and J. A. Melkebeek, "Comparison of Jiles and Preisach hysteresis models in magnetodynamics ," *IEEE Transactions on Magnetics*, vol. 31, pp.3551 - 3553, 1995.

[50] L. Prandtl, "Ein gedankenmodell zur kinetischen theorie der festen Korper," *ZAMM,* vol. 8, pp. 85-106, 1928.

[51] C. Ragusa, "An analytical method for the identification of the Preisach distribution function," *J. Magnetism and Magnetic Materials*, vol. 254-255, pp. 259-261, 2003.

[52] P. M. Sain, M.K. Sain and B. F. Spencer, "Models for hysteresis and application to structural control," *Proc. American control Conf.*, pp. 16-20, 1997.

[53] A. Salvini and F.R. Fulginei,, "Genetic algorithms and neural networks generalizing the Jiles-Atherton model of static hysteresis for dynamic loops", *IEEE Transactions on Magnetics*, vol. 38, pp. 873-876, 2002.

[54] R. R. Selmic and F. L. Lewis, "Backlash compensation in nonlinear systems using dynamics inversion by neural networks," *Proc. 1999 IEEE Int. Conf. Control Applications*, pp. 1163-1168, Aug. 1999.

[55] J.-J. E. Slotine and W. Li, *Applied Nonlinear Control*, Englewood Cliff, NJ: Prentice-Hall, 1991.

[56] B. P. Spencer, Jr. *Reliability of Randomly Excited Hysteresis Structures. Lecture Notes in Engineering*, vol.21. New York: Springer-Verlag, 1986.

[57] C.-Y. Su, Y. Stepanenko, J. Svoboda and T. P. Leung, "Robust adaptive control of a class of nonlinear systems with unknown backlash-like hysteresis," *IEEE Trans. on Automatic Control*, vol. 45, pp. 2427-2432, 2000.

[58] X. Tan and J. S. Baras, "Modeling and control of a magnetostrictive actuator," *Proc. of the 41st IEEE conference on Decision and Control*, Las Vegas, Nevada, USA, Dec. 2002.

[59] G. Tao and P.V. Kokotovic, "Adaptive control of plants with unknown hystereses," *IEEE Trans. on Automatic Control*, vol. 40, pp. 200-212, 1995.

[60] G. Tao and F. L. Lewis (Eds), *Adaptive Control of Nonsmooth Dynamic Systems*, Springer, 2001.

[61] M.-S. Tsai and J.-S. Chen, "Robust tracking control of a piezoactuator using a new approximate hysteresis model," *Tran. of ASME* vol.125, pp.96-102, 2003.

[62] V. I. Utkin, "Variable structure systems with sliding modes (Survey Paper)," *IEEE Trans. on Automatic Control*, vol. 22, pp. 212-222, 1977.

[63] A. Visintin (ed), *Phase Transitions and Hysteresis. Lecture Notes in Mathematics*, Vol. 1584. Berlin: Springer-Verlag, 1994.

[64] G. Webb, A. Kurdila and D. Lagoudas "Adaptive hysteresis model for model reference control with actuator hysteresis," *J. Guidance, Control and Dynamics*, vol.23, pp.459-465, 2000.

[65] J-D. Wei and C-T. Sun, "Constructing hysteresis memory in neural networks ," *IEEE Trans. System, Man, and Cybernetics-part B: Cybernetics*, vol.30, pp. 601-609, 2000.

[66] Y.-K. Wen, "Method for random vibration of hysteretic systems ," *J. Engr. Mech.*, vol.102, pp. 249-263, 1976.

[67] Y. Yu, Z. Xiao, E.-B. Lin and N. Naganathan, "Analytic and experimental studies of a wavelet identification of Preisach model of hysteresis," *J. Magnetism and Magnetic Materials*, vol. 208, pp. 255-263, 2000.